VTT PUBLICATIONS 712

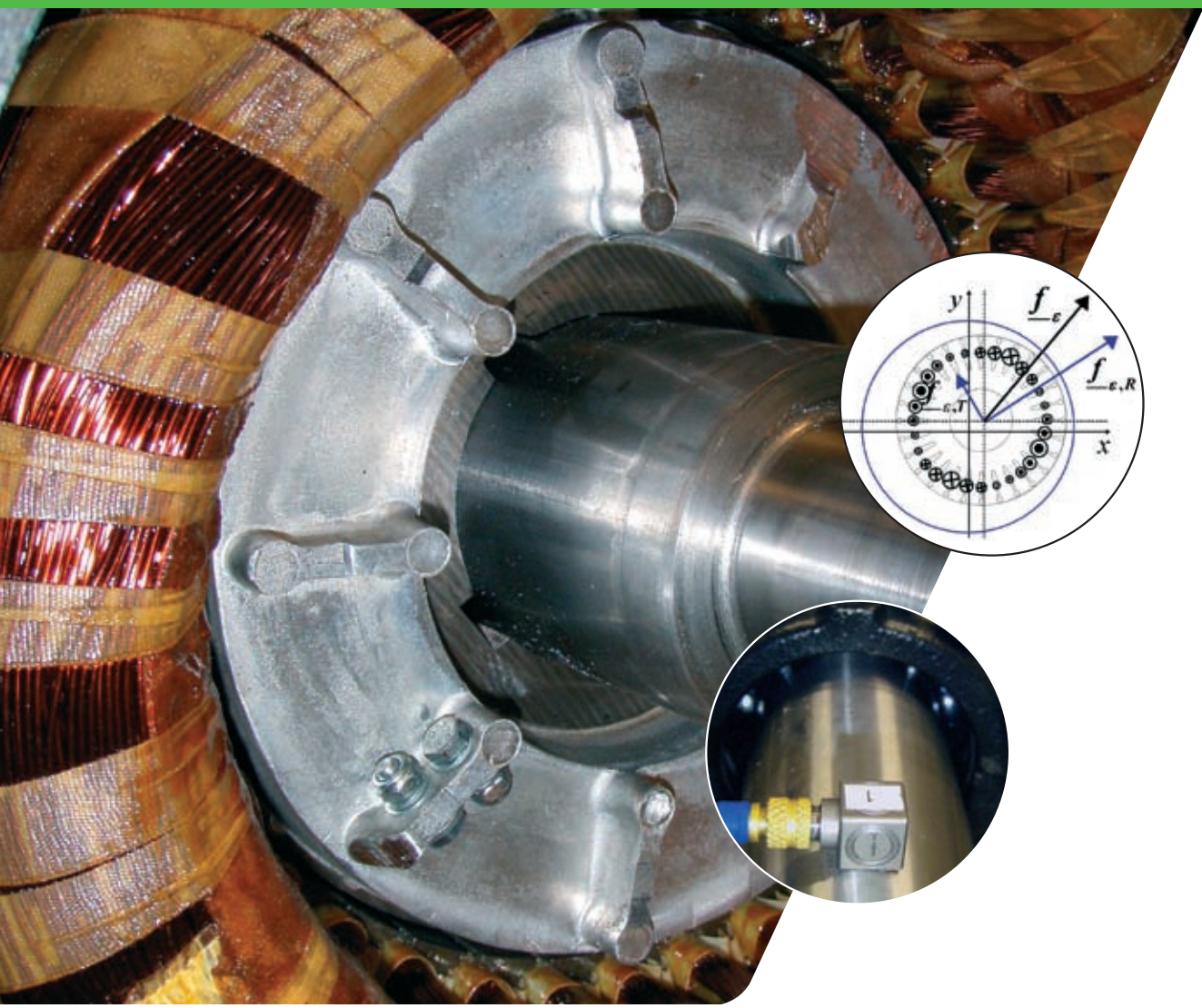

Antti Laiho

Electromechanical modelling and active control of flexural rotor vibration in cage rotor electrical machines

VTT PUBLICATIONS 712

Electromechanical modelling and active control of flexural rotor vibration in cage rotor electrical machines

Antti Laiho

VTT

Helsinki University of Technology
Faculty of Electronics, Communications and Automation
Department of Electrical Engineering

DOCTORAL DISSERTATION

Dissertation for the degree of Doctor of Science in Technology to be presented with due permission of the Faculty of Electronics, Communications and Automation for public examination and debate in Auditorium S4 at Helsinki University of Technology (Espoo, Finland) on the 18th of September, 2009, at 12 noon.

ISBN 978-951-38-7348-6 (soft back ed.)
ISSN 1235-0621 (soft back ed.)

ISBN 978-951-38-7349-3 (URL: http://www.vtt.fi/publications/index.jsp)
ISSN 1455-0849 (URL: http://www.vtt.fi/publications/index.jsp)

JULKAISIJA – UTGIVARE – PUBLISHER

VTT, Vuorimiehentie 3, PL 1000, 02044 VTT
puh. vaihde 020 722 111, faksi 020 722 4374

VTT, Bergsmansvägen 3, PB 1000, 02044 VTT
tel. växel 020 722 111, fax 020 722 4374

VTT Technical Research Centre of Finland, Vuorimiehentie 3, P.O. Box 1000, FI-02044 VTT, Finland
phone internat. +358 20 722 111, fax + 358 20 722 4374

Technical editing Mirjami Pullinen

Edita Prima Oy, Helsinki 2009

Electromechanical modelling and active control of flexural rotor vibration in cage rotor electrical machines [Sähkömekaaninen mallinnus ja aktiivinen roottorin poikittaisvärähtelyjen hallinta häkkiroottorilla varustetussa induktiokoneessa]. Espoo 2009. VTT Publications 712. 91 p. + app. 84 p.

Keywords induction machine, electromagnetic actuator, rotor-dynamics, self-bearing machine, bearingless drive, mechanical vibration, active control

Abstract

The main objective of this thesis is to develop new tools for model-based control of flexural rotor vibration in cage induction machines. In order to exert the control force on the rotor, a built-in force actuator based on self-bearing principle is considered. A low-order parametric electromechanical model coupling the eccentric-rotor machine, the actuator and rotor-dynamics is developed. Furthermore, numerical analysis of the actuator-rotor system is considered. The numerical analysis is based on time-discretised finite element analysis of the electromagnetic fields in the two-dimensional cross-section of the machine. The finite element analysis is used to estimate the parameters of the low-order model. The numerical analysis provides a tool for both designing the actuator and testing the control algorithms.

In the thesis, a control algorithm, previously used mainly in active magnetic bearings for compensation of harmonic disturbance forces, is applied by using the built-in force actuator. In the simulations, the control algorithm is embedded in the numerical analysis. The modelling and model-based control are verified by experiments. A 30 kW two-pole cage induction motor with an extended rotor shaft is used for measurements.

The results both from simulations and experiments show that, by using the built-in force actuator, the model-based controller is suitable for flexural rotor vibration suppression in a cage induction machine. In particular, the stable operation at the critical speed of the machine can be achieved by using the methodology presented in this research.

Electromechanical modelling and active control of flexural rotor vibration in cage rotor electrical machines [Sähkömekaaninen mallinnus ja aktiivinen roottorin poikittaisvärähtelyjen hallinta häkkiroottorilla varustetussa induktiokoneessa]. Espoo 2009. VTT Publications 712. 91 s. + liitt. 84 s.

Avainsanat induction machine, electromagnetic actuator, rotor-dynamics, self-bearing machine, bearingless drive, mechanical vibration, active control

Tiivistelmä

Tämän väitöskirjan tavoite on uusien menetelmien kehittäminen poikittaisten roottorivärähtelyjen mallipohjaiseen vaimennukseen häkkiroottorilla varustetussa induktiokoneessa. Työssä käytetään laakerittoman sähkökoneen voimantuottomekanismia voiman tuottamisessa roottoriin. Tutkimuksessa rakennetaan matalakertalukuinen sähkömekaaninen malli, joka kytkee toisiinsa roottorin epäkeskon liikkeen, voima-aktuaattorin ja roottoridynamiikan. Työssä tutkitaan lisäksi aktuaattori-roottori-systeemin numeerista analyysiä. Numeerinen analyysi perustuu sähkömagneettisten kenttien aika-diskretisoituun elementtimenetelmä-perustaiseen analyysiin koneen kaksiulotteisessa poikkileikkauksessa. Elementtimenetelmää käytetään matalakertalukuisen mallin parametrien estimoinnissa. Numeerinen analyysi antaa työkaluja aktuaattorin suunnitteluun ja säätöalgoritmien testaukseen.

Tässä työssä sovelletaan aiemmin pääasiassa aktiivimagneettilaakereissa harmonisten herätteiden kompensoinnissa käytettyä säätöalgoritmia käyttäen koneen sisäänrakennettua voima-aktuaattoria. Simuloinneissa säätöalgoritmi on sisällytetty numeeriseen analyysiin. Työssä mallinnus ja mallipohjainen säätö verifioidaan kokeellisesti. Mittauksissa käytetään kaksinapaista häkkiroottorilla ja pidennetyllä roottoriakselilla varustettua 30 kW:n induktiokonetta.

Sekä simulaatioista että kokeista saadut tulokset osoittavat, että sisäänrakennettua voima-aktuaattoria hyödynnettäessä mallipohjainen säädin soveltuu poikittaisten roottorivärähtelyjen aktiivivaimennukseen häkkiroottorilla varustetussa induktiokoneessa. Tässä työssä esitetty menetelmä mahdollistaa koneen stabiilin toiminnan kriittisellä pyörimisnopeudella.

Preface

This research work was carried out as a part of ACRVEM (Active Control of Rotor Vibration in Electrical Machines) project during 2006–2008. The aim of the project was to develop tools for attenuation of flexural rotor vibration in electrical machines. The project was funded by Academy of Finland and VTT Technical Research Centre of Finland. The funding parties are gratefully acknowledged. The research partners in the project were Department of Mathematics and Systems Analysis at Helsinki University of Technology (HUT), Department of Automation and Systems Technology at HUT, Department of Electrical Engineering at HUT and VTT Technical Research Centre of Finland. This work was conducted in Department of Electrical Engineering at HUT and VTT Technical Research Centre of Finland. The project was interdisciplinary in the sense that it involved electrical engineering, control engineering, mechanical engineering and practical implementation of the laboratory set-up. Hence, I am greatly indebted to many people with whom it was a pleasure to work within these years.

I wish to thank my supervisor Professor Antero Arkkio for guidance and supervision throughout the project. I am greatly indebted to Dr. Timo Holopainen, ABB Electrical Machines, for co-operation, encouragement and inspiring discussions. I would like to express sincere gratitude to Dr. Kari Tammi, Dr. Kai Zenger, Dr. Andrej Burakov, Mr. Juha Orivuori and Mr. Anssi Sinervo for fruitful co-operation in ACRVEM project. I would like to devote special thanks to Mr. Ari Haavisto for his invaluable and kind assistance in experimental part of this project. I am grateful to all the laboratory members in Team of Electromechanics at HUT for friendly atmosphere and creative discussions. In particular, I am grateful to Dr. Anna-Kaisa Repo for introducing evolution algorithms. At the beginning of the experimental part of the work, I received essential guidance with the dSpace system from Professor Marko Hinkkanen, Power Electronics Laboratory at HUT, to whom I am grateful.

I would like to express gratitude to Mr. Pekka Koskinen and Mr. Ismo Vessonen, VTT Industrial Systems, for all the arrangements and opportunity to work in this long-term project. I am grateful to colleagues in VTT Industrial Systems, for a friendly and innovative working atmosphere. Especially, I am grateful to Dr. Seppo Aatola, Mr. Aki Kinnunen, Mr. Jarkko Keinänen, Mr. Kalle Vehviläinen and Mr. Vesa Nieminen for a kind help with issues related to vibration measurements. I wish to thank Mr. Paul Klinge and Mr. Kai Katajamäki for invaluable help with structural finite element modelling. I am thankful to Mr. Antti Hynninen, Mr. Petteri Kokkonen and Mr. Juha Virtanen for guidance with issues related to structural mechanics and beyond. I am grateful to Dr. Erkki Lantto and Mr. Ville Tommila, High Speed Tech Oy Ltd, for valuable suggestions and discussions regarding active magnetic bearings and control algorithms. During the simulation part of the work, I received invaluable help from Dr. Sami Kanerva, ABB Electrical Machines, and Dr. Slavomir Seman, ABB Drives, to whom

I would like to express my gratitude. I would also like to thank Pedro Jover, ABB Electrical Machines, for a nice team work in measuring the vibrations of electrical machines with healthy and not-so-healthy rotors.

I am grateful to my parents, Leila and Raino, and my brother, Ari, for all support and dedication. I am grateful to my friends for support and almost oriental understanding. Finally, I would like to express my deepest gratitude to Julia for her love and encouragement.

Espoo, August 10, 2009

Antti Laiho

List of Publications

This thesis is based on the following original publications.

I A. Laiho, T. P. Holopainen, P. Klinge and A. Arkkio, "Distributed model for electromechanical interaction in rotordynamics of cage rotor electrical machines", *Journal of Sound and Vibration*, vol. 302, no. (4–5), pp. 683–698, 2007.

II A. Laiho, K. Tammi, A. Burakov, A. Arkkio and K. Zenger, "A built-in force actuator for active control of lateral rotor vibration in cage induction electrical machines", *Journal of Sound and Vibration*, vol. 320, no. 3, pp. 496–515, 2009.

III A. Laiho, K. Tammi, K. Zenger and A. Arkkio, "A model-based flexural rotor vibration control in cage induction electrical machines by a built-in force actuator", *Electrical Engineering (Archiv für Electrotechnik)*, vol. 90, no. 6, pp. 407–421, 2008.

IV A. Laiho, A. Sinervo, J. Orivuori, K. Tammi, A. Arkkio and K. Zenger, "Attenuation of harmonic rotor vibration in a cage rotor induction machine by a self-bearing force actuator", *IEEE Transactions on Magnetics*, pp. 1–12 (in press).

V A. Laiho, K. Tammi, J. Orivuori, A. Sinervo, K. Zenger and A. Arkkio, "Electromechanical interaction in eccentric-rotor cage induction machine equipped with a self-bearing force actuator", *Journal of System Design and Dynamics*, vol. 3, no. 4, pp. 519–529, 2009.

Contents

Appendices of this publication are not included in the PDF version.
Please order the printed version to get the complete publication
(http://www.vtt.fi/publications/index.jsp).

Abbreviations

AMB	active magnetic bearing
CC	convergent control
CPU	central processing unit
DFT	discrete fourier transformation
DOF	degree of freedom
FE	finite element
FEA	finite element analysis
FEM	finite element method
FRF	frequency-response function
LTI	linear time-invariant
LTP	linear time-periodic
LQR	linear quadratic regulator
MMF	magnetomotive force
ODE	ordinary differential equation
PC	personal computer
PEM	prediction-error method
PID	proportional-integral-derivative
PM	permanent magnet
RL	resistor-inductor
RMS	root mean square
SRC	synchronous response control
UMP	unbalanced magnetic pull

Symbols and Notation

B	air-gap flux density [T]
$\hat{B}_k$	peak value of flux density harmonic k [T]
$\underline{\hat{B}}_k$	space-vector of flux density harmonic k [T]
$\underline{B}_k$	complex amplitude of flux density harmonic k [T]
C	damping matrix [Ns/m]
d_r	diameter of rotor core [m]
f	force [N]
f_c	control force [N]
f_{ex}	excitation force [N]
$\underline{f}_{\epsilon}$	force of unbalanced magnetic pull (UMP) [N]
$\underline{f}_{\epsilon,R}$	radial UMP [N]
$\underline{f}_{\epsilon,T}$	tangential UMP [N]
$\underline{g}_{p\pm1}$	cage-current variables [A]
G	gyroscopic matrix [Ns/m]
$\mathcal{H}$	frequency-response matrix [m/V]
$\underline{\hat{i}}_c$	space-vector of control winding current [A]
$\underline{\hat{i}}_{c,0}$	modulated space-vector of control winding current [A]
$\underline{\hat{i}}_{r,k}$	space-vector of rotor cage current harmonic k [A]
$\underline{\hat{i}}_{r,k,0}$	modulated space-vector of rotor cage current harmonic k
I	identity matrix [-]
j	imaginary unit [-]
k_0	negative stiffness coefficient [N/m]
K	stiffness matrix [N/m]
l_r	length of rotor core [m]
L_c	inductance of control winding [H]
$L_{r,k}$	rotor cage inductance of harmonic k [H]
m	(modal) mass of rotor [kg]
M	mass matrix [kg]
$M_{r,c,p+1}$	mutual inductance of control winding and rotor cage [H]
N	number of slices [-]
N_ℓ	number of nodes on slice [-]
p	number of pole-pairs [-]
R_c	resistance of control winding [Ω]
$R_{r,p\pm1}$	rotor cage resistance of harmonic component k [Ω]

s	Laplace variable [1/s], slip [-]
t	time [s]
T_s	sample time [s]
u	displacement vector [m]
u_x	horizontal displacement [m]
u_y	vertical displacement [m]
$\underline{\hat{u}}_c$	space-vector of control winding supply voltage [V]
$\underline{\hat{u}}_{c,0}$	modulated space-vector of control winding supply voltage [V]
u_{rc}	rotor center displacement [m]
v_c	control input [V]
x	horizontal coordinate [m]
$X_{c,\epsilon,p+1}$	eccentricity coupling factor of control winding [m]
$X_{r,\epsilon,k}$	eccentricity coupling factor of rotor cage harmonic k [m]
y	vertical coordinate [m]
$\underline{z}_r$	rotor centre position [m]
$\underline{z}_r^\ell$	rotor centre position on slice [m]
$\underline{z}_s^\ell$	averaged stator deformation on slice [m]
α_k	convergence parameter [-]
γ_k	convergence parameter [-]
δ_0	radial air-gap length [m]
$\delta_{p,1}$	Kronecker delta [-]
η	modal vector [m$\sqrt{\text{kg}}$]
θ	angular coordinate [rad]
μ_0	air-gap permeability [N/A^2]
Ξ	damping ratio matrix [-]
Φ	modal matrix [1/$\sqrt{\text{kg}}$]
φ_p	initial phase angle of fundamental flux [rad]
φ_s	phase angle of fundamental flux [rad]
φ_w	phase angle of rotor whirling [rad]
$\underline{\hat{\psi}}_{r,k}$	space-vector of rotor cage flux linkage harmonic k [Wb]
ω_m	angular frequency of rotor rotation [rad/s]
ω_s	supply (angular) frequency [rad/s]
ω_w	angular frequency of rotor whirling [rad/s]
Ω	natural frequency matrix [rad/s]

e^X	exponential function $\exp(X)$
$\underline{\hat{X}}$	space-vector X
$\underline{X}$	complex number X
$\underline{\hat{X}}^r$	space-vector X in rotor coordinates
$\underline{\hat{X}}^s$	space-vector X in stator coordinates
$\underline{X}^*$	complex conjugate of complex number $\underline{X}$
$\lvert\underline{X}\rvert$	absolute value of complex number $\underline{X}$
$\dot{X}$	time-derivative of X
$X^\dagger$	pseudo-inverse of matrix X
$\mathrm{Re}(\underline{X})$	real part of complex number $\underline{X}$
$\mathrm{Im}(\underline{X})$	imaginary part of complex number $\underline{X}$
$\lVert X\rVert_2$	square norm of vector X

1 Introduction

...On the shaft was shining copper,
And the bow was strong and wondrous,
But alas! It was ill-natured... [1]

1.1 Background

In rotating machinery, passive or active vibration control is generally needed to prevent excessive rotor vibration, which can lead to fatigue or malfunction. A long-term operation close to critical speed is usually not possible due to an excessive vibration level which may break the machine or lead to fatigue. Usually, the critical-speed operation is avoided by designing the machine to operate either below or above the critical speed and the critical speeds are passed quickly. In some applications such as variable-speed drives, the rotor vibration may, however, be a strongly restrictive issue because the optimal running speed cannot be reached due to increased vibration. On the other hand, in electrical machine design, the critical speed is a limiting factor, that affects the design process in a restrictive manner. The power of an electrical machine is related to the length of the rotor core, which cannot be extended above a certain limit without structural modifications because of increased vibration.

In an electrical machine, an unbalanced magnetic field distribution in the air-gap between the stator and rotor generates a force on the rotor. The phenomenon is referred to as unbalanced magnetic pull (UMP). The eccentric rotor motion distorts the air-gap which results in a non-uniform permeance distribution and, consequently, asymmetric field distribution. Hence, the eccentric rotor motion (or rotor-dynamics) is coupled with the magnetic fields in the air-gap. This results in a coupled electromechanical system in which the rotor motion affects the magnetic field distribution which, in turn, generates a force on the rotor resulting in displacement response.

The radial UMP component reduces the stiffness between the stator and rotor of the machine which changes the eigenfrequencies of the vibration modes having relative motion between the stator and rotor. The tangential component of the UMP is related to electromechanical damping. In a cage induction machine, the tangential component is induced by currents in the rotor cage and parallel paths of the stator winding. The currents are generated by the additional air-gap fields due to the eccentric rotor motion. The tangential UMP component may have an influence on the rotor-dynamic stability.

In addition to the coupling between the mechanical and electromagnetic systems, the UMP provides means of actively generating force on the rotor provided that the field asymmetry can be controlled. Using the unbalanced magnetic field distribution on force production has been utilised in active magnetic bearings (AMBs), for instance. Later, the methodology was adopted in self-bearing (bea-

ringless) electrical machines. Along with AMB, the self-bearing force actuation provides a built-in non-contact actuator, which generates a controlled force on the rotor.

An electrical machine under eccentric rotor motion and equipped with a self-bearing force actuator is a coupled electromechanical system. The system can be controlled by currents causing the unbalance in the air-gap field distribution. The system involves transient magnetic fields, circuits and a mechanical system consisting of rotor-dynamics of the rotor and structural dynamics of the bearings, housing and foundation. The model-based control design for such a system involves modelling of the electromechanical actuator-rotor system.

1.2 Aim of the work

The main objective of this thesis is to provide means for electromechanical modelling of a cage induction machine for the needs of model-based control of rotor vibration. The main application of the research is linked to large machines with low critical speeds. The work provides simulation and analytical tools for the design of the force actuator for vibration control in cage induction machines. For purposes of investigating actuator-rotor dynamics, a system simulator is built.

Special focus is put on the coupling of structural mechanical modelling with an analysis of transient magnetic fields by using low-order parametric models. The parametric models are formulated such that they can be readily used in control design. The modelling is restricted to linear time-invariant (LTI) models. The LTI model covers the governing dynamical phenomena in the actuator-rotor system. However, in the thesis, some effects beyond the LTI model are brought out.

In the thesis, by using the self-bearing force actuator, the goal is also to investigate and demonstrate a control algorithm previously used for attenuation of harmonic vibration components in rotating machinery and AMBs. The experimental results of a cage induction machine with extended rotor shaft are presented. The scope of the work is to demonstrate active force generation, rotor vibration attenuation and critical speed operation in a cage induction machine.

In summary, the scope of the work involves

1) development a computationally efficient analytical model for flexural rotor vibration in cage rotor electrical machines. The model should couple low-frequency phenomena in rotor vibration with electromagnetic fields in the machine. The 3-D rotor and stator deflections should be included in the model. In addition, the model is to be based on physical parameters which could be estimated numerically or measured,

2) modelling of the actuator-rotor system by using a low-order LTI formalism. The requirement for the model is that it can be applied in a real-time

controller. In addition, the model should be based on physical parameters which can be measured or estimated numerically,

3) development of numerical tools for simulated rotor vibration control by using the built-in force actuator. The aim of the analysis is to obtain a virtual plant for the design of the force actuator and, also, for testing the control algorithms. The analysis should be detailed in the sense that, for instance, stator or rotor slotting and saturation of magnetic materials would be included,

4) experimental verification of the modelling and proposed control design for attenuation of flexural rotor vibration. The control of dominating vibration frequencies of the rotor and stable operation at the critical speed should be demonstrated.

1.3 Scientific contribution

1) A method for coupling a low-order parametric model of an eccentric-rotor electrical machine to a three-dimensional (3-D) structural mechanical model of the machine in modal analysis framework is developed. The methodology provides computationally efficient analytical tools for studying 3-D rotor vibration effects in electrical machines.

2) The effect of electromechanical interaction on flexural rotor vibration in an electrical machine is examined by using the parametric force model and structural finite-element analysis (FEA) in a common framework. The results indicate that the electromechanical interaction has an effect on the rotor bending vibration modes of the machine. The damping of the modes having relative motion between the stator and rotor are affected by the electromechanical interaction. Furthermore, the damping stems from the circulating currents in the rotor cage due to the eccentric rotor motion. The response of the machine to rotor mass unbalance is affected by the electromechanical interaction, as well.

3) A built-in force actuator is considered for attenuation of flexural rotor vibration. For the cage rotor induction machine equipped with the built-in force actuator, a system simulator based on FEA is built. It is shown that the simulator provides a suitable tool for control design prior to implementing the control strategies in a real machine.

4) A low-order linear time-invariant parametric model is developed for an eccentric-rotor cage induction machine equipped with the built-in force actuator. In particular, the unbalanced magnetic pull induced by both the eccentric rotor motion and the currents in the supplementary winding is modelled in a common framework. The model is verified against more detailed

numerical simulations based on finite element analysis. The parameters of the LTI model are estimated by applying numerical optimisation based on evolutionary algorithms.

5) Model-based control design is proposed by using the identified parametric model. A control strategy for attenuating the harmonic vibration components of the rotor rotation is proposed. The modelling and control design are verified against experiments. Flexural rotor vibration attenuation is demonstrated in a 30 kW two-pole cage induction motor with an extended rotor shaft. In particular, it is shown that the proposed approach enables stable operation at the critical speed of the machine.

1.4 Publications

Publication I

In this paper, the electromechanical interaction in electrical machines is considered. The main contribution of the paper is to extend the technique developed by Holopainen *et al.* [2] to cover 3-D structural mechanics finite-element method (FEM). The methodology provides means of studying 3-D rotor vibratory effects in electrical machines by a computationally efficient parametric model. The results provide a basic framework in which rotor vibration modes are coupled in modal superposition formalism to an electromagnetic system.

The methodology presented in this paper provides means of including the effect of the UMP on the analysis of electrical machine vibrations. The effect of electromechanical interaction on rotor-dynamics is demonstrated by two numerical examples. The results predict that the UMP may have an effect on the rotor bending modes. In particular, the effect of electromechanical damping due to rotor currents is included in the analysis.

The paper has been written by Antti Laiho. The distributed model was developed by Antti Laiho and Timo Holopainen. The co-author, Timo Holopainen, made a contribution through his expertise in analytical modelling of eccentric-rotor electrical machines. Furthermore, Timo Holopainen contributed to the writing with his understanding of the background of the electromechanical interaction in electrical machines. Paul Klinge contributed with comments on coupling and system order reduction of structural finite element models with gyroscopic elements. Professor Antero Arkkio contributed to the article by supervision and valuable comments and discussions.

Publication II

In this paper, the dynamics of the force actuator is considered by using a system simulator based on the time-discretised magnetic field FEA and structural

mechanics FEM. A detailed modelling of stator and rotor slotting as well as saturation of magnetic materials is included in the system simulator. The effect of various rotating magnetic fields in the air-gap on the force production of the actuator is examined.

The presented simulation results indicate that the actuator-rotor system is linear with respect to the input voltage of the control winding. However, the results show that the system is considerably non-linear with respect to the excitation force. A further observation is made that the static rotor eccentricity induces an oscillating UMP component at double supply frequency. The effect is not included in the eccentric-rotor model formulated within the LTI formalism. However, by linearity with respect to the input voltage, and by knowing the external disturbance force level, a conclusion is made that LTI formalism provides a good approximation of the actuator-rotor system dynamics.

An LTI model of the actuator-rotor system is then built. The LTI model covers the dominating dynamics of the eccentric-rotor cage induction machine equipped with a supplementary stator winding for lateral force generation. Such effects as high-order components of the air-gap flux density, unipolar flux, and saturation of magnetic materials are not included in the analytical model. The model is identified by using the black-box models against data from the system simulator. The validity of the identified LTI model is verified against finite element (FE) simulations.

This paper has been written by Antti Laiho. The eccentric-rotor LTI model of the actuator-rotor system was developed by Antti Laiho. Kari Tammi contributed through his expertise on active force production and vibration control. Andrej Burakov contributed through his expertise on analytical modelling of electromagnetic fields. He derived the first voltage-flux equations for the actuator-rotor system with centralised rotor. The eccentric-rotor model presented in the paper is based on his derivation. The original idea to examine the actuator-rotor system was by Professor Antero Arkkio. Furthermore, Professor Antero Arkkio made a contribution to the development of the finite element model used in the system simulator. Kai Zenger contributed to the article through his expertise in active control. Furthermore, he supervised the work and gave valuable comments.

Publication III

This paper presents modelling, simulation and control design for an eccentric-rotor cage induction machine equipped with a built-in force actuator. The working principle of the actuator is based on the self-bearing machine force actuator. A system simulator based on time-discretised finite-element magnetic field analysis is built. Here, the magnetic field analysis is coupled with the structural FEA in modal formalism. The methodology provides a system simulator which can be used in actuator design.

Furthermore, a low-order parametric model for the voltage-fed control winding

with eccentric rotor motion is built. The parameter estimation is carried out by applying numerical optimisation based on evolutionary algorithms and the system simulator. The dynamics of the actuator-rotor system are examined. The results indicate that the voltage-fed actuator brings out additional dynamics stemming from the resistor-inductor (RL) circuit of the control winding.

The active control of flexural rotor vibration is considered by using the built-in force actuator and a control algorithm specially developed for rotating machinery. A control strategy for attenuating the rotor vibration at dominating discrete frequencies is considered. In addition, a wide frequency-band compensator is applied in order to compensate the actuator-rotor dynamics close to the rotation frequency of the rotor.

This paper has been written by Antti Laiho. The parametric actuator-rotor model for rotor vibration control was developed by Antti Laiho. The co-author, Kari Tammi, proposed the convergent control algorithm and made a contribution to control design. Kai Zenger contributed through his expertise in control engineering with valuable suggestions and discussions. Professor Antero Arkkio supervised the work and made a contribution to the development of the finite element model used in the system simulator.

Publication IV

In this paper, the active rotor vibration control is experimentally demonstrated in a 30 kW two-pole cage induction motor equipped with a four-pole control winding. The identification of the actuator-rotor model developed in Publication II and Publication III is carried out. Hence, the model-based vibration control for the rotation-speed harmonics by using the technique developed in Publication III is applied.

The main contribution of the paper is to demonstrate the attenuation of harmonic vibration components of the rotor by using the self-bearing force actuator and synchronous response control (SRC) algorithm. The performance of control on the vibration in machine bearings, foundation and housing are considered, as well. The results show that the control scheme proves to be suitable for the attenuation of harmonic rotor-vibration components in a cage induction machine.

This paper has been written by Antti Laiho. The co-authors, Anssi Sinervo and Juha Orivuori, made a contribution in measurements, modal analysis and assembling the laboratory test set-up. Kari Tammi contributed to the article through his expertise in practical implementation of control algorithms for vibration attenuation in rotating machinery. He took part in constructing the measurement set-up for experiments. In addition, he contributed to the mechanical design of the machine used in the experiments. Professor Antero Arkkio designed the stator winding in the machine. Furthermore, he supervised the work and gave valuable comments. Kai Zenger contributed to the article with his expertise in control engineering. In addition, he gave valuable suggestions related to the

control design.

Publication V

This paper provides experimental vibration attenuation results for a cage induction machine by using the self-bearing force actuator. Special focus is on a simplified control algorithm in which the algorithm used in Publication IV is reduced to attenuate only the first dominating rotor speed harmonic. The analytical modelling is performed in the rotor coordinate system in complex formalism which enables a simplified control design by using SRC. Also, the identification of the actuator-rotor system is carried out for a single frequency (DC in a rotor coordinate system).

The results show that the simplified control scheme is efficient for vibration suppression in the case the rotor performs forward whirling. A drawback of the simplified control design is that the backward whirling of the rotor is not controlled. This may have a considerable influence on the control when the rotation speed nears the critical speed.

The paper has been written by Antti Laiho. The co-authors, Anssi Sinervo and Juha Orivuori, made a contribution in measurements, modal analysis and assembling the laboratory test set-up. Kari Tammi contributed to the article through his expertise in practical implementation of control algorithms for vibration attenuation in rotating machinery. Professor Antero Arkkio and Kai Zenger contributed to the article by supervising the work.

Contribution in publications

The contribution of the author and the co-authors is listed in Table (1).

Table 1: Contribution of the author and the co-authors in percentages in each publication. The details of the contribution are given in the text in Sec. 1.4.

publication	author	co-author 1	co-author 2	co-author 3	co-author 4	co-author 5
I	60	25	5	10		
II	55	10	15	10	10	
III	60	15	10	15		
IV	55	15	15	5	5	5
V	55	5	15	15	5	5

1.5 Structure of the work

This work consists of three major topics: (1) electromechanical modelling based on coupled rotor-dynamics and forces related to the asymmetric distribution of magnetic field in the air-gap, (2) modelling and analysis of the actuator-rotor system and (3) control of the flexural rotor vibration by using the force actuator. The work is divided into the following parts:

1) A literature survey on the issues related to the work is given in Sec. 2. In addition, some overview and background of the issues closely linked to the work are discussed.

2) The methods developed in the work are discussed in Sec. 3. The discussion is based on the author's publications listed in Sec. 1.4 and reprinted at the end of this thesis.

3) The results from the modelling, simulations and experiments are considered in Sec. 4. Most of the results are published in the publications listed in Sec. 1.4. However, some unpublished results of the recent work are presented, as well. In fact, in Sec. 4.2 results from the linear and non-linear FEM are compared giving more insight into the effects not covered by LTI models. Furthermore, the results related to the critical speed operation in Sec. 4.4 are not included in the publications.

4) The main results achieved in the work are discussed in Sec. 5. Moreover, the limitations of the approach and further research is considered.

5) Finally, the work is summarised and conclusions are made in Sec. 6.

2 Literature survey

The literature survey is divided into three main areas of research consisting of

1) electromechanical interaction in electrical machines based on unbalanced magnetic fields. The main focus is on the force exerted on the rotor due to the unbalanced flux-density distribution in the air-gap. The study is restricted to cage rotor machines,

2) working principle, modelling and rotor position control related to a built-in force actuator based on the working principle of the actuator used in self-bearing machines,

3) attenuation of flexural rotor vibration by using the built-in force actuator.

The electromechanical modelling and model-based control design of the actuator-rotor system naturally couples all these fields under a common framework.

This literature review focuses on analysis and control of flexural rotor vibration in electrical machines needed in model-based control. More thorough literature reviews of the electromechanical interaction and unbalanced magnetic pull in electrical machines were given by Tenhunen [3] and Burakov [4]. A detailed survey on coupled rotor-dynamics and electromechanical interaction was given by Holopainen [5] and Kalita [6]. A recent literature review on control methods applied in general rotating machinery was given by Tammi [7].

2.1 Electromechanical interaction

The working principle of an electrical machine is based on the rotating magnetic fields in the machine. The torque is generated by resulting tangential forces exerted on the rotor. Due to effects such as non-ideality of the air-gap geometry, rotor misalignment, stator or rotor slotting and saturation, additional forces induced by the unbalanced magnetic field distribution are acting between the stator and rotor of the machine. These forces are a source for the stator and rotor vibration which may cause noise and increased bearing wear.

This work is restricted to rotor vibration and hence to magnetic forces exerted on the rotor. However, the magnetic forces induced by the air-gap magnetic field act between the stator and rotor. In literature, the forces exerted on the stator have received more attention. This is most probably because the spatial force distribution along the air-gap periphery, even with a symmetric air-gap field distribution and concentric rotor, may excite the stator and induce problems with noise, for instance.

In an electrical machine, an asymmetric magnetic field distribution generates a net force on the rotor. The unbalanced magnetic field distribution may originate from stator or rotor non-ideal geometries [8], stator and rotor slotting [9],

saturation [10] or eccentric rotor motion [11], for instance. The effect of the UMP was observed already in the early 20th century by Rosenberg [12].

In the thesis, the studied sources for the UMP are restricted to (1) eccentric rotor motion and (2) additional magnetic field component induced by a supplementary winding placed among the torque-producing main winding. The eccentric rotor motion induces an asymmetric permeance distribution along the air-gap. Consequently, the originally symmetric field distribution becomes unbalanced. The effect of the UMP on vibration characteristics of an electrical machine is, in the first approximation, that the natural rotor bending frequencies are reduced due to the radial pull. The effect is referred to as negative spring effect. Particularly, the UMP affects those vibration modes which include relative motion between the stator and rotor.

In general, for large eccentricities, the UMP becomes a non-linear function of the rotor eccentricity. From a rotor-dynamic point of view, this leads to non-linear dynamical systems [13, 14]. However, it has been observed from measurements that the UMP is linear roughly up to 20 % eccentricity [15] which is, in practical applications, already an intolerably large value. Motivated by observation, the UMP is commonly assumed to be a linear function of rotor eccentricity. For small eccentricities, it is common practice in industry to model the effect of the UMP on vibration characteristics of an electrical machine by adding negative stiffnesses between the stator and rotor.

Frohne [16] considered cylindrical rotor whirling in an asynchronous machine. By using a sinusoidally distributed permeance along the rotor periphery with linear dependency on the rotor eccentricity, he concluded that the eccentric-rotor air-gap field can be approximated by the fundamental field with p pole pairs and with additional field components of $p \pm 1$ pole pairs (Fig. 1 and Fig. 2). In particular, in the stator coordinate system, the radial component of the air-gap flux-density is given by

$$\begin{aligned} B(t,\theta) &= \hat{B}_p \cos(\omega_s t + \varphi_p - p\theta) \\ &\quad + \hat{B}_{p-1} \cos((\omega_s - \omega_w)t + \varphi_p - \varphi_w - (p-1)\theta) \\ &\quad + \hat{B}_{p+1} \cos((\omega_s + \omega_w)t + \varphi_p + \varphi_w - (p+1)\theta) \end{aligned} \tag{1}$$

where t is time, θ is the angular position along the rotor periphery, p is number of pole pairs, $\hat{B}_p$ is the fundamental flux density, $\hat{B}_{p\pm1}$ are the eccentricity harmonic flux densities, ω_s is the supply angular frequency, ω_w is the angular frequency of rotor whirling, φ_p and φ_w are the initial phase angles of the fundamental field and rotor eccentricity, respectively.

Früchtenich *et al.* [17] studied eccentric rotor motion in an asynchronous machine equipped with a cage rotor. The induced rotor cage currents were included in the analysis, as well (Fig. 3). They concluded that the eccentric rotor motion induces rotor cage currents which have an effect on the UMP. In fact, the induced rotor cage currents generate magnetic flux components with $p \pm 1$ pole

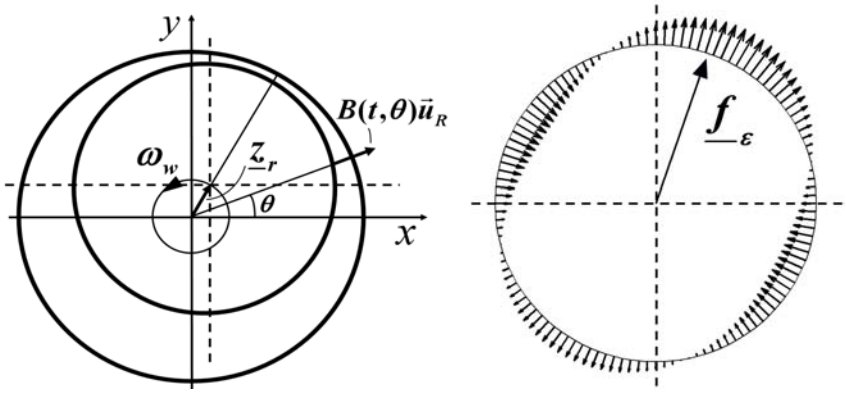

(a) (b)

Figure 1: Schematic picture of cylindrical rotor whirling and the radial magnetic flux density distribution in the air-gap: (a) cylindrical rotor whirling on the transversal plane perpendicular to the rotor axis and (b) the unbalanced magnetic flux density distribution in the air-gap due to the eccentric rotor motion in a four-pole machine with the net force $\underline{f}_\epsilon$ exerted on the rotor.

pairs which, in general, oppose the asymmetric air-gap field and hence make the air-gap field more symmetric. The rotor cage currents not only have an effect on the radial magnetic pull ($\underline{f}_{\epsilon,R}$ in Fig. 3), but also induce a tangential UMP component ($\underline{f}_{\epsilon,T}$ in Fig. 3). In conclusion, the circulating $p \pm 1$ currents in the rotor cage reduce the radial UMP and generate a tangential UMP component. Furthermore, it was deduced that at rotor whirling frequencies

$$\omega_w = \frac{1 - s(1 \pm p)}{p} \omega_s, \tag{2}$$

the $p \pm 1$ harmonic rotor current becomes zero. In Eq. (2), the slip s is given by $s = (\omega_s - p\omega_m)/\omega_s$ where ω_m is the angular frequency of rotor rotation. Hence, approximately at the whirling frequencies given by Eq. (2), there is a local maximum in the radial UMP. Furthermore, Früchtenich *et al.* [17] coupled the model for the UMP to a mechanical rotor model leading to a system of second-order ordinary differential equations (ODEs).

Arkkio *et al.* [18] presented a frequency-domain model for the UMP by using a transfer function

$$\underline{f}_\epsilon(s) = \underline{K}(s)\underline{z}_r(s) \tag{3}$$

where $\underline{f}_\epsilon$ is the force (UMP) exerted on the rotor, s denotes the Laplace variable and $\underline{z}_r$ is the rotor displacement in the stator reference frame. In Eq. (3), the Laplace variable s is reduced to $s = j\omega_w$ in whirling rotor motion with angular

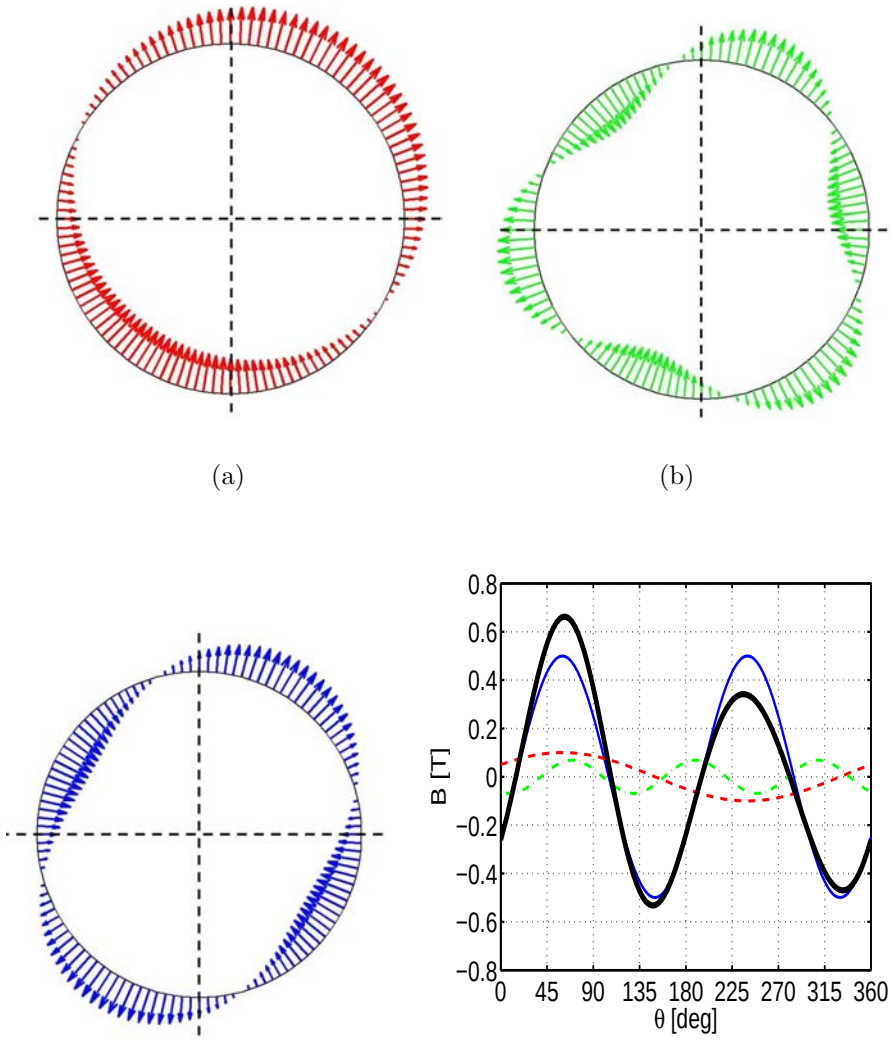

Figure 2: Radial air-gap flux density distribution in a four-pole machine with additional two-pole and six-pole field components induced by the eccentric rotor motion: (a) two-pole eccentricity field, (b) six-pole eccentricity field, (c) main four-pole field and (d) fields along the air-gap periphery; resultant asymmetric field from Fig. 1(b) (thick solid line), four-pole field (thin solid line), two-pole field (dashed line) and six-pole field (dash-dotted line).

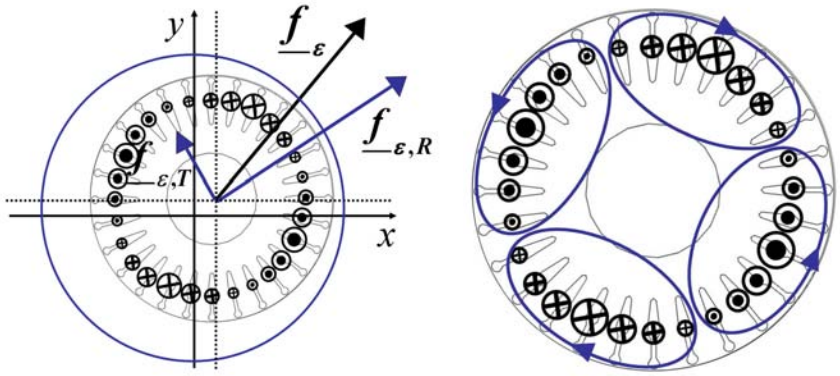

(a) (b)

Figure 3: Unbalanced magnetic pull exerted on the eccentric rotor. (a) force exerted on the rotor and (b) four-pole magnetic field lines and cage currents in the rotor bars induced by eccentric rotor motion in a two-pole cage induction machine. The notation $\odot$ means that a current is flowing in the $+z$ direction while $\otimes$ means that it is flowing in the $-z$ direction.

frequency ω_w. In [18], the transfer function $\underline{K} = \underline{K}(s)$ was given by

$$\underline{K}(s) = \left[k_0 + \frac{k_{p-1}}{s - z_{p-1}} + \frac{k_{p+1}}{s - z_{p+1}} \right] \tag{4}$$

where k_0 is the spring constant due to the radial UMP, $k_{p\pm1}$ are parameters depending on the the fundamental flux and $z_{p\pm1}$ denote the system poles in the complex plane. In their analysis, Arkkio *et al.* [18] considered cylindrical rotor whirling in cage induction machine. In cylindrical whirling, the rotor centre line is aligned with the stator bore. The rotor centre follows a circular path and the air-gap is axially uniform. In [18], the UMP was simulated by time-discretised FEA of the magnetic fields in a 2-D machine cross-section. Furthermore, they verified the simulation results against measurements carried out for a 15 kW four-pole cage induction machine equipped with magnetic bearings which were used to measure the force (UMP) exerted on the rotor [19]. Furthermore, a low-order parametric model

$$\underline{\dot{q}}_{p-1} = z_{p-1}\underline{q}_{p-1} + k_{p-1}\underline{z}_r \tag{5}$$

$$\underline{\dot{q}}_{p+1} = z_{p+1}\underline{q}_{p+1} + k_{p+1}\underline{z}_r \tag{6}$$

$$\underline{f}_{\epsilon} = k_0\underline{z}_r + \underline{q}_{p-1} + \underline{q}_{p+1} \tag{7}$$

for the UMP was introduced. In comparison with the time-discretised FEM, the analytical model given by Eqs. (5) – (7) provides a computationally considerably more efficient means of studying the UMP. The fact that the model was

formulated for a general cylindrical rotor motion makes the formalism particularly useful. By fitting the transfer function given by Eq. (4) to results from the time-stepping FEA carried out for several whirling frequencies, Arkkio *et al.* [18] estimated the parameters in Eq. (4). Hence, the time-domain system given by Eqs. (5) – (7) was readily applicable to transient analysis. By applying the Laplace transform, the ODE system given by Eqs. (5) – (7) leads to the transfer function given by Eq. (4). However, the physical meaning of the force variables $\underline{q}_{p\pm1}$ is hidden.

The effect of the UMP on rotor-dynamics of the cage induction machine under arbitrary eccentric rotor motion was considered by Holopainen [5]. Holopainen *et al.* [2] derived a model for the UMP in which the rotor is subjected to arbitrary eccentric rotor motion. In the model the rotor is assumed to be parallel to the stator so that the air-gap is uniform along the rotor shaft but the rotor centre displacement in a 2-D machine cross-section is treated as a degree of freedom. The model is in parametric form based on physical quantities. As well, the rotor-cage $p \pm 1$ currents were included in the model. In [2], the space-vectors for the $p \pm 1$ radial air-gap flux-density were given by

$$\underline{\hat{B}}_{p-1} = \frac{1}{2\delta_0}\underline{\hat{B}}_p \underline{z}_r^* + \frac{\mu_0}{\delta_0} k_{r,p-1} \underline{\hat{i}}_{r,p-1} \tag{8}$$

$$\underline{\hat{B}}_{p+1} = \frac{1}{2\delta_0}\underline{\hat{B}}_p \underline{z}_r + \frac{\mu_0}{\delta_0} k_{r,p+1} \underline{\hat{i}}_{r,p+1} \tag{9}$$

where $\underline{\hat{B}}_p$ is the space-vector of the fundamental flux density, $\underline{\hat{i}}_{r,p\pm1}$ are the space-vectors of harmonics $p\pm1$ of the rotor cage current, δ_0 is the (effective) radial air-gap length, μ_0 is air-gap permeability and $k_{r,p\pm1}$ are real-valued coupling factors related to rotor design and saturation.

From the Maxwell stress tensor, by using the radial component of the flux density [20], the eccentricity force exerted on the rotor is given by

$$\underline{f}_\epsilon = \frac{\pi d_r l_r}{4\mu_0}\left[\underline{\hat{B}}_{p-1}^* \underline{\hat{B}}_p + \underline{\hat{B}}_p^* \underline{\hat{B}}_{p+1}\right] \tag{10}$$

where d_r is diameter of the rotor core and l_r is axial length of the rotor core. Eq. (10) yields, by using Eqs. (8) and (9),

$$\underline{f}_\epsilon = \frac{\pi d_r l_r}{4\mu_0\delta_0}\left[|\underline{\hat{B}}_p|^2 \underline{z}_r + \mu_0 k_{r,p-1} \underline{\hat{B}}_p \underline{\hat{i}}_{r,p-1}^* + \mu_0 k_{r,p+1} \underline{\hat{B}}_p^* \underline{\hat{i}}_{r,p+1}\right]. \tag{11}$$

By using Eqs. (8) and (9) and the analysis of rotor-cage currents based on discrete Fourier transformation (DFT) [2, 21], the $p \pm 1$ flux linkages of the rotor cage are given by

$$\underline{\hat{\psi}}_{r,p-1} = L_{r,p-1} \underline{\hat{i}}_{r,p-1} + X_{r,\epsilon,p-1} \underline{\hat{B}}_p \underline{z}_r^* \tag{12}$$

$$\underline{\hat{\psi}}_{r,p+1} = L_{r,p+1} \underline{\hat{i}}_{r,p+1} + X_{r,\epsilon,p+1} \underline{\hat{B}}_p \underline{z}_r \tag{13}$$

where $L_{r,p\pm1}$ are rotor cage inductances of harmonics $p\pm1$ and $X_{r,\epsilon,p\pm1}$ are eccentricity coupling factors of rotor cage harmonics $p\pm1$. The voltage-flux equations in stator reference frame are given by [22]

$$0 = R_{r,p\pm1}\hat{\underline{i}}_{r,p\pm1} + \frac{\mathrm{d}\hat{\underline{\psi}}_{r,p\pm1}}{\mathrm{d}t} - j(p\pm1)\omega_m\hat{\underline{\psi}}_{r,p\pm1} \tag{14}$$

where $R_{r,p\pm1}$ are the rotor cage resistances of harmonics $p\pm1$. By substituting Eqs. (12) and (13) to Eq. (14), the equations for the cage current harmonics $p\pm1$ are given by

$$\begin{aligned} 0 &= \frac{\mathrm{d}\hat{\underline{i}}_{r,p-1}}{\mathrm{d}t} + \left[\frac{R_{r,p-1}}{L_{r,p-1}} - j(p-1)\omega_m\right]\hat{\underline{i}}_{r,p-1} \\ &\quad + \frac{X_{r,\epsilon,p-1}}{L_{r,p-1}}\left[\frac{\mathrm{d}}{\mathrm{d}t}(\hat{\underline{B}}_p\underline{z}_r^*) - j(p-1)\omega_m\hat{\underline{B}}_p\underline{z}_r^*\right] \qquad (15) \\ 0 &= \frac{\mathrm{d}\hat{\underline{i}}_{r,p+1}}{\mathrm{d}t} + \left[\frac{R_{r,p+1}}{L_{r,p+1}} - j(p+1)\omega_m\right]\hat{\underline{i}}_{r,p+1} \\ &\quad + \frac{X_{r,\epsilon,p+1}}{L_{r,p+1}}\left[\frac{\mathrm{d}}{\mathrm{d}t}(\hat{\underline{B}}_p\underline{z}_r) - j(p+1)\omega_m\hat{\underline{B}}_p\underline{z}_r\right]. \qquad (16) \end{aligned}$$

The cage current dynamics given by Eqs. (15) and (16) describes the cage current $p\pm1$ components induced by eccentric rotor motion. In the case of rotor whirling under constant operational conditions, it holds

$$\begin{aligned} \underline{z}_r(t) &= \underline{z}_0 e^{j\varphi_w(t)} \qquad (17) \\ \hat{\underline{B}}_p(t) &= \underline{B}_p e^{j\varphi_s(t)} \qquad (18) \end{aligned}$$

where $\underline{z}_0$ and $\underline{B}_p$ are complex constants, $\dot{\varphi}_w = \omega_w$ and $\dot{\varphi}_s = \omega_s$. By substituting Eqs. (17) and (18) to Eqs. (15) and (16), the criteria given by Eq. (2) are obtained. Furthermore, by using Eqs. (15) and (16), the substitution of Eqs. (17) and (18) to Eq. (11) leads to

$$\begin{aligned} \underline{f}_\epsilon(t) &= \frac{\pi d_r l_r}{4\mu_0\delta_0}\left[|\underline{B}_p|^2 - \mu_0 k_{r,p-1}\frac{jX_{r,\epsilon,p-1}(\omega_w-\omega_{p-1})|\underline{B}_p|^2}{R_{r,p-1}+jL_{r,p-1}(\omega_w-\omega_{p-1})}\right. \\ &\quad \left. - \mu_0 k_{r,p+1}\frac{jX_{r,\epsilon,p+1}(\omega_w+\omega_{p+1})|\underline{B}_p|^2}{R_{r,p+1}+jL_{r,p+1}(\omega_w+\omega_{p+1})}\right]\underline{z}_0 e^{j\varphi_w(t)} \qquad (19) \end{aligned}$$

where $\omega_{p\pm1} = \omega_s - (p\pm1)\omega_m$. The transfer function in Eq. (19) is of the same form with Eq. (4). Furthermore, $\omega_w = \mp\omega_{p\pm1}$ in Eq. (19) corresponds to the frequencies in Eq. (2).

The constant-flux assumption in Eq. (18) results in time-varying coefficients in the force given by Eq. (11). In order to extract the time-dependent coefficients, Holopainen [5] used the cage-current variables

$$\begin{aligned} \underline{g}_{p-1} &= \hat{\underline{i}}^*_{r,p-1}e^{j\varphi_s} \qquad (20) \\ \underline{g}_{p+1} &= \hat{\underline{i}}_{r,p+1}e^{-j\varphi_s}. \qquad (21) \end{aligned}$$

As a result a model for the UMP, analogous to the parametric model in Eqs. (5) – (7), is obtained. The main development is that the parameters and variables of the model have a clear physical meaning. In the model, the force exerted on the rotor by the UMP is given by

$$\underline{f}_{\epsilon} = k_0 \underline{z}_r + c_{p-1}\underline{g}_{p-1} + c_{p+1}\underline{g}_{p+1} \tag{22}$$

where

$$k_0 = \frac{\pi d_r l_r |\underline{B}_p|^2}{4\mu_0\delta_0},\ c_{p-1} = \frac{\pi d_r l_r k_{r,p-1}\underline{B}_p}{4\delta_0},\ c_{p+1} = \frac{\pi d_r l_r k_{r,p+1}\underline{B}_p^*}{4\delta_0}. \tag{23}$$

In the case of a two-pole machine, the component $p-1=0$ referring to unipolar flux is neglected and k_0 is divided by 2. In Fig. 3(b), the four-pole rotor cage current distribution is schematically depicted in a two-pole cage induction machine rotor with 28 rotor bars.

In Eq. (22), the parameter k_0 stands for a negative spring constant which corresponds to the magnetic pull in the direction of the shortest air-gap. The parameters $c_{p\pm1}$ are in general complex-valued and the cage current variables $\underline{g}_{p\pm1}$ not only contribute to the radial UMP but are responsible for the tangential UMP component, and hence, electromechanical damping and stability issues [23]. In [5], the cage current dynamics is given by

$$\dot{\underline{g}}_{p-1} + (\tau_{p-1}^{-1} - j\omega_{p-1})\underline{g}_{p-1} + b_{p-1}\dot{\underline{z}}_r - jb_{p-1}\omega_{p-1}\underline{z}_r = 0 \tag{24}$$

$$\dot{\underline{g}}_{p+1} + (\tau_{p+1}^{-1} + j\omega_{p+1})\underline{g}_{p+1} + b_{p+1}\dot{\underline{z}}_r + jb_{p+1}\omega_{p+1}\underline{z}_r = 0 \tag{25}$$

where $\tau_{p\pm1} = L_{r,p\pm1}/R_{r,p\pm1}$, $b_{p-1} = \underline{B}_p^* X_{r,\epsilon,p-1}/L_{r,p-1}$ and $b_{p+1} = \underline{B}_p X_{r,\epsilon,p+1}/L_{r,p+1}$.

In addition to the circulating cage currents, parallel paths in the stator winding affect considerably the UMP [11,18,24]. This is because the eccentricity fluxes with $p \pm 1$ pole pairs induce circulating currents in the stator winding making the air-gap field more symmetric, and thus, reducing the UMP. Furthermore, the above analysis was carried out for a general machine with $2p$ poles. However, a two-pole machine ($p = 1$) is a special case in which the unipolar (homopolar) flux $p - 1 = 0$ may generate forces on the rotor [25, 26]. In this work, the unipolar flux is neglected.

In addition to the analytical formulations, the UMP has been analysed numerically by FEM. Presently, a transient 3-D FEA of an eccentric-rotor electrical machine is not available within reasonable computation time. Hence, a 2-D FEM is used. The effect of end-windings was taken into account by including end-winding impedances in the circuit equations [27, 28].

Earlier, a 3-D extension of a 2-D electromagnetic FEM of an electrical machine was developed by Tenhunen [3]. In the model, 2-D FEM slices perpendicular to the rotor are applied. The separate slices are connected by continuity conditions. However, as was pointed out by Tenhunen *et al.* [29], the computational effort grows almost linearly with the number of 2-D slices included. Hence, the number of slices is strongly restricted by the computational time.

2.2 Self-bearing force actuator

2.2.1 Overview

As was already discussed in Sec. 2.1, in an electrical machine, an asymmetric field distribution in the air-gap generates a net force on the rotor. The mechanism provides a means of an active generation of force on the rotor, provided that the asymmetry of the field distribution can be controlled (Fig. 4). The force actuation based on unbalanced field distribution around the rotor is industrialised in active magnetic bearing (AMB) technology [30, 31]. The AMBs offer some advantages compared to the traditional sliding- or rolling-element bearings. Indeed, AMB provides non-contact action, no lubrication needed, longer life-cycle, controlled bearing force, active rotor vibration control, built-in tools for diagnostics, high-speed and high-temperature operation. In high-speed applications, the AMBs are generally used and the related technology has achieved a mature state. As a disadvantage, AMB needs a power input and sophisticated means of active control. So far, AMB technology has not made a breakthrough in large applications.

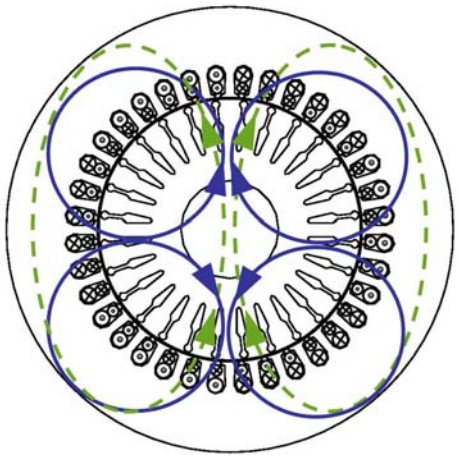

Figure 4: Magnetic field distribution in a two-pole machine equipped with four-pole supplementary winding for force generation. The four-pole field induces an asymmetry in the two-pole field distribution so that a net force is exerted on the rotor. In the figure, the flux density is enhanced on the upper part of the air-gap and, consequently, an upward force is generated.

In the late 1980s and beginning of the 1990s, a new bearingless (self-bearing) concept was introduced in AC machinery [32–38]. In a self-bearing machine, the rotor position is controlled by unbalancing the magnetic flux density distribution in the air-gap. Since the torque-producing flux density of an electrical machine is typically of the order 0.5–1.0 T, only a small unbalance of this field generates a large net force on the rotor. This can be seen from Eq. (10), where the $2p$ pole field is distorted by eccentricity fields with $p \pm 1$ pole pairs.

A self-bearing machine can be understood as a hybrid design consisting of an integrated AMB and electrical machine. The working principle is analogous to AMBs but there are some fundamental differences. In self-bearing technology, less iron is needed to produce the demanded force since the main torque-producing winding affects the generated force, as well. Furthermore, no additional axial space is needed due to the built-in nature of the concept. This is an advantage since a longer rotor shaft may induce rotor vibrations. On the other hand, in a self-bearing actuator, additional dynamics are involved because the force production is coupled to the machine operation. This can be regarded as a disadvantage of the concept. Moreover, additional losses may be induced in the rotor and stator.

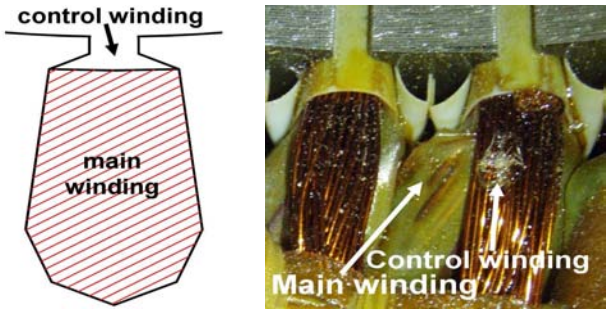

(a) (b)

Figure 5: The supplementary winding (control winding) design in the machine stator. The supplementary winding is distributed to the stator slots in the wedge area and occupies about 10 % of the total cross-sectional area of a single slot. The picture (b) is taken from the set-up used in Publication IV and Publication V in which a 30 kW two-pole induction motor was equipped with a supplementary four-pole winding.

The following literature survey is restricted to the force-actuation methodology of induction-type self-bearing machines. However, other machine types such as the switched reluctance and permanent magnet (PM) bearingless machines are within the bearingless concept as well [39]. The bearingless drive concept has been applied and industrialised in many, mostly low-power, applications such as blood pumps.

In the literature, two design principles for the stator of the bearingless induction machine are presented:

1) The stator winding is composed of two separate (three-phase) windings distributed to the stator slots. One is for the torque-production and occupies roughly 90% of the slot cross-sectional area. The other, referred to as "supplementary winding", is used for producing a transversal force on the rotor (Fig. 5). The concept was introduced by Chiba *et al.* [35].

2) A single winding is used both for producing torque and transversal force. The design was introduced by Salazar *et al.* [33, 36]. In this design, the individual stator winding phases are divided and supplied so that both rotation and rotor positioning are provided. Another single-winding design was proposed by Khoo *et al.* [40,41]. In the design, the stator phases are divided in parallel paths. Hence, the paths are connected by bridges equipped with power supplies to generate currents which produce an unbalanced field distribution in the air-gap.

In addition to the active control of rotor position or vibration, both of these winding structures can be used for passive reduction of UMP [6,42]. This work is restricted to the design principle in which two stator windings are used [35]. In a $2p$ pole machine, the supplementary winding is distributed in the stator slots so that it produces an air-gap field with $p-1$ or $p+1$ pole pairs. Hence, the originally symmetric $2p$ pole torque-producing field is unbalanced and a net force is exerted on the rotor. A typical induction machine design is a two-pole supplementary winding in a four-pole machine or a four-pole supplementary winding in a two-pole machine [39].

From a practical point of view, the manufacturers of electrical machines are familiar with installing two separate windings in stator slots, for instance, when producing double-speed induction motors. However, the produced torque is reduced when using the separate-winding design. Indeed, the current density in a stator slot is restricted by resistive heating. If 10% of the slot area is occupied by the supplementary winding, the current in the torque-producing winding has to be reduced by 10%. The generated torque is proportional to the air-gap flux-density and the rotor current. Since the current density – and hence the air-gap flux density – remains the same, the torque is reduced by 10%. This can be regarded as a disadvantage of the concept. On the other hand, the dimensions for the supplementary winding have to be carefully designed in terms of the demanded maximum value of the lateral force.

2.2.2 Working principle and analytical modelling

The following discussion is restricted to bearingless cage induction machines which are equipped with individual stator winding sets for torque and lateral force production. The commonly-used and highly industrialised cage-rotor design is challenging for self-bearing force actuation. This is due to the rotor-cage currents which are induced by the currents of the supplementary winding. The cage currents induce additional dynamics to the actuator-rotor system. Indeed, the cage currents affect the unbalanced field distribution having an effect on the generated force. Consequently, the actuator force becomes more difficult to orientate.

From the beginning of the 1990s, force-actuation methodology of the self-bearing machine has been modelled both analytically and numerically. The con-

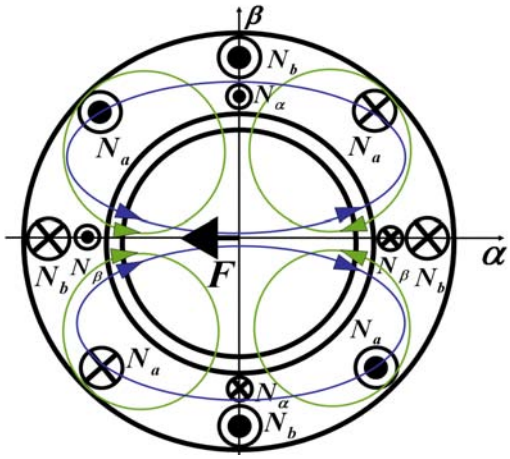

Figure 6: Force-actuation methodology for a four-pole (N_a, N_b) machine with a two-pole (N_α, N_β) supplementary winding. The construction was introduced by Chiba *et al.* [35].

cept of a bearingless induction motor, to the best knowledge of the author, was introduced for the first time by Salazar *et al.* [33] and Chiba *et al.* [35]. Chiba *et al.* [35] considered a four-pole bearingless cage induction machine equipped with a two-pole winding for generation of lateral force on the rotor. The motor cross-section with equivalent two-phase winding schema is shown in Fig. 6. In their work, Chiba *et al.* deduced that the control force $F = (F_\alpha, F_\beta)^T$ exerted on the rotor is given by

$$\begin{pmatrix} F_\alpha \\ F_\beta \end{pmatrix} = MI \begin{bmatrix} -\cos(2\omega t) & \sin(2\omega t) \\ \sin(2\omega t) & \cos(2\omega t) \end{bmatrix} \begin{pmatrix} i_\alpha \\ i_\beta \end{pmatrix}. \tag{26}$$

In Eq. (26), M is the spatial derivative of mutual inductance between the two- and four-pole windings in terms of the virtual work when rotor is displaced from the stator bore centre. Furthermore, i_α and i_β denote the currents supplied to the two-pole supplementary winding. The currents supplied to the four-pole main winding are given by

$$i_a = I\cos(2\omega t) \tag{27}$$
$$i_b = I\sin(2\omega t) \tag{28}$$

where I is the peak value of the current and 2ω the supply frequency of the four-pole winding. In Fig. 6, the flux-density field lines are illustrated for the case $i_b = 0 = i_\beta$. In this case, the two-pole supplementary winding increases the air-gap flux density on the left-hand side (arrows in same direction) and decreases on the right-hand side (arrows in opposite direction). Consequently, the force is directed to $-\alpha$ direction. As was noted in [35], Eq. (26) predicts that the actuator force is modulated by the four-pole main-winding currents. Secondly,

the generated force is proportional to the supplementary winding currents. In the literature, the studied bearingless induction machine design is in most cases a four-pole machine with two-pole supplementary winding or vice-versa. A study on bearingless induction machines with different numbers of poles was carried out by Okada *et al.* [43].

In [35], a feedback control system was constructed for rotor positioning. Indeed, the analytical expression given by Eq. (26) was used to calculate the current commands of the supplementary winding from the force demand (F_α^*, F_β^*). The force demand was obtained from a proportional-integral-derivative (PID) controller which used the rotor centre position measured by air-gap sensors.

Chiba *et al.* [44] deduced analytically the actuator force by assuming sinusoidal MMF distributions and cylindrical rotor and stator (no slotting effects). The parameter M in Eq. (26) yielded

$$M = \frac{\mu_0 \pi l R N_2 N_4}{8 g_0^2} \tag{29}$$

in which l is the axial length of the rotor, R is radius of the rotor, g_0 is radial air-gap length, and N_2 and N_4 are the number of turns in the two-pole and four-pole winding, respectively.

In [45], the influence of the induced rotor-cage currents in a bearingless induction motor was considered. The analysis was carried out for a four-pole motor with a supplementary two-pole winding. It was indicated that there is no mutual coupling between the two- and four-pole windings provided that the rotor is concentric with the stator bore (zero eccentricity). However, as was pointed out by Chiba *et al.*, currents in the supplementary two-pole winding induce circulating currents in the rotor cage which affect the generated actuator force on the rotor. Indeed, the equalising rotor-cage currents reduce the asymmetry of the air-gap flux-density distribution and, consequently, reduce the generated radial force. In [45], an equivalent circuit was built for frequency-domain analysis of circuits consisting of rotor cage, main four-pole winding and the supplementary two-pole winding.

Nomura *et al.* [46] considered a phase delay in the generation of the actuator force in a bearingless cage induction machine. In their work, a four-pole motor with a two-pole supplementary winding design was considered. The phase delay stems from the equalising currents induced in the rotor cage. Furthermore, it was concluded that the phase delay in force generation may result in a decrease of phase margin in the feed-back control loop of the rotor position and, consequently, result in an instability. In [46], a phase lead-lag compensator was proposed in order to enhance the rotor position control in a feedback schema used in [35].

A different approach to handle the effect of circulating rotor-cage currents was proposed by Chiba *et al.* [47]. In their approach, a pole-specific rotor design was proposed. In the design, for a four-pole bearingless machine, the rotor cage is constructed from four-pole circuits which are isolated from each other. In this

construction, the currents in the supplementary two-pole winding do not induce currents in the rotor cage and, hence, the force-current relationship in Eq. (26) holds. Especially, the force is directly generated by the supplementary winding currents without phase delay. In comparison with the commonly-used cage rotor design, the proposed construction demands a more ponderous manufacturing process. From an industrial point of view, this can be regarded as a disadvantage of the construction.

In the analysis of the self-bearing force actuation, for simplicity, it is a common practice to neglect the effect of the rotor eccentricity in the force generation. The assumption can be justified by the fact that given the rotor position control is successful, the UMP induced by eccentric rotor motion becomes zero. In the derivation of the actuator force, the principle of virtual work has been commonly used. Hence, the force is obtained as spatial derivatives of the co-energy functional. The spatial dependence of the co-energy functional stems from the mutual inductances between the main and supplementary windings which depend linearly on the rotor eccentricity. As a result, a force independent from the eccentricity is obtained. The spatially-dependent inductances were directly applied in the development of a sensorless (self-sensing) bearingless induction motor [48, 49].

In general, in addition to the mechanical excitation forces, the bearingless machine force actuator has to compensate the UMP exerted on the rotor in the case of eccentric rotor motion. The need for compensating the UMP was brought out by Nomura *et al.* [46]. However, their analysis was concentrated on the effect of equalising currents in the rotor cage induced by the currents of the supplementary winding. To the author's best knowledge, Baoguo *et al.* [50] were the first to include the effect of the eccentric rotor in the analytical model of a bearingless induction motor. They pointed out the necessity of an enhanced modelling of the actuator force by including the UMP induced by eccentric rotor motion. It was emphasised that, in an actual motor, a rotor eccentricity is always present due to variation of machine load or the actuator force. In [50], for a four-pole induction motor with a two-pole supplementary winding, the analytical expression for the resultant force exerted on the rotor due to currents in the supplementary winding and the eccentric rotor was given by

$$F_x = \frac{\pi r l}{2\mu_0}\left[B_2 B_4 \cos(\varphi_4 - \varphi_2) + \epsilon B_4^2 \cos\alpha\right] \tag{30}$$

$$F_y = \frac{\pi r l}{2\mu_0}\left[B_2 B_4 \sin(\varphi_4 - \varphi_2) + \epsilon B_4^2 \sin\alpha\right] \tag{31}$$

where r is the radius of the rotor, l is length of the rotor stack, μ_0 is air-gap permeability and ϵ is rotor eccentricity. Furthermore, B_2 and B_4 denote the peak values of the two- and four-pole air-gap flux-densities, respectively, φ_2 and φ_4 are the initial phase angles of the two- and four-pole MMFs, respectively, and α is the direction of the minimum air-gap.

Yikang *et al.* formulated an analogous model to the one presented by Baoguo

et al. [50]. In the model, the analytical expressions were formulated for the actuator force in case of an eccentric rotor. Furthermore, the model was formulated in terms of the air-gap fluxes. Later, Zhang *et al.* [51] introduced an analytical model for rotor position control in a self-bearing induction machine. In the model, the radial UMP component was included into the model. In addition, they considered the equations of motion for the rotor system in the form

$$F_{dx} + F_{sx} - F_x = m\ddot{x} \tag{32}$$

$$F_{dy} + F_{sy} - F_y = m\ddot{y} \tag{33}$$

where F_{dx} and F_{dy}, F_{sx} and F_{sy}, F_x and F_y denote the disturbance, the UMP induced by eccentric rotor motion, and actuator forces in x- and y- directions, respectively. Furthermore, m denotes the rotor mass.

Cai *et al.* [52] derived an analytical model of radial actuator force in a bearingless four-pole wound-rotor induction motor with a two-pole supplementary winding. In their model, the exerted force on the rotor was calculated from the principle of virtual work. As a result, the force exerted on the rotor was given in terms of the rotor eccentricity and supplementary winding currents. Particularly, they concluded that, by including non-linear terms in the eccentric-rotor air-gap permeance distribution, an oscillating UMP component at double supply frequency appears. This agrees with the results obtained by Guo *et al.* [53]. However, the currents of the two-pole supplementary winding were not induced in the four-pole wound-rotor considered by Cai *et al.* [52]. Hence, naturally the equalising rotor currents were not considered. The pole-specific cage rotor [47] has a similar effect on the induced rotor cage currents as the wound-rotor design.

In addition to controlling the rotor position, the self-bearing force actuation technology can be utilised for rotor vibration suppression in a machine with conventional bearings. The force actuation methodology was proposed for vibration control in rotating machinery by Watanabe [54]. Active vibration control by using self-bearing generator was examined by Khoo *et al.* [55]. More recently, the self-bearing actuator was applied to vibration attenuation and critical speed operation by Chiba *et al.* [42]. When the synchronous forward whirling dominates the rotor vibration, the force demand is rotating synchronously with the rotor. This is an advantage since the induced rotor-cage currents are small.

In the analysis of the self-bearing cage induction machine, there is a need for further development. So far, only few authors have considered analytically the effect of the eccentric rotor motion in the actuator force. Furthermore, in the models including the UMP, only the radial UMP component has been studied. However, as it was discussed in Sec. 2.1, the tangential component of the UMP may have a significant effect on the dynamics and stability of the system. In fact, not only the supplementary winding produces oscillating currents in the rotor cage. As was surveyed in Sec. 2.1, the eccentric rotor induces currents in the rotor cage, as well. So far, the rotor-cage currents induced by the eccentric rotor

motion have not been included in any analytical model of a force actuator in a bearingless induction machine.

The torque-producing stator winding, the supplementary winding for force generation, the eccentric cage rotor and the mechanical rotor system is a coupled electromechanical system. In the literature, the following electromechanical effects are not included in analytical studies:

1) the rotor-cage currents induced by eccentric rotor motion,

2) the coupled electromechanical system consisting of actuator-rotor dynamics and rotor-dynamics of the rotor.

2.2.3 Numerical modelling

In the literature, there are only few studies in which numerical methods (most often FEM) are applied to analyse the force actuator of a bearingless induction machine. In particular, the number of studies including eccentric rotor motion is limited. To reduce the computational work, the assumption of axial symmetry is commonly used. In the case of an eccentric rotor, due to lack of symmetry, the whole 2-D machine cross-section has to be included.

Chiba *et al.* [56] examined the effect of magnetic saturation on the force actuator in an induction-type bearingless motor by using FEM. Cai *et al.* [57] investigated the force production mechanism in a bearingless wound-rotor induction motor by using a 2-D time-discretised FEM. They considered a design consisting of a four-pole torque-producing winding, a two-pole supplementary winding and a wound four-pole rotor. For comparison, a squirrel-cage rotor design was studied as well. It was concluded that, in comparison to the squirrel-cage rotor design, a much larger actuator force is generated on the rotor in the wound-rotor design.

Baoguo *et al.* [50] modelled both analytically and numerically by FEM the bearingless induction motor with rotor eccentricity. They estimated the parameters of the analytical model by FEM. The FEA was carried out for static rotor eccentricity. A different approach was introduced in [58]. A dynamic reluctance mesh was used for simulations of a four-pole self-bearing induction machine with a two-pole supplementary winding. A self-bearing design with a single-winding construction was studied by using FEM by Ferreira *et al.* [59] and Khoo *et al.* [40,60].

So far, numerical analysis of the self-bearing induction machines has been restricted to the force generated on the rotor. The electromechanical actuator-rotor coupling has been left without further analysis. However, the rotor-dynamics may couple with the generated force, depending on the rotor eccentricity, which results in a coupled electromechanical system. The time-discretised 2-D FEM provides a reliable tool for analysing coupled electromechanical systems [61, 62].

2.3 Control design and built-in force actuator

The control design associated with the position control of the self-bearing induction machine is, in almost all studies, restricted to conventional PID controllers. Recently, however, Kauss *et al.* [63] obtained promising results in applying a controller based on linear quadratic regulator (LQR) in a vertical-rotor bearingless induction machine. The force actuator mechanism of a bearingless induction machine, especially, with a squirrel-cage rotor design, brings out challenges for the rotor position controller [45, 46, 64]. As was discussed in Sec. 2.2.1, the AMB is a technology analogous to self-bearing machines. In AMBs, in addition to PIDs, various controllers have been studied [31]. Especially, control issues related to the suppression of harmonic vibration components have gained special attention. Compensation of periodic disturbances has also been applied in a bearingless slice motor [65].

In any rotating machinery, typically, the main sources for rotor vibration are the unbalanced mass harmonics [66, 67]. In electrical machines, additional harmonic forces are induced from the rotating electromagnetic fields in the machine air-gap. Hence, the rotor vibration in electrical machines is typically dominated by a small number of vibration components related to the rotation speed and the various rotating magnetic fields in the air-gap.

Burrows *et al.* [68] introduced a control method for the compensation of harmonic disturbance forces exerted on a rotor. In their work, analytical derivations and a simulated example was given. Furthermore, they proposed that AMB can be used in a practical implementation of the control method presented. In an electrical machine, due to a small air-gap between the rotor and stator, the force actuation on the rotor centre is problematic. However, the built-in force actuator used in a self-bearing machine provides a means of force generation at the mid-span between the bearings.

Later, Burrows *et al.* [69], used an extended version of the algorithm [68] for the control of synchronous rotor vibration in a flexible rotor. In [69], the vibration attenuation was demonstrated by using an experimental rig consisting of a flexible rotor supported by journal bearings. A single AMB unit was used for the force actuation. Burrows *et al.* concluded that a single AMB unit can be used both for the system identification and actuation of control force.

Narrow frequency-band controllers that are compensating discrete dominating harmonics of the disturbance force were proposed by various authors [70–76]. These algorithms are referred to as the mass unbalance compensation algorithms, or SRC algorithms [77]. The SRC algorithms have previously been used for rotor-bearing systems, AMBs and helicopter rotors, for instance.

Knospe *et al.* [73] developed an SRC algorithm referred to as "Convergent Control" (CC). The CC algorithm was systematically compared with other flexural rotor vibration suppression algorithms [7]. Motivated by the results, the CC algorithm was chosen for this work. The robustness issues of the CC algo-

rithm were considered by Knospe *et al.* [78]. In the following, the CC algorithm equipped with instantaneous coefficient update [79] is surveyed. The analysis is based on the results described by [7, 75, 80].

An excitation force composed of integral multiples of rotor rotation frequency and exerted on the rotor is given by

$$f_{ex}(t) = \mathrm{Re}\left\{\sum_{k=0}^{N_f} \hat{f}_{ex}^{k} e^{j\varphi_k(t)}\right\} \tag{34}$$

where $\varphi_k(t)$ denotes the phase of the excitation force harmonic k with $\dot{\varphi}_k = \omega_k = k\omega_m$ and the coefficients $\hat{f}_k$ are given by

$$\hat{f}_{ex}^{k} = f^k \begin{pmatrix} 1 \\ -j \end{pmatrix} \tag{35}$$

with f^k denoting the amplitude of the harmonic excitation force.

Assuming a linear system, the rotor response to the excitation is given by

$$u_{rc}(t) = \mathrm{Re}\left(\sum_{k=0}^{N_f} \hat{u}_{rc}^{k} e^{j\varphi_k(t)}\right) \tag{36}$$

where the Fourier coefficient of the rotor displacement $\hat{u}_{rc}$ at angular frequency ω_k is given by

$$\hat{u}_{rc}^{k} = \mathcal{H}(j\omega_k)\hat{v}_c^k + \mathcal{H}_{ex}(j\omega_k)\hat{f}_{ex}^{k} = \mathcal{H}(j\omega_k)\hat{v}_c^k + \hat{d}^k$$

where $\mathcal{H}$ and $\mathcal{H}_{ex}$ are the frequency-response matrices of the system in the LTI formalism [81], $\hat{v}_c^k$ is the control input voltage Fourier coefficient at frequency ω_k and $\hat{d}^k$ is the corresponding Fourier coefficient of the disturbance. The CC algorithm [82] minimises the output displacement Fourier coefficients $\hat{u}_{rc}^k$ at frequency ω_k. Indeed, the aim of the control is to minimise the square norm of the measured rotor displacement given by

$$\|\hat{u}_{rc}^{k}\|_2 = \|\mathcal{H}(j\omega_k)\hat{v}_c^k + \hat{d}^k\|_2. \tag{37}$$

In the CC algorithm, the minimisation is carried out by a law analogous to the gradient method which gives the Fourier coefficients $\hat{v}$ of the control input in discrete-time by

$$\hat{v}_c^k(n) = \gamma_k \hat{v}_c^k(n-1) - \alpha_k \mathcal{A}_k \hat{u}_{rc}^{k}(n) \tag{38}$$

where $0 < \gamma_k \leq 1$, $\alpha_k > 0$ are the parameters related to the convergence of the algorithm and n refers to time-instant $t_n = nT_s$ with T_s denoting the sample time. In Eq. (38), the matrix $\mathcal{A}_k$ is given by

$$\mathcal{A}_k = \mathcal{H}(j\omega_k)^{\dagger} \tag{39}$$

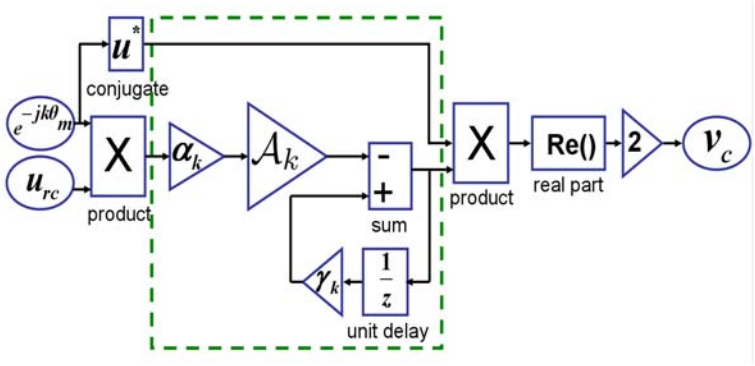

Figure 7: The CC algorithm and instantaneous coefficient update for the attenuation of a single excitation force harmonic k. In the figure, the unit delay operator is given by $z^{-1}\hat{v}_c^k(n) = \hat{v}_c^k(n-1)$.

where † denotes the pseudo-inverse operator which is needed when the (rotor) displacement is measured at multiple points. Effectively, the aim of the recursive law given by Eq. (38) is to adapt the control force to compensate the disturbance force on a specific frequency.

In Fig. 7, the CC algorithm is schematically depicted. For the Fourier coefficient calculation, instantaneous coefficient update [7, 75, 79] was applied. Indeed, the instantaneous Fourier coefficient update and the resulting control input are given by

$$\hat{u}_{rc}^k(n) = u_{rc}(n)e^{-jk\theta_m(n)} \tag{40}$$

$$v_c(n) = 2\mathrm{Re}\left[\sum_{k=0}^{N_f} \hat{v}_c^k(n)e^{jk\theta_m(n)}\right]. \tag{41}$$

A discrete-time equivalent feedback compensator can be built for the CC algorithm [7]. Hence, the CC controller leads to an LTI system in discrete-time.

The instantaneous coefficient update given by Eqs. (40) and (41) has been used in practical applications [79]. The mass unbalance compensation algorithms have been under active research since 1980s [68]. This is because unbalanced mass excitation is the primary source of flexural rotor vibration in most rotating machine applications [66]. In AMBs, however, modern control theory including H_∞ -control and other techniques based on μ -synthesis have been applied, as well [31].

3 Methods of analysis

3.1 Electromechanical modelling

As discussed in Sec. 2.1, 3-D electromechanical modelling of electrical machines demands a considerable amount of computational effort. A full-scale 3-D transient electromechanical analysis of an electrical machine is a challenge even for present personal computers (PCs). For this reason, 2-D models are commonly used for electromechanical analysis. In 2-D models, the assumption of axial isotropy (uniform air-gap in the axial direction) is used. End windings can approximately be included in a 2-D model [28]. However, 3-D effects such as conical rotor motion (non-uniform air-gap) and skewed stator slots or rotor bars need an enhanced model. A model consisting of 2-D FEM slices perpendicular to the rotor axis was presented by Tenhunen [83]. Another technique in which the extension in the axial direction is accomplished analytically is considered in the following.

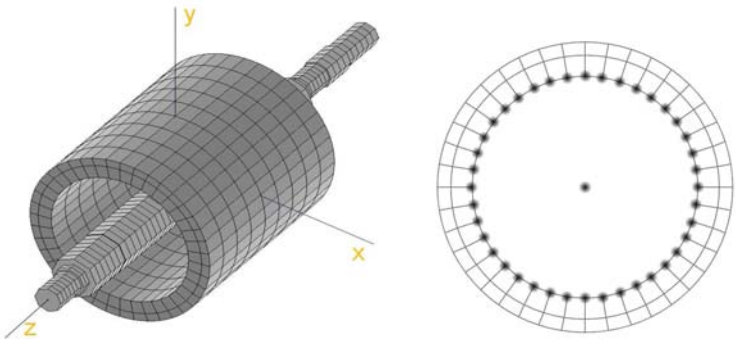

(a) Stator core and rotor FE models.

(b) Stator inner core nodes of a slice with rotor node in the middle.

Figure 8: Slicing the structural mechanics FE models of the stator and rotor. The stator deformation is implemented by averaging the deformations of the stator inner core nodes by Eq. (42).

The electromechanical model developed by Holopainen [5] was extended in the structural modal analysis framework. The method developed in Publication I offers a technique for coupling the parametric electromechanical model of an eccentric-rotor cage induction machine to a structural mechanics FE model of the machine. The coupling is performed in modal form which enables an efficient system order reduction by modal synthesis. The electromechanical model is based on modelling the $p \pm 1$ eccentricity harmonics of the magnetic flux in the machine air-gap. The forces exerted on the rotor due to the stator or rotor non-ideal

shapes, slotting harmonics, saturation of magnetic materials or unipolar flux (two-pole machines) were neglected.

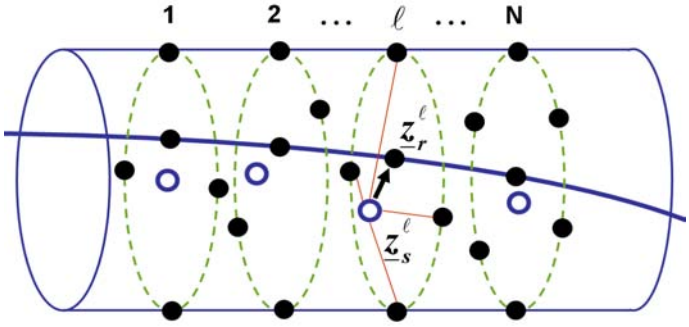

Figure 9: Distributed model and averaging process. The rotor centre line inside the stator core.

In Fig. 8(a), a 3-D structural FE mesh of the stator with the rotor modelled as a beam is shown. The structural FE model is sliced axially. As a result, slices with a single rotor beam node and multiple stator core nodes shown in Fig. 8(b) are obtained. Let the number of slices be N with a number of N_ℓ ($\ell = 1, \ldots, N$) stator core nodes included in each slice (Fig. 9). Hence, the averaged stator deformation in complex plane for slice ℓ is given by

$$\underline{z}_s^\ell = \frac{1}{N_\ell} \sum_{\sigma=1}^{N_\ell} \left\{ u_x(n_\sigma^\ell) + j u_y(n_\sigma^\ell) \right\} \tag{42}$$

where $u_x(n_\sigma^\ell)$ and $u_y(n_\sigma^\ell)$ are the x- and y- displacement degrees of freedom (DOFs) of the stator inner core node n_σ^ℓ, respectively.

By applying Eq. (22), the force exerted on the rotor is obtained. Indeed, by slicing in z direction and including the averaged stator degrees of freedom given by Eq. (42), the transversal electromagnetic force exerted on the rotor node of slice ℓ is given by

$$\underline{f}_\epsilon^\ell = \frac{1}{N} \left[k_0(\underline{z}_r^\ell - \underline{z}_s^\ell) + c_{p-1}\underline{g}_{p-1} + c_{p+1}\underline{g}_{p+1} \right]. \tag{43}$$

By averaging $\underline{z}_r^\ell - \underline{z}_s^\ell$ in z direction over the stator bore, the dynamical equations for the cage current variables given by Eqs. (24) and (25) are obtained as

$$\dot{\underline{g}}_{p-1} + (\tau_{p-1}^{-1} - j\omega_{p-1})\underline{g}_{p-1} + \frac{b_{p-1}}{N} \sum_{\ell=1}^{N} (\dot{\underline{z}}_r^\ell - \dot{\underline{z}}_s^\ell) - \frac{j b_{p-1} \omega_{p-1}}{N} \sum_{\ell=1}^{N} (\underline{z}_r^\ell - \underline{z}_s^\ell) = 0 \tag{44}$$

$$\dot{\underline{g}}_{p+1} + (\tau_{p+1}^{-1} + j\omega_{p+1})\underline{g}_{p+1} + \frac{b_{p+1}}{N} \sum_{\ell=1}^{N} (\dot{\underline{z}}_r^\ell - \dot{\underline{z}}_s^\ell) + \frac{j b_{p+1} \omega_{p+1}}{N} \sum_{\ell=1}^{N} (\underline{z}_r^\ell - \underline{z}_s^\ell) = 0. \tag{45}$$

It can be seen from Eqs. (44) and (45) that the model predicts zero rotor-cage currents when the rotor performs conical rigid body movement (conical whirling). This agrees with the results obtained by Tenhunen *et al.* [83] by using a more detailed multi-slice FEA. When the equalising rotor-cage currents become zero, it can be seen from Eq. (43) that, under conical rotor whirling, the amplitude of the force is independent from the whirling frequency. This agrees with the FE results [83], as well. However, Tenhunen *et al.* [83] found from the measurements that the moment produced by the UMP on conical rotor motion varies with whirling frequency. They suggested that the variation stems from the inter-bar rotor-cage currents [84]. The inter-bar currents are not included in the electromechanical model presented in this work. The averaging method presented here works best for rotor bending modes which in most cases dominate within the low-frequency domain.

The structural mechanics of the machine is governed by

$$M\ddot{u} + (C + G)\dot{u} + Ku = f \tag{46}$$

where u denotes the DOF vector and M, C and K denote the mass, damping and stiffness matrices, respectively [67]. The gyroscopic matrix $G = G(\omega_m)$ depends on the rotation speed. In Publication I, gyroscopic disks [85] were used to model the gyroscopic effect. The excitation forces are collected in f.

The electromechanical system modelled by Eq. (43) and Eqs. (44) and (45) is written in the real-entry matrix form before coupling it with the mechanical model given by Eq. (46). As a result, in Publication I, a model for the coupled electromechanical system of the cage induction machine is given in the form

$$\ddot{\eta} + (2\Omega\Xi + \Phi^T G\Phi)\dot{\eta} + (\Omega^2 - \Phi^T K_0\Phi)\eta - \Phi^T Q g = \Phi^T f \tag{47}$$

$$\dot{g} + K_c\Phi\eta + B\Phi\dot{\eta} + Ag = 0. \tag{48}$$

In Eq. (47), modal superposition $u = \Phi\eta$ with η denoting the modal coordinate vector was applied [86]. The mass-normalised modal matrix $\Phi = (\phi^{(1)}, \ldots, \phi^{(n)})$ is built from the n lowest mechanical vibration modes and the diagonal matrix Ω is composed of the mechanical eigenfrequencies. Furthermore, the scaling relations are given by

$$\Phi^T M\Phi = I \tag{49}$$

$$\Phi^T K\Phi = \Omega^2 \tag{50}$$

$$\Phi^T C\Phi = 2\Omega\Xi \tag{51}$$

where the entries of Ξ include the damping ratios of mechanical vibration modes which can be obtained from the modal testing of the machine. In Eqs. (47) and (48), the real-entry matrices K_0, Q, K_c, B and A are composed of the electromechanical parameters from Eq. (43) and Eqs. (44) and (45). Furthermore, the state vector g consists of real and imaginary parts of the cage current variables $\underline{g}_{p\pm1}$ in Eqs. (44) and (45).

The coupled electromechanical model given by Eqs. (47) and (48) couples the rotor and stator deformations with the electromechanical system characterized by the UMP and the rotor-cage currents induced by the distortion of the air-gap. The effect of electromechanical interaction on the vibration modes was numerically studied in Publication I.

3.2 Built-in force actuator

The model for an eccentric-rotor cage induction machine equipped with a built-in force actuator was developed in space-vector formalism in Publication II and Publication III. The model for the eccentric-rotor cage induction machine developed by Holopainen [2] was coupled with the voltage-flux equations written for the control winding. The model for an eccentric-rotor cage induction machine [2] was adopted because the model was developed in parametric form for an arbitrary rotor eccentricity. This enables system identification by using impulse or noise excitation. In addition, the parametric model leads to a formulation in a standard LTI form which enables the use of various tools of control engineering developed for the LTI systems.

The parametric model was developed in the stator coordinate system with the origin fixed to the centre of the stator bore (Fig. 11). Hence, the model was coupled to the mechanical model by the technique developed in Publication I. In this work, a voltage-driven control winding is considered. This differs from the commonly-used current-driven system [39]. A voltage-driven system inherently includes passive means of rotor vibration attenuation when the control winding is not excited (short-circuited control winding) [42, 87]. A disadvantage of the voltage-driven system is the more complex dynamics. This is due to the RL circuit of the control winding which has to be taken into account in the modelling.

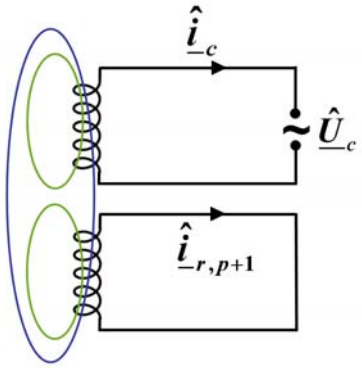

Figure 10: The control winding and the rotor cage are magnetically coupled.

As a result, a system model is obtained in a standard LTI form in Publication II and Publication III. The model enables control design by using the well established theory of control engineering [81]. The main assumptions of the analytical model are the following:

1) direct coupling between the control winding and the main stator winding is negligible,

2) magnetic fields are studied in a transversal 2-D machine cross-section where the control force is applied. The tangential component of the magnetic field is neglected,

3) saturation of the magnetic materials is neglected; the voltage and flux equations are linearised at an operation point,

4) higher spatial harmonic field components are neglected,

5) there are no parallel branches in the stator winding,

6) unipolar flux is neglected.

The condition that the torque-producing main winding is not directly magnetically coupled with the control winding can be achieved by a proper geometrical design of the control winding. The rotor cage, however, couples these two windings through eccentric rotor motion (Fig. 10). This phenomenon is included in the model. The 3-D effects such as skewed rotor bars are not included in the model. However, some 3-D effects can be included by adopting the distributed model for UMP presented in Publication I. In most analytical studies of UMP, the tangential component of the magnetic flux density is assumed to be negligible. Indeed, based on the measurements, Binns *et al.* [20] concluded that the tangential component of the flux density can be neglected when considering UMP. In the numerical FEA study presented in Publication II, the tangential component of the fundamental flux was 5.0% of the radial component (1.0% slip).

The saturation of magnetic materials has a reducing effect on both UMP [10] and the actuated control force [39]. In the design of an electrical machine, an aim is to minimize the higher harmonic field components in the air-gap in order to avoid problems of noise and vibration. The higher air-gap harmonics may interact with the rotor eccentricity and produce a net force on the rotor. Typically, stator and rotor slot harmonics are the dominating higher harmonics in the air-gap. As a first approximation, the UMP induced by the stator and rotor slot harmonics can be regarded as independent of the whirling frequency of the rotor [2, 9, 88]. This implies that, as a first approximation, the effect of the slot harmonics on UMP can be included in the negative stiffness (k_0 in Eq. (22)).

Parallel branches in the stator winding induce additional dynamics to the actuator-rotor system. The eccentric rotor motion induces equalising currents in the parallel branches which reduce UMP. In addition, parallel branches may induce anisotropy to an eccentric-rotor machine [89]. The circulating currents induced in the parallel paths affect the actuator force, as well. In general, the actuator force is decreased due to the circulating currents which make the flux distribution more symmetric. Most importantly, the control winding and main

torque-producing winding become magnetically coupled through parallel paths in the stator winding. A more detailed analytical model is needed in order to include the effect of parallel branches in the stator winding. The unipolar flux may induce vibration especially in two-pole machines [26, 90].

The control winding is magnetically linked to the rotor cage (Fig. 10). In order to obtain a model of the actuator-rotor system, voltage-flux equations of the control winding are coupled with the voltage-flux equations of the rotor cage given by Eq. (14). The voltage-flux equations for a $2p$ pole cage induction machine equipped with a $2(p+1)$ pole control winding are written in the stator coordinate system by

$$\hat{\underline{u}}_c = R_c \hat{\underline{i}}_c + \frac{\mathrm{d}\hat{\underline{\psi}}_{c,p+1}}{\mathrm{d}t} \tag{52}$$

$$0 = R_{r,p+1} \hat{\underline{i}}_{r,p+1} + \frac{\mathrm{d}\hat{\underline{\psi}}_{r,p+1}}{\mathrm{d}t} - j(p+1)\omega_m \hat{\underline{\psi}}_{r,p+1} \tag{53}$$

$$0 = R_{r,p-1} \hat{\underline{i}}_{r,p-1} + \frac{\mathrm{d}\hat{\underline{\psi}}_{r,p-1}}{\mathrm{d}t} - j(p-1)\omega_m \hat{\underline{\psi}}_{r,p-1} \tag{54}$$

where $\hat{\underline{u}}_c$ is the voltage supplied to the control winding, $\hat{\underline{i}}_c$ is the current in the control winding, $\hat{\underline{i}}_{r,p\pm1}$ are the cage current harmonics $p \pm 1$, R_c is the control winding resistance, $R_{r,p\pm1}$ are the rotor-cage resistances for the $p \pm 1$ cage current harmonics. Furthermore, $\hat{\underline{\psi}}_{c,p+1}$ denotes the space-vector of the $p+1$ harmonic flux through the control winding and $\hat{\underline{\psi}}_{r,p\pm1}$ denote the space-vectors of the $p \pm 1$ harmonic fluxes through the rotor cage.

The magnetic flux linkages of the control winding and rotor cage are given by

$$\hat{\underline{\psi}}_{c,p+1} = L_c \hat{\underline{i}}_c + M_{r,c,p+1} \hat{\underline{i}}_{r,p+1} + X_{c,\epsilon,p+1} \hat{\underline{B}}_p \hat{\underline{z}}_r \tag{55}$$

$$\hat{\underline{\psi}}_{r,p+1} = L_{r,p+1} \hat{\underline{i}}_{r,p+1} + M_{r,c,p+1} \hat{\underline{i}}_c + X_{r,\epsilon,p+1} \hat{\underline{B}}_p \hat{\underline{z}}_r \tag{56}$$

$$\hat{\underline{\psi}}_{r,p-1} = L_{r,p-1} \hat{\underline{i}}_{r,p-1} + X_{r,\epsilon,p-1} \hat{\underline{B}}_p \hat{\underline{z}}_r^* \tag{57}$$

where L_c is the control winding inductance, $M_{r,c,p+1}$ is the mutual inductance between the control winding and rotor cage for the $p+1$ magnetic flux harmonic, $X_{c,\epsilon,p+1}$ is coefficient related to $p+1$ flux harmonic induced by the eccentric rotor motion and coupled with the control winding, $L_{r,p\pm1}$ are the inductances of the rotor cage for $p \pm 1$ cage-current harmonics and $X_{r,\epsilon,p\pm1}$ are the coefficients related to $p \pm 1$ harmonic fluxes through the rotor cage induced by eccentric rotor motion [2].

The force exerted on the rotor due to the asymmetric air-gap field is calculated by using the Maxwell stress tensor. In Publication II and Publication III, the force

$\underline{f}_c$ exerted on the rotor was given by

$$\begin{aligned}\underline{f}_c &= \frac{\pi d_r l_r}{4\mu_0\delta_0}\left[\left(1-\frac{1}{2}\delta_{p,1}\right)|\underline{\hat{B}}_p|^2\underline{z}_r + \mu_0 k_{r,p-1}\underline{\hat{B}}_p\underline{\hat{i}}^*_{r,p-1} + \mu_0 k_{r,p+1}\underline{\hat{B}}^*_p\underline{\hat{i}}_{r,p+1}\right. \\ &+ \left.\mu_0 k_{c,p+1}\underline{\hat{B}}^*_p\underline{\hat{i}}_{c,p+1}\right] \qquad (58)\end{aligned}$$

where $\mu_0 = 4\pi\cdot 10^{-7}$ N/A^2 is the permeability of free space, and d_r, l_r and δ_0 denote the rotor-core diameter, rotor-core length and radial air-gap length, respectively. In Eq. (58), $\underline{\hat{B}}_p$ denotes the space-vector of the fundamental component of the magnetic flux density induced in the air-gap by the torque-producing main stator winding. Furthermore, "$*$" denotes complex conjugation and δ is Kronecker delta which here argues that for a two-pole machine ($p = 1$) the coefficient of $|\underline{\hat{B}}_p|^2\underline{z}_r$ is divided by 2. The coupling factors $k_{r,p\pm1}$ and $k_{c,p+1}$ give the MMF spatial harmonics in the air-gap produced by the currents $\underline{\hat{i}}_{r,p\pm1}$ and $\underline{\hat{i}}_{c,p+1}$, respectively.

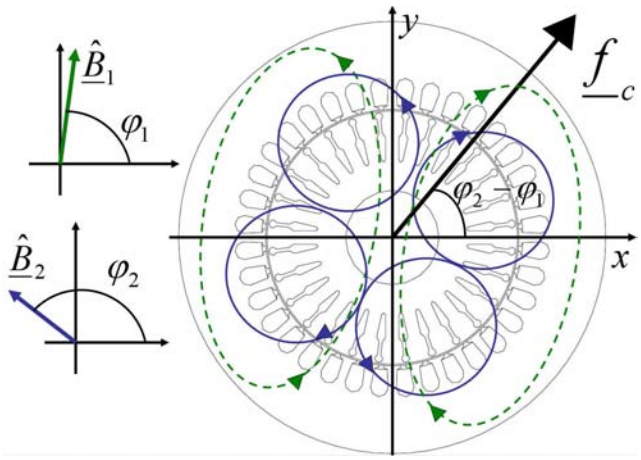

Figure 11: Force exerted on the rotor as an effect of the two-pole (dashed line) and the four-pole (solid line) fields.

In this thesis, the machine is assumed to be in a steady-state operation condition. Thus, the machine is assumed to operate at constant-flux operation conditions given by

$$\underline{\hat{B}}_p(t) = \underline{B}_p e^{j\varphi_s(t)} \qquad (59)$$

where $\underline{B}_p$ is a complex constant and $\dot{\varphi}_s = \omega_s$ in which ω_s denotes the supply frequency (rad/s) of the main winding. Substitution of Eq. (59) in Eq. (58) shows that a control winding current of frequency ω_c results in a rotating force at angular frequency $\omega_c - \omega_1$. In Fig. 11, the generation of a rotating force is schematically depicted for a two-pole machine with a four-pole supplementary winding. In Publication II and Publication III, a modulation of the control winding voltage supply and the rotor-cage and control-winding currents was used in

order to transform the actuator-rotor system to a standard LTI system in which an excitation at a specific frequency results in a response at the same frequency. The model developed in Publication II and Publication III is given by

$$\begin{aligned}
\underline{\hat{u}}_{c,0} &= (R_c + j\omega_s L_c)\underline{\hat{i}}_{c,0} + L_c\frac{\mathrm{d}\underline{\hat{i}}_{c,0}}{\mathrm{d}t} + M_{r,c,p+1}\frac{\mathrm{d}\underline{\hat{i}}_{r,p+1,0}}{\mathrm{d}t} + j\omega_s M_{r,c,p+1}\underline{\hat{i}}_{r,p+1,0} \\
&\quad + X_{c,\epsilon,p+1}\underline{B}_p(j\omega_s\underline{z}_r + \dot{\underline{z}}_r) \qquad (60)\\
0 &= (R_{r,p+1} + j\omega_{p+1}L_{r,p+1})\underline{\hat{i}}_{r,p+1,0} + L_{r,p+1}\frac{\mathrm{d}\underline{\hat{i}}_{r,p+1,0}}{\mathrm{d}t} + M_{r,c,p+1}\frac{\mathrm{d}\underline{\hat{i}}_{c,0}}{\mathrm{d}t} \\
&\quad + j\omega_{p+1}M_{r,c,p+1}\underline{\hat{i}}_{c,0} + X_{r,\epsilon,p+1}\underline{B}_p(j\omega_{p+1}\underline{z}_r + \dot{\underline{z}}_r) \qquad (61)\\
0 &= (R_{r,p-1} + j\omega_{p-1}L_{r,p-1})\underline{\hat{i}}_{r,p-1,0} + L_{r,p-1}\frac{\mathrm{d}\underline{\hat{i}}_{r,p-1,0}}{\mathrm{d}t} \\
&\quad + X_{r,\epsilon,p-1}\underline{B}_p(j\omega_{p-1}\underline{z}_r^* + \dot{\underline{z}}_r^*) \qquad (62)\\
\underline{f}_c &= \frac{\pi d_r l_r}{4\mu_0\delta_0}\left[\left(1 - \frac{1}{2}\delta_{p,1}\right)|\underline{B}_p|^2\underline{z}_r + \mu_0 k_{r,p-1}\underline{B}_p\underline{\hat{i}}^*_{r,p-1,0} + \mu_0 k_{r,p+1}\underline{B}^*_p\underline{\hat{i}}_{r,p+1,0}\right. \\
&+ \left.\mu_0 k_{c,p+1,0}\underline{B}^*_p\underline{\hat{i}}_{c,0}\right] \qquad (63)
\end{aligned}$$

where

$$\omega_{p\pm1} = \omega_s - (p \pm 1)\omega_m. \qquad (64)$$

Furthermore, modulation of the supply voltage and currents given by

$$\begin{aligned}
\underline{\hat{u}}_c &= \underline{\hat{u}}_{c,0}e^{j\varphi_s} \qquad (65)\\
\underline{\hat{i}}_c &= \underline{\hat{i}}_{c,0}e^{j\varphi_s} \qquad (66)\\
\underline{\hat{i}}_{r,p\pm1} &= \underline{\hat{i}}_{r,p\pm1,0}e^{j\varphi_s} \qquad (67)
\end{aligned}$$

was applied. The phase angle of the main field $\varphi_s = \varphi_s(t)$ can be measured with a coil installed in the stator slots, or, obtained from the frequency converter. The modulation transforms the system to an LTI system with time-invariant coefficients.

In Publication I, a method for coupling the electromechanical model of an eccentric-rotor cage induction machine to a structural mechanical model in modal form was presented. In Publication II and Publication III, the technique was used in coupling the actuator-rotor model to the mechanical rotor model. As a result, an actuator-rotor model in a standard LTI formalism with real-entry matrices was introduced. The model is given by

$$\begin{aligned}
\dot{q} &= Aq + Bv + Gf_{ex} \qquad (68)\\
u_{rc} &= Cq \qquad (69)
\end{aligned}$$

where

$$A = \left[\begin{array}{c|c|c} -2\Omega\Xi & \Phi_{rc}^T P_{em}\Phi_{rc} - \Omega^2 & \Phi_{rc}^T C_{em} \\ \hline I & 0 & 0 \\ \hline S_{em}\Phi_{rc} & Q_{em}\Phi_{rc} & A_{em} \end{array}\right], \tag{70}$$

$$B = \begin{bmatrix} 0 \\ 0 \\ B_{em} \end{bmatrix}, G = \begin{bmatrix} \Phi_{rc}^T \\ 0 \\ 0 \end{bmatrix}, C = \begin{bmatrix} 0 & \Phi_{rc} & 0 \end{bmatrix}, q = \begin{pmatrix} \dot{\eta} \\ \eta \\ i \end{pmatrix}. \tag{71}$$

In order to obtain Eqs. (68) and (69), modal superposition [86] was used with a modal matrix Φ_{rc}, Ω denoting the diagonal matrix containing the eigenfrequencies and Ξ the damping ratios. Furthermore, u_{rc} denotes the rotor centre displacement and η the modal coordinates. The entries of the matrices A_{em}, P_{em}, C_{em}, S_{em}, Q_{em} include the resistances, inductances and other electromechanical parameters from Eqs. (60) – (63). The state vector q is composed of the modal velocities $\dot{\eta}$, the modal coordinates η and the control winding and rotor cage currents collected in the vector $i = (\mathrm{Re}(\underline{i}), \mathrm{Im}(\underline{i}))^T$ where $\underline{i} = (\hat{\underline{i}}_{c,0}, \hat{\underline{i}}^*_{r,p-1,0}, \hat{\underline{i}}_{r,p+1,0})^T$. The control winding supply is given by $v = (\mathrm{Re}(\hat{\underline{u}}_{c,0}), \mathrm{Im}(\hat{\underline{u}}_{c,0}))^T$.

The model given by Eqs. (68) and (69) is an LTI model with $2n + 6$ states ($2n+4$ for a two-pole machine) where n denotes the number of modes included in the modal superposition. In this thesis, the focus is on the rotor bending modes which typically describe the low-frequency vibratory behaviour of a rotor. The model is analogous with the actuator-rotor LTI model developed for the AMBs by Maslen *et al.* [91].

3.3 Simulations and finite element modelling

In Publication II and Publication III, a virtual plant or system simulator for the actuator-rotor system was built. The simulator is based on the 2-D time-stepping FEA of the magnetic fields on the machine cross-section under rotor rotation and eccentric rotor motion [28]. A typical FE mesh on the machine cross-section is shown in Fig. 12. Non-linear magnetic materials were used in the simulations in order to examine the influence of saturation of the magnetic materials on the actuator force. Furthermore, a detailed stator slot meshing was used in order to bring out the effect of the higher air-gap field harmonics. The currents induced in the rotor cage were included in FEA. The end rings were modelled by using circuit equations. The field-circuit FEA was encoded into a SIMULINK block [61] and connected to the LTI block of the mechanical rotor model.

The block diagram of the actuator-rotor system is shown in Fig. 13. In the figure, the system is disturbed by an excitation force f_{ex} typically dominated by rotating components at frequencies of integer multiples of rotor rotation frequency [66]. Another source for the excitation is the UMP. The control force f_c given

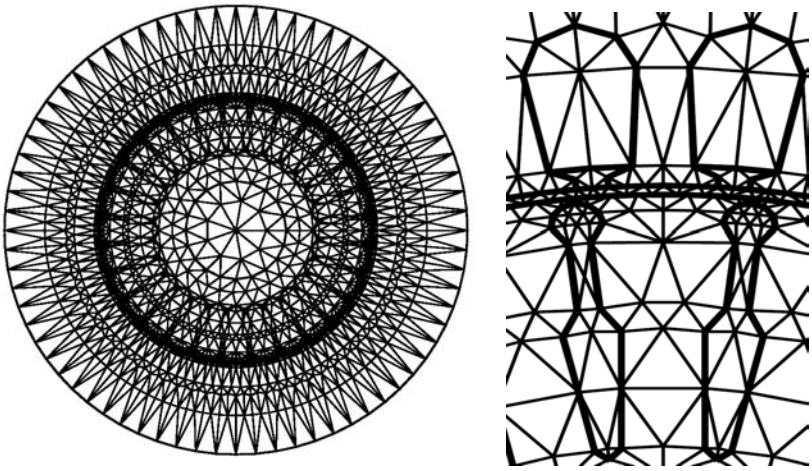

(a) (b)

Figure 12: The FEM mesh for a two-pole cage induction machine used in the simulations: (a) mesh consists of 4400 linear triangular elements with 2765 nodes, (b) section of the mesh showing air-gap region with stator and rotor slots.

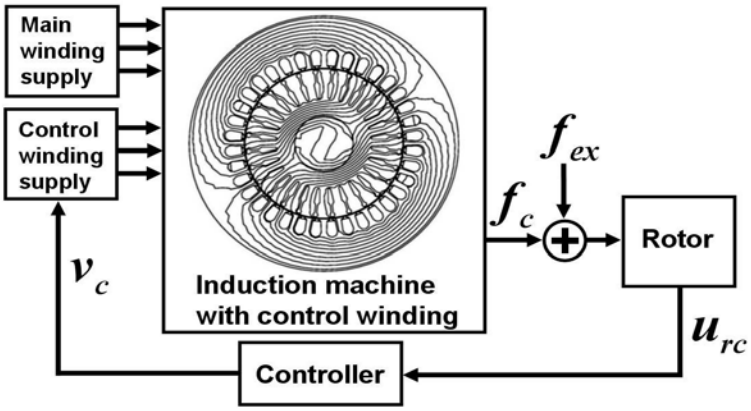

Figure 13: A schematic view of the induction machine with a control-winding construction acting as a built-in force actuator.

by the actuator and disturbance force f_{ex} are exerted to the machine rotor which results in the rotor centre displacement u_{rc}. The rotor vibration controller takes the rotor displacement as an input and gives the control winding voltage as an output which is fed to the control winding terminals.

3.4 System identification

In 1983, in the early years of AMB technology, Burrows *et al.* [68] proposed that, in a set-up with conventional bearings, an AMB unit located in the middle of the bearing span would provide potential for system identification. In electrical machines, an actuator installation problem arises due to the small air-gap between the stator and rotor. However, the actuator principle in a self-bearing machine concept enables force generation on the rotor in the middle of the bearing-span.

The main objective of the identification in this work is to provide a valid model for the model-based vibration control. To this end, the actuator-rotor model given by Eqs. (68) and (69) is identified by using the following methods:

1) optimisation in time-domain based on evolutionary algorithms [92,93]. Noise input was supplied to the control winding and the rotor displacement was obtained as output. The parameters of the LTI system were estimated by the differential evolution algorithm [94, 95] in Publication III,

2) black-box identification by using the subspace method [96]. The LTI model was identified against the system simulator in Publication II,

3) prediction-error method (PEM) [97] was used in frequency-domain in Publication IV. Band-limited white noise was supplied to the control winding and the rotor displacement was measured with the disturbance subtracted [98],

4) a single value of the frequency-response function (FRF) at a specific frequency was estimated by using a rotating space-vector voltage supply in Publication V. An analytical expression was deduced for the FRF at rotation frequency of the rotor. Hence, the parameters were estimated by using both analytical methods and measurements.

The LTI model structure in Eqs. (68) and (69) including arbitrary eccentric rotor motion enables various input voltage signals to be used in the identification process. In this work, both black-box (with a fixed number of states predicted by the analytical model) and parametric identification routines were used. Furthermore, both the simulation and measured data were used. The non-idealities of the rotor shaft (bowed rotor) set demands on the vibration control. The effect of the control-winding supply on the rotor vibration was obtained by subtracting the uncontrolled rotor displacement signal from the overall rotor displacement [98]. In fact, the measured rotor displacements and currents in the control winding fluctuated because of a small slip. First, the measurement without control winding

supply was performed for a full period of the slip. Then, by applying interpolation and using the tacho signal, the measurements without control winding supply were subtracted from the measurement with a non-zero supply. The details of the method are presented in [98].

3.5 Control design

The CC algorithm [82] discussed in Sec. 2.3 is applied on rotor vibration attenuation in a cage induction machine equipped with a built-in force actuator. The force actuator was introduced in Sec. 2.2. The actuator-rotor system was modelled in an LTI formalism in Eqs. (68) and (69).

In simulations performed in Publication II and Publication III, it resulted that the RL circuit of the control winding induces a sharp resonance peak at the main-winding supply frequency. The actuator dynamics is involved because the supplementary winding was voltage fed. This results in a strong system phase shift close to the supply frequency. Especially at a small slip, this induces difficulties in estimating the FRF at the first rotor rotation speed harmonic (unbalance mass excitation frequency) which is needed for the CC controller in Eqs. (38) and (39). For this reason, in order to smooth the phase shift, a wide-band compensator was proposed in Publication III. In addition, the wide frequency-band control is to compensate random excitation and to make the plant more insensitive to changes in dynamics. The changes in dynamics follow from the changing operational conditions of the machine. In terms of the actuator-rotor dynamics, the governing dynamical changes are declared by the changing fundamental air-gap flux density, slip and rotation speed.

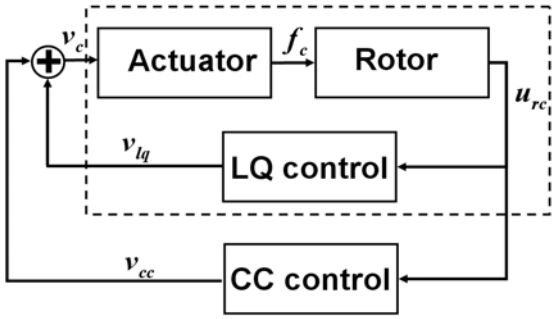

Figure 14: Modified plant formed by the LQ control (inside dashed-line box). The CC control is applied for the modified plant.

In Publication III, a linear quadratic (LQ) state-feedback control [81] was used in order to compensate the actuator dynamics. Hence, a CC algorithm was designed for the modified process (Fig. 14). In Publication III, the modified process was formulated based on the state-space model (Eqs. (68) and (69)) in

the LTI formalism by

$$\frac{\mathrm{d}}{\mathrm{d}t}\begin{pmatrix} q \\ \hat{q} \end{pmatrix} = \left[\begin{array}{c|c} A & -BK_{lq} \\ \hline K_{ob}C & A - K_{ob}C - BK_{lq} \end{array}\right]\begin{pmatrix} q \\ \hat{q} \end{pmatrix} + \begin{bmatrix} B \\ B \end{bmatrix} v_{cc} + \begin{bmatrix} G \\ 0 \end{bmatrix} f_{ex} \quad (72)$$

$$u_{rc} = \begin{bmatrix} C & 0 \end{bmatrix}\begin{pmatrix} q \\ \hat{q} \end{pmatrix}. \quad (73)$$

where $\hat{q}$ is the estimated state vector and the observer gain is denoted by K_{ob}. The LQ compensator for the plant is given by the state feedback law by means of the estimated state $\hat{q}$ by

$$v_{lq} = -K_{lq}\hat{q}. \quad (74)$$

where K_{lq} is the negative feedback LQ gain. The overall control-voltage input $v_c = v_{lq} + v_{cc}$ is a sum of the LQ compensator signal v_{lq} and the actual CC control signal v_{cc}. For the modified process given by Eqs. (72) and (73), the CC algorithm is constructed by using the FRF estimates for the modified process in Eq. (39) to build the control law given by Eq. (38).

4 Results

4.1 Electromechanical modelling

In Publication I, the distributed electromechanical model for an eccentric-rotor electrical machine was introduced. The model was applied for a 7 MW asynchronous motor and 21 MVA synchronous generator. The main parameters of the machines are listed in Table (2). The parameters of the electromechanical force model were estimated by FE simulations of the machines [4,28]. Hence, the identified electromechanical model was coupled to a structural FE model. The mechanical damping was neglected in order to bring out the effect of electromechanical interaction on system damping. The structural FE model of the 21 MVA generator is shown in Fig. 15.

Table 2: The main parameters of the example machines. The number of parallel paths used in the analysis was 1. The actual number of parallel paths is given in parenthese. The generator is a salient-pole machine, and for the radial air-gap length, the minimum value is given.

parameter	7 MW motor	21 MVA generator
number of pole-pairs	1	7
number of phases	3	3
number of parallel paths	1(1)	1(7)
inner diameter of stator core [mm]	630	2020
radial air-gap length [mm]	6.5	11
connection	star	star
rated voltage [V]	6000	13800
rated frequency [Hz]	50	60
rated speed [rpm]	2980	514
rated current [A]	743	893
rated power [MW]/[MVA]	7.0	21.3
rated slip [%]	0.597	0
rotor mass [kg]	2997	25400
bearing span [mm]	2600	3350

The effect of electromechanical interaction on the rotor vibration characteristics was studied by using the distributed electromechanical model given by Eqs. (47) and (48). The 21 MVA generator and 7 MW motor modal data is presented in Table (3) and Table (4), respectively. In the tables, the frequencies f and f_0 stand for the natural vibration frequencies of the electromechanical model

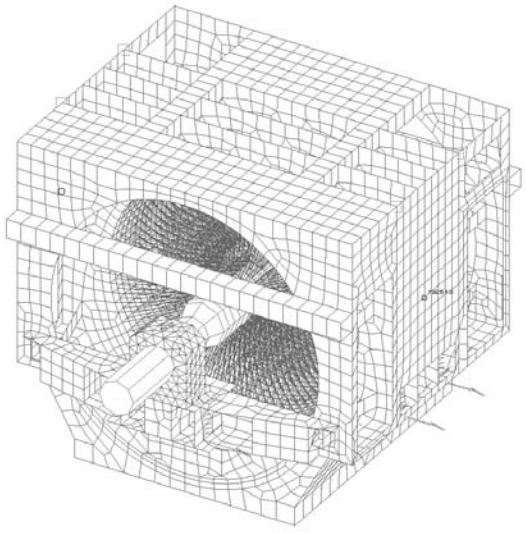

Figure 15: The structural mechanics FE model of the 21 MVA generator.

and mechanical model, respectively. Furthermore, the electromagnetic damping ratios ξ are presented.

The results indicate that the electromechanical interaction has an effect on the rotor bending modes. In addition to the reduction of the rotor bending natural frequencies, the damping of the bending modes in the 21 MVA generator has increased (Table (3)). The effect of the electromechanical interaction on the other modes is small. Particularly, the model predicts that the rotor-cage currents are not induced in the conical rotor deformation. Consequently, the electromechanical damping in Table (3) for the conical mode is zero. However, the modal frequency of the conical mode is slightly reduced due to axially distributed radial magnetic pull.

Table 3: Modal analysis data of the rotor bending and electromechanical modes of the 21 MVA generator at the rated speed.

mode	f_0 [Hz]	f [Hz]	Δf [%]	ξ [%]
electromechanical 1		8.20		88.34
electromechanical 2		8.97		37.72
bearing block	11.04	10.92	-1.12	0.27
rotor bending 1	20.83	19.85	-4.71	1.20
rotor bending 2	23.21	22.43	-3.37	0.73
	41.08	41.06	-0.06	0.01
conical	42.65	42.53	-0.29	0.00

Due to the dynamics induced by the rotor-cage currents, additional electrome-

chanical modes are included in the electromechanical model. These modes are related to the electromagnetic properties of the rotor cage (resistances and inductances). However, the results show that these modes are well damped which is a consequence of the RL properties of the rotor. The results of modal analysis for the 7 MW motor listed in Table (4) show that the effect of the electromechanical interaction is restricted to the negative spring effect i.e. the electromechanical damping is negligible.

Table 4: The calculated modal data for the 7 MW motor at the rated speed.

mode	f_0 [Hz]	f [Hz]	Δf [%]	ξ [%]
rotor bending 1	27.46	26.59	-3.15	-0.009
rotor bending 2	35.29	34.65	-1.83	-0.010
electromechanical		49.40		1.000

The modal analysis data for 21 MVA generator and 7 MW motor is plotted against rotation frequency in Fig. 16 and Fig. 17, respectively. Results were obtained from Eqs. (47) and (48). The mechanical damping was neglected in order to bring out the effect of electromechanical interaction. Gyroscopic disks [85] were used to model the gyroscopic effect.

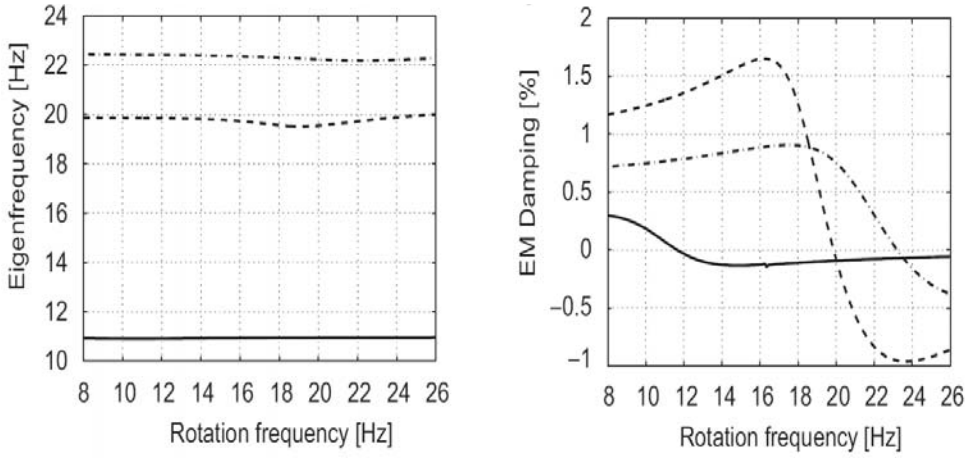

(a) (b)

Figure 16: Eigenanalysis data for 21MVA generator plotted against rotational frequency: (a) eigenfrequencies, (b) damping factors. Bearing block mode (solid line), rotor bending mode 1 (dashed line), rotor bending mode 2 (dash-dotted line).

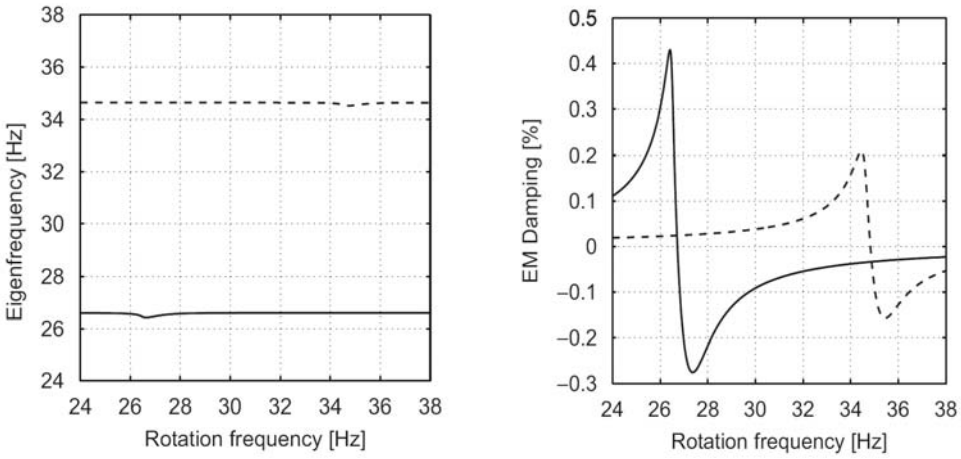

(a) (b)

Figure 17: Eigenanalysis data for 7MW motor plotted against rotational frequency: (a) eigenfrequencies, (b) damping factors. Rotor bending mode 1 (solid line), rotor bending mode 2 (dashed line).

In Fig. 18, the response of the 7 MW motor and 21 MVA generator to the unbalanced mass excitation is shown for the electromechanical and mechanical systems. The negative spring effect (radial UMP) is manifested by a shift in the responses of the electromechanical system. Mostly due to the asymmetric bearings, the rotor performs elliptic whirling which in turn induces rotor-cage currents depending on the whirling frequency. The tangential UMP component related to the cage currents affect the damping of the system and hence, the receptance. The results indicate that the electromechanical interaction has an effect on the rotor vibration excited by the unbalanced mass close to the rotor bending modes. Indeed, the negative/positive electromechanical damping (Fig. 16(b),Fig. 17(b)) increases/decreases the unbalance response.

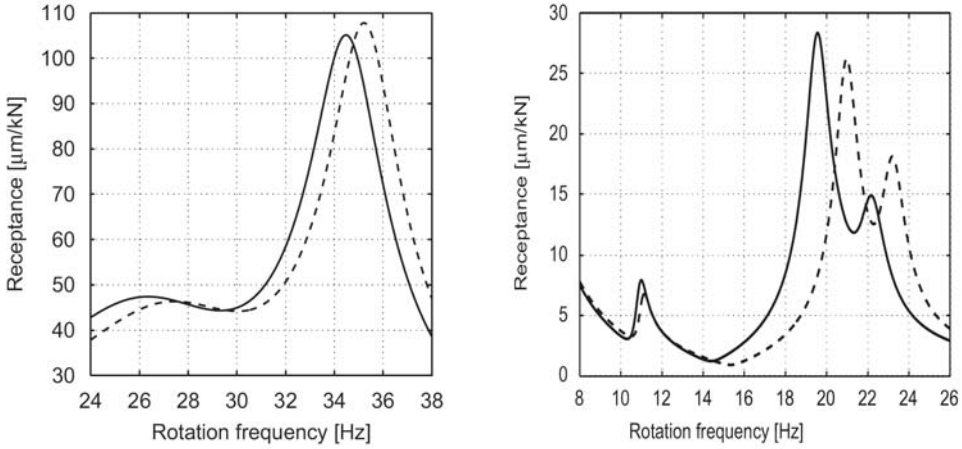

(a) 7 MW motor

(b) 21 MVA generator

Figure 18: Unbalanced mass frequency-receptance calculated by employing the electromechanical (solid line) and mechanical (dashed line) formulation.

4.2 Actuator-rotor FEM simulation and identification

In Publication II and Publication III, the actuator-rotor system under arbitrary eccentric rotor motion was studied. The equations were derived for a general $2p$ pole cage induction machine. The simulations were carried out for a 30 kW two-pole cage induction machine with an extended rotor shaft.

In Publication II, based on FE simulations, it was concluded that the actuator-rotor system can be approximated as an LTI system. However, it was pointed out that the disturbance force manifests non-linearity and, therefore, the excitation force level has to be known in order to use LTI models. In addition, the tangential component and higher harmonics of the magnetic flux density were not included in the analytical model. The results from FEM in Publication II show that the tangential component of the fundamental flux density was 4.99% (concentric rotor), 4.98% (10% static eccentricity) and 4.99% (synchronous whirling, 10% eccentricity) of the corresponding radial component. In Fig. 19, the stator and rotor slot harmonics obtained from FEA in Publication II with concentric rotor and without control winding supply are shown. In this case, the analytical model presented in Publication II is restricted to the radial component of the fundamental ($p = 1$) harmonic for which the value of 0.65 T is obtained in Fig. 19. The two-pole motor has 28 rotor bars and 36 stator slots which results to the first rotor and stator slot harmonics of orders $Q_r \pm 1 = 27, 29$ and $Q_s \pm 1 = 35, 37$, respectively [99]. The corresponding frequencies (50 Hz main winding supply, 1.0% slip) are $Q_r\omega_m \pm \omega_1 = 1436$ Hz, 1336 Hz (rotor slot harmonics) and $\pm\omega_1 = \pm 50$ Hz (stator slot harmonics).

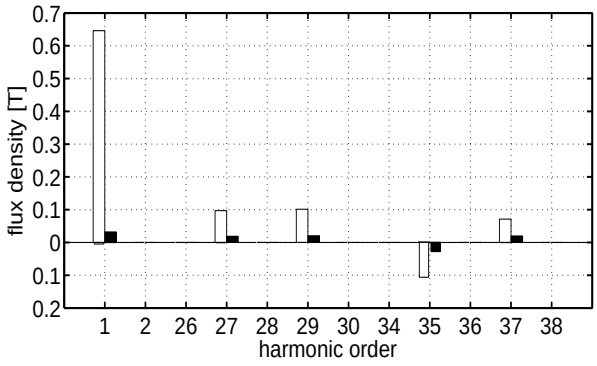

Figure 19: Harmonic content of the magnetic field in simulations presented in Publication II: radial (white bars) and tangential (black bars) component of the magnetic flux density. Upward and downward bars denote the harmonics travelling in positive (clock-wise) and negative (anti-clockwise) directions, respectively.

In Publication III, the system identification was carried out by estimating the parameters of the actuator-rotor LTI system by using optimisation based on evolutionary algorithms. In Fig. 20 and Fig. 21, identification results from Publication III are presented in which the low-order parametric actuator-rotor

model given by Eqs. (68) and (69) is identified against results from FEA. The identification results show a good agreement with FE simulations at the low-frequency domain roughly up to 100 Hz. However, there is dynamics not included in the LTI system around 150 Hz.

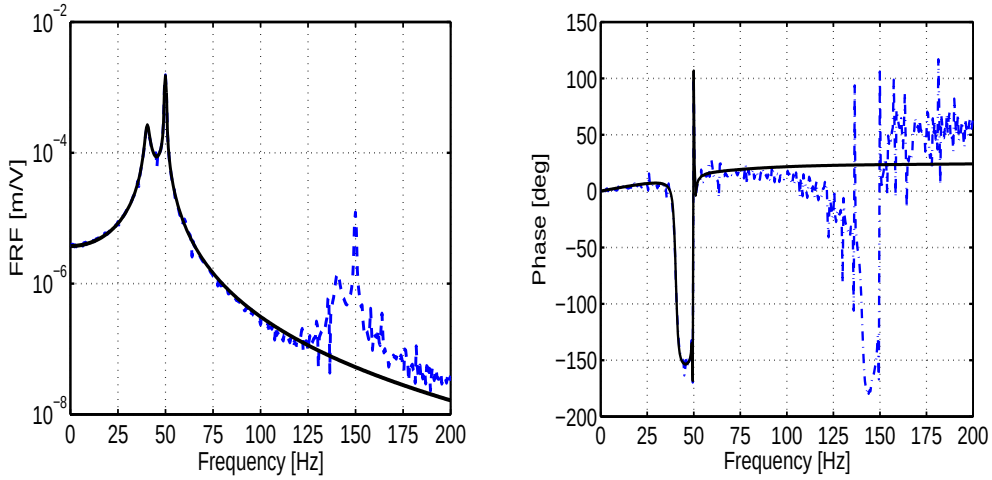

(a) (b)

Figure 20: Simulated FRF between the input voltage component 1 and horizontal displacement by using FEM (dashed line) and identified LTI model (solid line): (a) FRF magnitude, (b) phase.

In Publication II, the FE simulations for the actuator-rotor system were carried out. It was concluded that even though the identified LTI model provides a good approximation of the actuator-rotor system, some effects are left beyond the scope of a low-order model. One of these effects is an oscillated UMP component induced by static rotor eccentricity. In Fig. 22, the rotor is subjected to a static eccentricity in the non-linear FEA (non-linear magnetic materials, single-valued magnetisation curve). The LTI model predicts a static force, but in FE simulations an oscillating force component at double supply frequency is present, as well. The validity of the LTI system in Fig. 20 and Fig. 21 is poor close to 150 Hz due to presence of additional dynamics not predicted by the LTI model.

In the FE simulation, 3-D effects such as unipolar flux and skewed rotor bars were not included. Hence, the oscillating force component was presumably induced by the stator or rotor slotting or saturation. In Fig. 23, the results from simulations by using linearised FEM (no saturation of magnetic materials) under static rotor eccentricity are shown. The UMP calculated by non-linear and linear FEA are compared in Table (5). The results indicate that saturation is not responsible for the oscillating component even though it has a strong effect on it. In terms of enhancing the LTI model, a more detailed air-gap analysis is needed

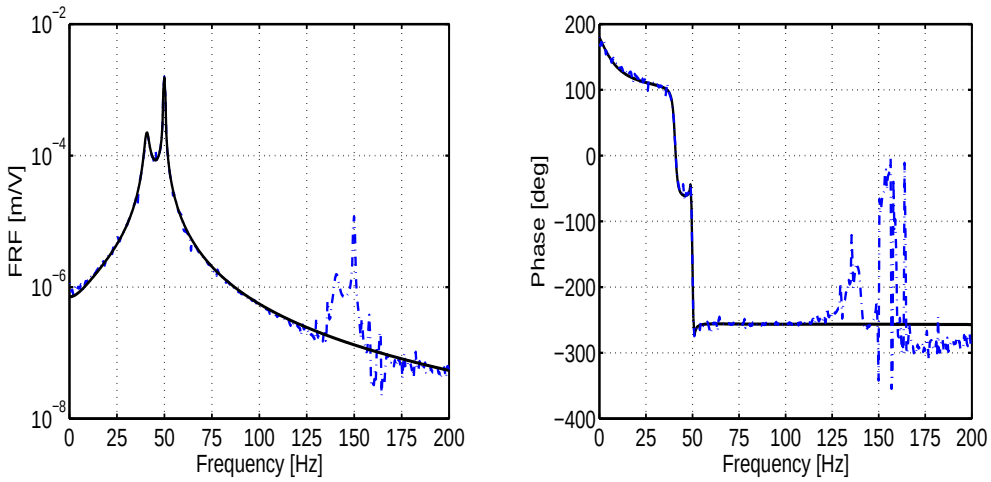

(a) (b)

Figure 21: Simulated FRF between the input voltage component 1 and vertical displacement by using FEM (dashed line) and identified LTI model (solid line): (a) FRF magnitude, (b) phase.

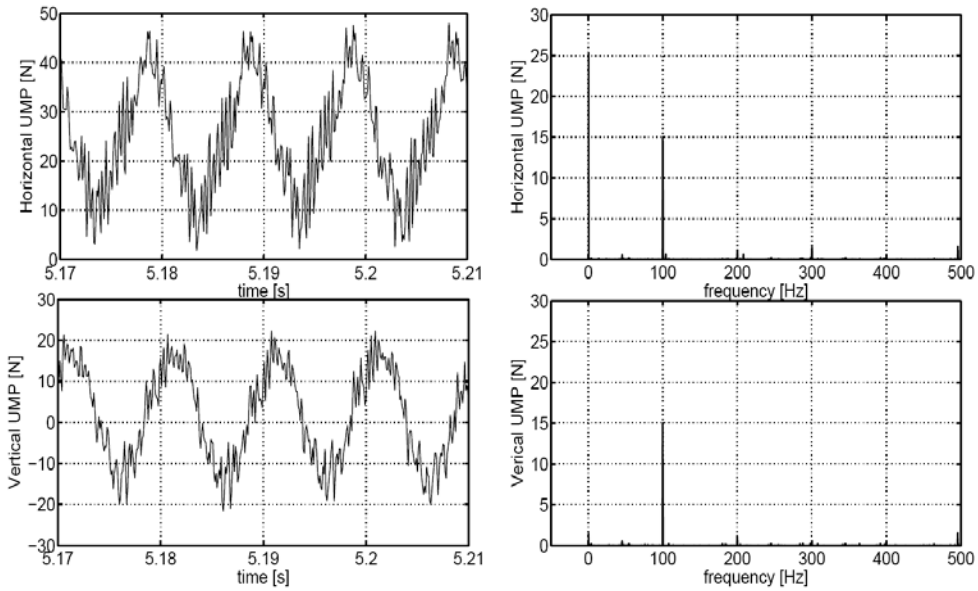

Figure 22: Simulated UMP (non-linear FEA) under static eccentricity of 100 μm in the horizontal direction without control winding input.

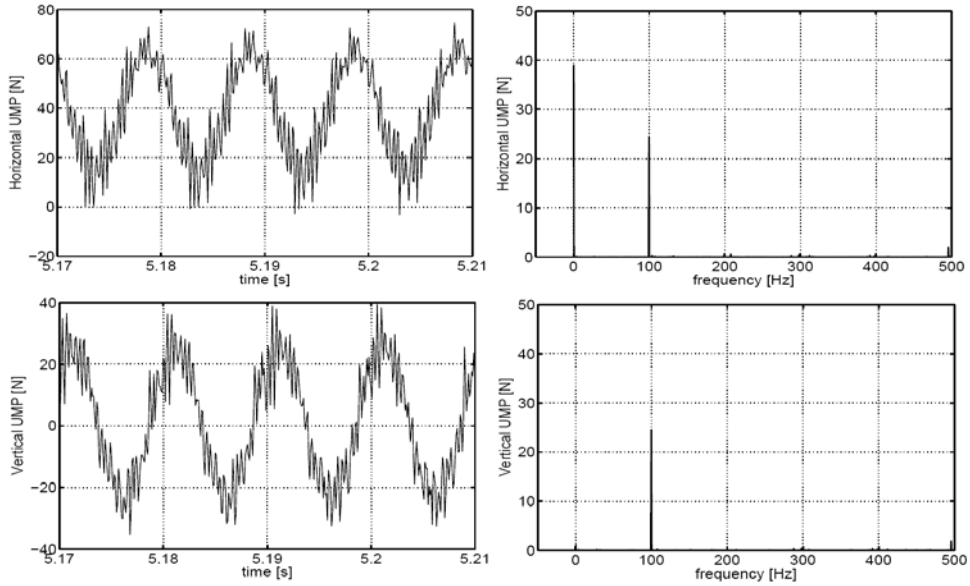

Figure 23: Simulated UMP (linearised FEA) under static eccentricity of 100 μm in the horizontal direction without control winding input.

in order to cover effects such as the oscillating UMP component. In general, the analysis leads to non-linear systems or linear time-periodic (LTP) systems.

Table 5: Simulated UMP from non-linear and linear FEA for static eccentricity of 10 % (100 μm) in the horizontal ($+x$) direction. The results from the linear FEA are in parentheses.

	0 Hz	100 Hz
horizontal UMP [N]	25.3 (39.1)	15.1 (24.5)
vertical UMP [N]	1.5 (1.1)	15.1 (24.5)

4.3 Simulated vibration attenuation

In Publication III, the system simulator (Fig. 13) for the actuator-rotor system was used to test the control algorithms in prior to the implementation in a real machine. The LQ compensator was designed with an observer and state-feedback. For the modified plant, the CC algorithm was used for attenuation of harmonic vibration components (Fig. 14).

In Fig. 24, a simulated vibration control result presented in Publication III is shown. The excitation force consisted of two harmonics: the first rotation-speed harmonic (43.4 N) and the second one (4.34 N). The results obtained from the simulations show that enough force is generated for vibration suppression and the force can be controlled.

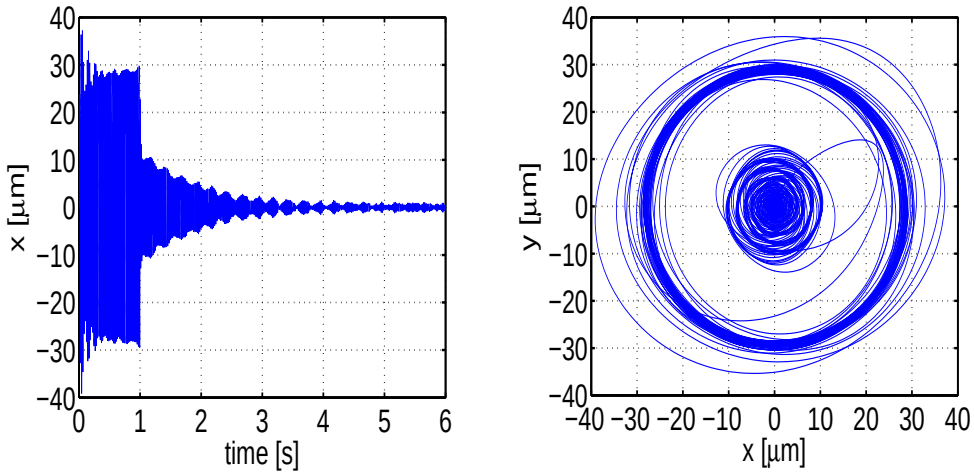

(a) (b)

Figure 24: Simulated rotor displacement by using time-discretised FEA. The LQ+CC controller is switched on at 1.0 s: (a) horizontal rotor displacement, (b) orbit.

4.4 Experimental system identification and vibration attenuation

In the following, experimental results from measurements carried out for a two-pole 30 kW cage induction motor are presented. The experimental set-up is shown in Fig. 25. The main parameters of the machine are listed in Table (6). Eddy-current displacement sensors were used to measure the rotor displacement close to the D-end end-shield. The fundamental flux was measured by using two-pole flux measurement windings and the control winding phase currents were measured by current shunts. The induced rotor cage currents were not measured. Instead, they were treated as non-measurable states of the actuator-rotor system. An experimental set-up for measuring the rotor cage currents was presented by Bottauscio *et al.* [100]. In Publication IV, prior to the model-based vibration control, the actuator-rotor system given by Eqs. (68) and (69) was identified by using the frequency-domain Prediction Error Method (PEM). The results of the identification are shown in Fig. 26 and Fig. 27.

In Publication IV and Publication V, the rotor vibration attenuation of a 30 kW two-pole cage induction motor was demonstrated. A two-pole cage induction machine was chosen for the reason that they are generally known to have rotor vibration problems [101–103]. The main aim was to demonstrate the CC algorithm by using the built-in force actuator in a real machine. Due to the flexible rotor, the machine could not be run at the rated operational conditions. However, the usage of CC algorithm by using a self-bearing actuator was successfully

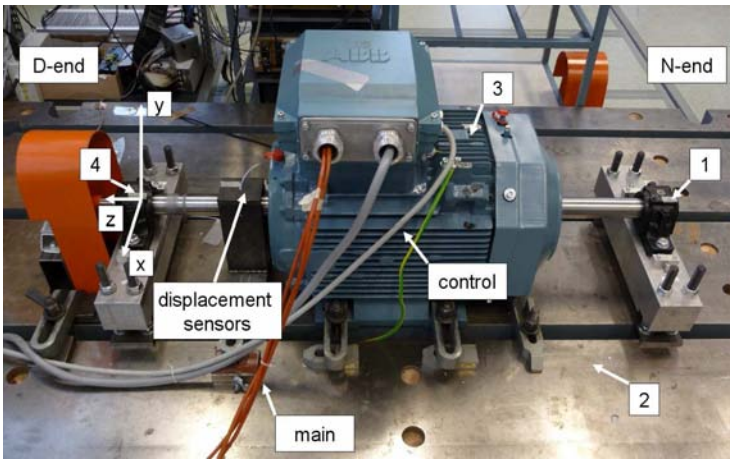

Figure 25: The 30 kW cage induction motor used in the experiments. The numbering refers to the accelometer positions '1' (N-end bearing), '2' (foundation), '3' (stator housing) and '4' (D-end bearing) from where vibration levels were measured in Publication IV.

Table 6: Main parameters of the induction motor used in the experiments (see Fig. 25). The values in parentheses are rated values of the machine with standard rotor.

parameter	value
rated supply frequency [Hz]	50
rated supply voltage (rms) [V]	400
connection	delta
rated current [A]	50
rated power [kW]	30
number of phases	3
number of parallel paths	1
number of poles	2
slip [%]	0.0 (1.0)
rotor mass (rotor core and shaft) [kg]	55.80
rotor shaft length [mm]	1560
radial air-gap length [mm]	1.0
first rotor bending mode [Hz]	36.94
rated rotation frequency [Hz]	49.5
control winding turns per phase	40

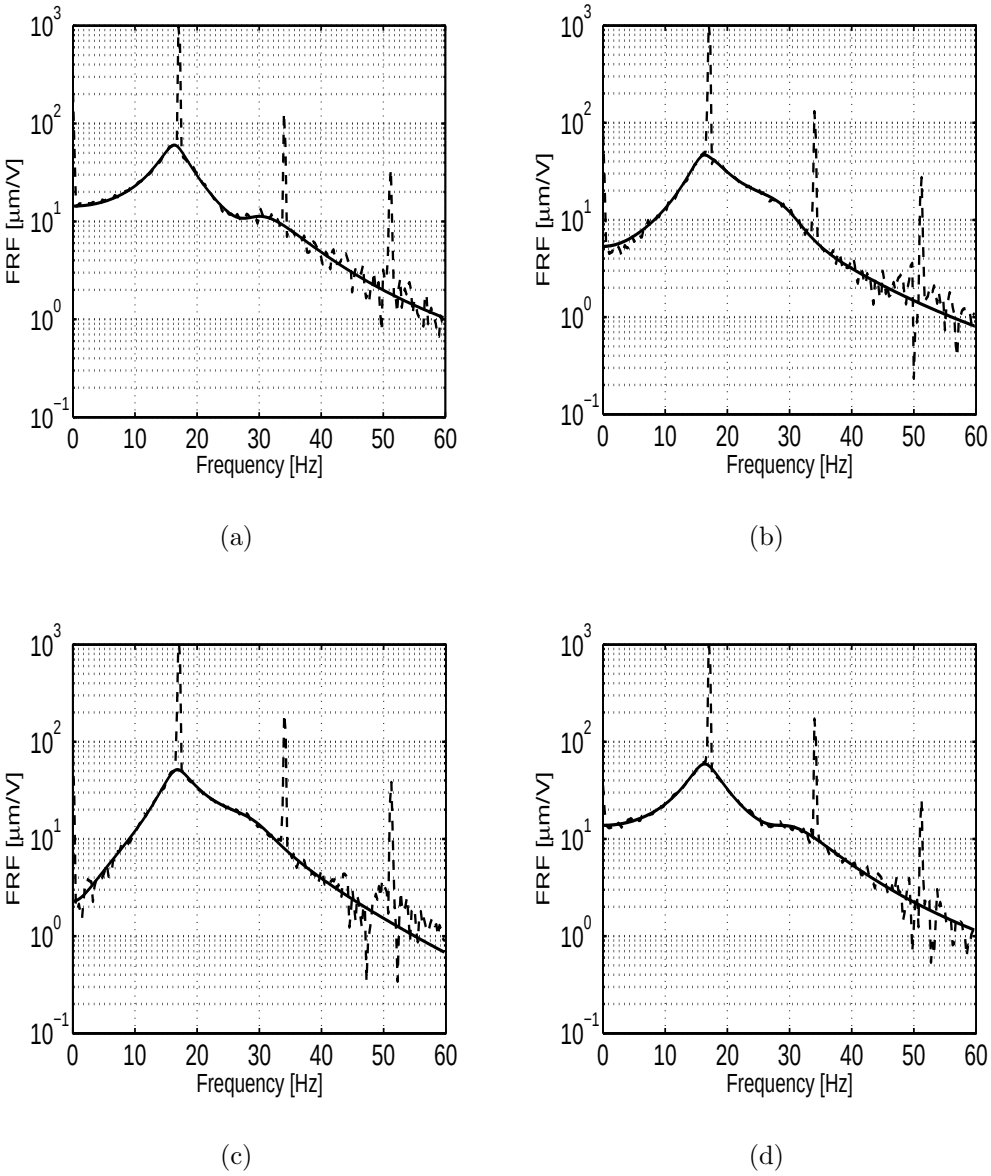

Figure 26: FRF amplitudes from the measurements (dashed line) and identification (solid line); (a) from $\mathrm{Re}(\underline{\hat{u}}_{c,0})$ to x, (b) from $\mathrm{Re}(\underline{\hat{u}}_{c,0})$ to y, (c) from $\mathrm{Im}(\underline{\hat{u}}_{c,0})$ to x, (d) from $\mathrm{Im}(\underline{\hat{u}}_{c,0})$ to y. The x and y coordinates refer to horizontal and vertical direction, respectively (Fig. 25).

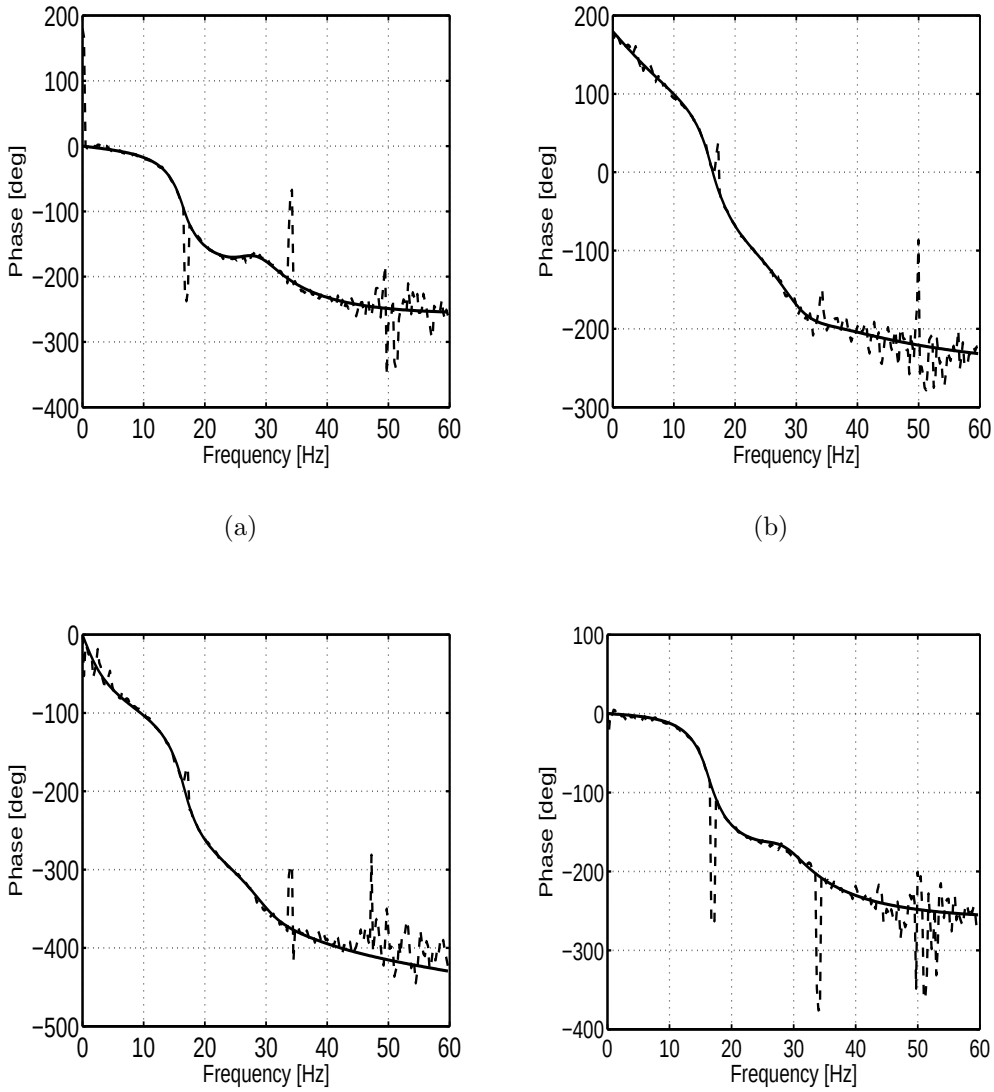

Figure 27: FRF phases from the measurements (dashed line) and identification (solid line); (a) from $\mathrm{Re}(\underline{\hat{u}}_{c,0})$ to x, (b) from $\mathrm{Re}(\underline{\hat{u}}_{c,0})$ to y, (c) from $\mathrm{Im}(\underline{\hat{u}}_{c,0})$ to x, (d) from $\mathrm{Im}(\underline{\hat{u}}_{c,0})$ to y. The x and y coordinates refer to horizontal and vertical direction, respectively (Fig. 25)

demonstrated. In Publication IV, several rotation speed harmonics were attenuated simultaneously. In Publication V, the emphasis is on the unbalance mass compensation which is performed by a simplified control design.

In the experiments, it resulted that the motor equipped with an extended rotor shaft could not be run at the rated operation condition without increased rotor vibration amplitudes and contact with auxiliary bearings. The mechanism behind the possible destabilizing forces (rotor-dynamic instability [23, 104, 105]) was not studied in detail. The first experiments on system identification and model-based control were completed with a stator main winding supply of 17 Hz and 15 A. The results were published in Publication IV. Later, in Publication V, the operation point was changed to 30.0 Hz and 6.0 A. Finally, by using the combined CC and LQ controller (Fig. 14), stable operation at a wide rotation speed range up to 50 Hz was achieved. In particular, a stable operation at critical speed (36.0 Hz) was demonstrated. These results were published in [98, 106, 107]. In the following, results by using CC control at rotation frequency of 17.0 Hz and results by using CC and LQ control at 36.0 Hz are presented.

At the rotation frequency of 17.0 Hz, the 15 A current supplied in main winding produced an air-gap field of 0.71 T (measured by two-pole flux measurement windings distributed to the stator slots). The CC algorithm was applied to operate on 4 harmonics (DC, 1st, 2nd and 3rd rotor speed harmonics). In Eq. (38), the parameters $\alpha_0 = 5.0 \cdot 10^{-5}$, $\alpha_1 = 20.0 \cdot 10^{-5}$, $\alpha_2 = 10.0 \cdot 10^{-5}$, $\alpha_3 = 10.0 \cdot 10^{-5}$ and $\gamma_0 = \gamma_1 = \gamma_2 = \gamma_3 = 1.0$ were used. The time-domain results of the vibration attenuation when the CC control was switched on is shown in Fig. 28.

In Publication IV, it was concluded that the reduction in the rotor vibration amplitudes was 97.0% and in the vibration level (vibration velocity in [mm/s]) the corresponding reduction was 57.0%. The general vibration levels at the machine bearings, foundation and housing were measured by accelometers. The overall vibration levels were reduced 4.0%–80.0% when the control was switched on. An exception was the D-end bearing block where the vibration level increased by 4.4%. The increase in vibration level was because the originally bowed rotor shaft was forced to the centre of the stator bore.

The control action can be clearly seen from the spectral analysis data of the rotor displacement shown in Fig. 29. The results show that the vibration attenuation is based on the reduction of the DC and the three harmonic peaks. In Fig. 30, the measured phase "a" current of the control winding is shown. The sources for the control winding current are (1) control winding voltage supply and (2) the rotor-cage four-pole current harmonics induced by eccentric rotor motion. The root mean square (RMS) values of the phase current for the controlled and uncontrolled case are 0.21 A and 0.31 A, respectively. The result manifests the strong influence of the currents induced from the rotor eccentricity. The influence is reduced when the eccentricity is reduced by the control.

In order to achieve wide-band vibration attenuation, the CC controller was coupled with a LQ controller. Especially, the results from simulations in Publi-

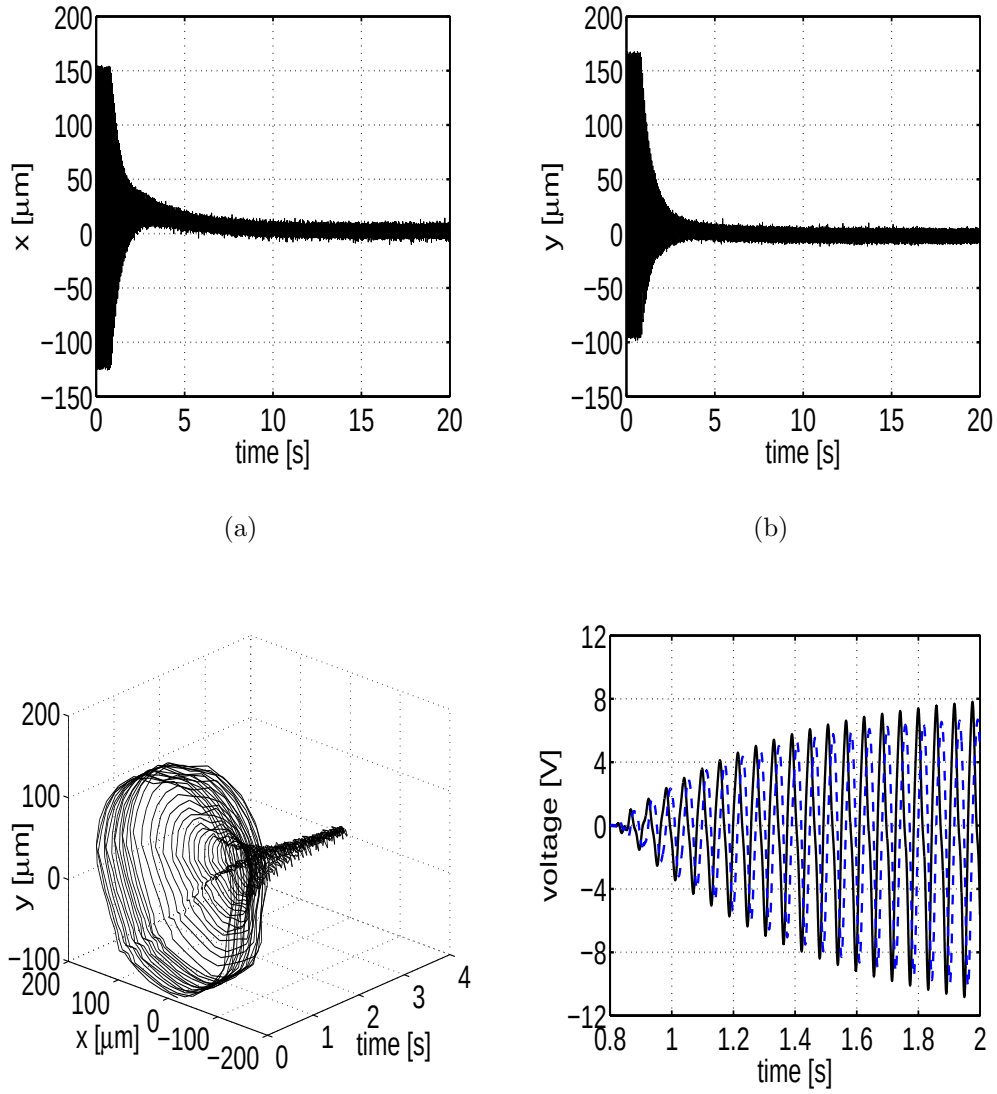

(a) (b)

(c) (d)

Figure 28: Vibration attenuation results from the experiments with the test machine. The control was switched on at $t = 0.8$ s; (a) horizontal rotor displacement, (b) vertical rotor displacement, (c) rotor orbit, (d) control input voltage $\underline{\hat{u}}_{c,0}$: real part (solid line) and imaginary part (dashed line).

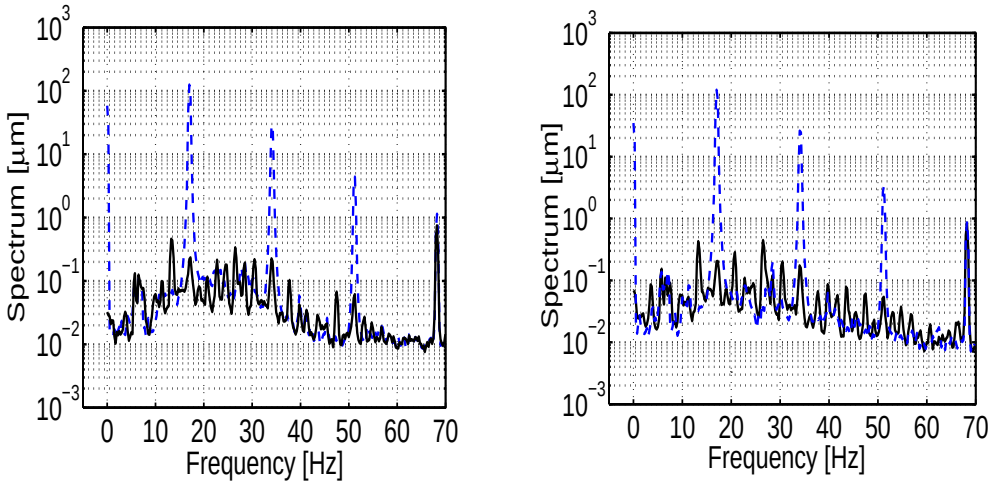

(a) (b)

Figure 29: Experimental results in the frequency-domain. Displacement spectra of the controlled (solid line) and uncontrolled system (dashed line); (a) x direction, (b) y direction.

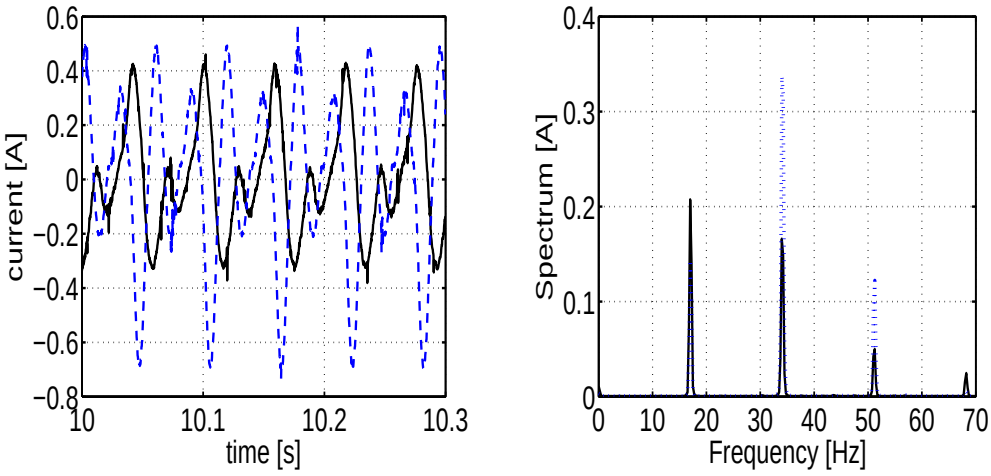

(a) (b)

Figure 30: The measured current in the control winding phase "a". Controlled system (solid line) and uncontrolled system (dashed line). (a) phase "a" current, (b) spectrum of the phase "a" current.

cation III predicted that rapid changes in the system phase may induce problems with a CC controller. The actuator-rotor system given by Eqs. (68) and (69) was identified by using PEM and band-limited noise in control winding input voltage at rotation frequency 32.0 Hz. Hence, based on the identification, a LQ controller was designed by Orivuori [107]. The CC controller was designed for rotation speed of 36.0 Hz. In fact, the machine was run at 36.0 Hz under LQ control and frequency response of the closed-loop system was experimentally estimated. The CC controller operating at the rotor rotation frequency ($k = 1$ in Eq. (38)) was coupled with the LQ controller by using Eqs. (72) and (73).

By using the preceding method for coupling CC and LQ controllers, a wide-band rotor vibration attenuation was achieved. The stable long-time operation was achieved on rotation speed range from 32 Hz to 50 Hz. Stable operation by using only the LQ controller [107] was demonstrated, as well. However, coupling of a CC controller enhanced the vibration attenuation. In particular, by using a combined LQ and CC controller, a long-time critical speed operation, not achievable without control, was demonstrated. In the following, previously unpublished results of the critical speed operation are presented. The identification, control design and implementation is a result of analysis in Publication III, LQ control design in [107] and implementation and data analysis presented in [98].

In Fig. 31, the measured rotor displacement from rundown from the rotation speed of 50 Hz is shown. In the rundown, the control winding and main winding were not supplied. The first flexural rotor bending mode is excited so that touch-down with the auxiliary bearing occurs approximately at 38.2 Hz (dashed line). From modal testing results in Publication IV, the bending mode was found at 36.94 Hz with damping ratio 0.68%. However, the electromechanical interaction (radial UMP) affects the bending mode by decreasing the natural frequency. In the rundown, the existence of the critical speed was demonstrated.

In the following, the results from experiments by using the combined CC and LQ control are presented. The rotation frequency of the rotor was 36.0 Hz (Fig. 31) and the machine was run without load. The stator main winding was supplied by 170.0 V and 15.5 A at supply frequency 36.0 Hz. This resulted in a two-pole field with peak value of 0.72 T (measured by two-pole flux measurement windings). In Fig. 32, the measured rotor displacement is shown. The machine could not be driven at this operation point without control (contact with touch-down bearings would not be avoided). In Fig. 32(a), the measured rotor displacement is shown with the initial rotor bow. In fact, the control objective was to minimise the difference between the measured displacement and initial bow, not to force the rotor to the middle of the stator bore. This approach minimises the net disturbance force exerted on the rotor. Due to the bowed rotor, the forces of the magnetic origin were enhanced. As was measured in Publication IV, forcing the rotor to the stator bore centre may increase vibration in bearings. In Fig. 32(b), the initial bow is subtracted from the measured displacement. The results show that the combined LQ and CC control works well and enables stable

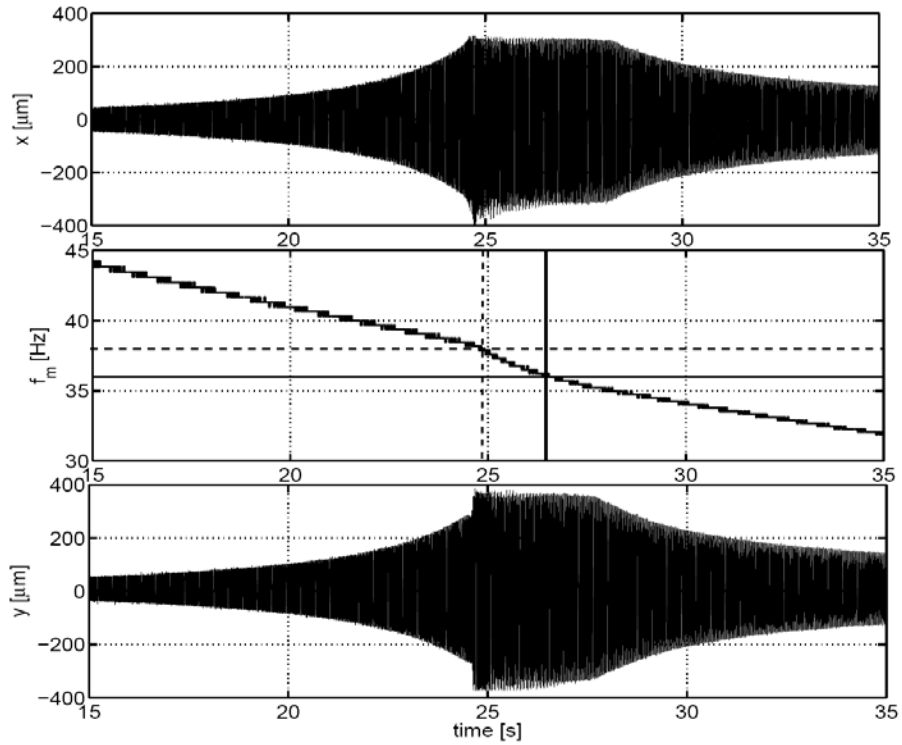

Figure 31: Measured rotor displacement data from the rundown without control or main winding supply. The rotor bending mode is excited and touch-down with auxiliary bearing occurs at the rotation speed of 38.2 Hz. In the middle, the rotor rotation frequency $f_m = \omega_m/(2\pi)$ is shown. Touch-down with safety bearings occurs at the rotation speed of 38.2 Hz (marked by dashed line). In addition, the rotation speed of 36.0 Hz is indicated by the solid line.

operation at the critical speed.

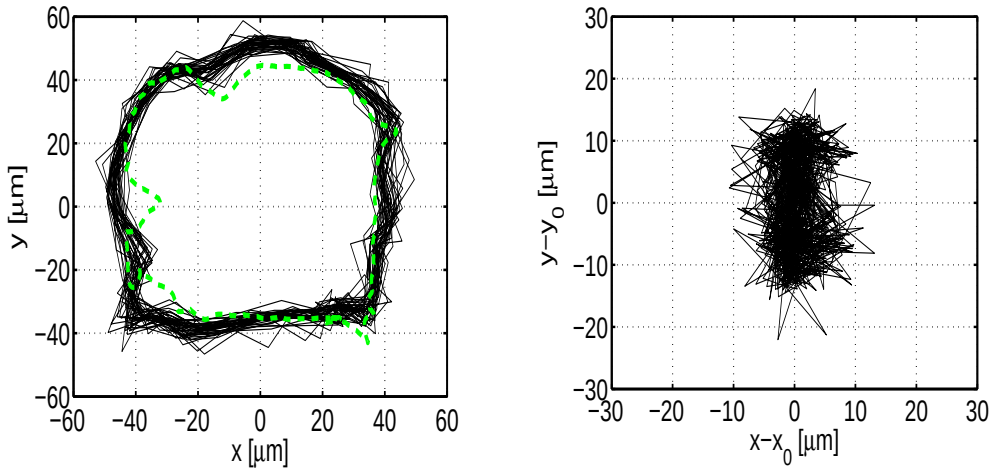

(a) (b)

Figure 32: The measured rotor displacement at 36.0 Hz rotation speed: (a) the rotor orbit (solid line) and rotor bow (dashed line), (b) the initial rotor bow subtracted from the rotor displacement.

In Fig. 33(a), the supply voltage $\underline{\hat{u}}_{c,0}$ to the control winding is shown. Main rotating components of the space-vector $\underline{\hat{u}}_{c,0}$ are 36.0 Hz (15.1 V), 0 Hz (4.6 V), 72.0 Hz (2.9 V) and −72.0 Hz (1.2 V). In Fig. 33(b), the rotating components of the rotor displacement $\underline{z}_r$ are shown. The spectrum was calculated from the measurement data by using methods developed in [98]. From the spectrum, it can be seen that the rotor motion is dominated by the forward whirling component (36.0 Hz).

In Fig. 34, the measured currents in the control winding are shown. The currents are induced by the control winding supply and, on the other hand, by eccentric rotor motion which produces an alternating four-pole eccentricity flux distribution in the air-gap. The main rotating components of the control winding current $\underline{\hat{i}}_c$ are 36.0 Hz (0.30 A) and 72.0 Hz (0.21 A).

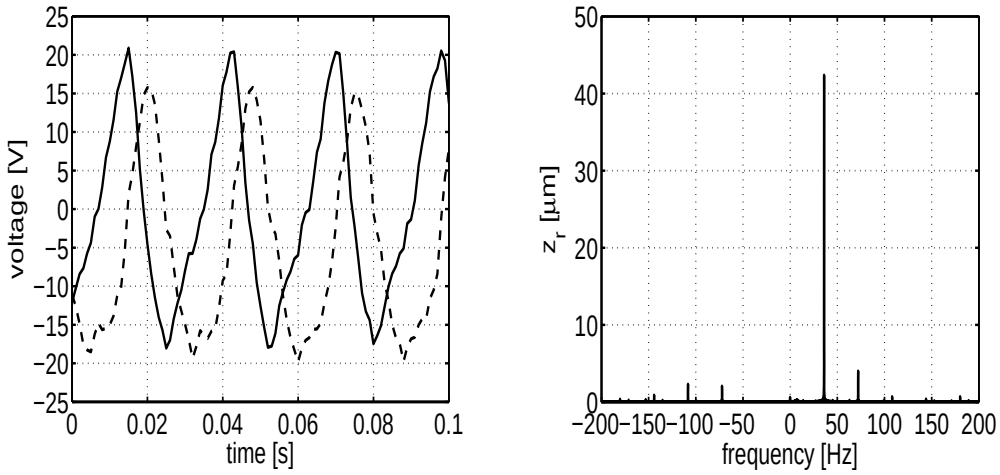

(a) (b)

Figure 33: The control winding supply voltage and the measured rotor displacement at 36.0 Hz rotation speed: (a) voltage space-vector $\underline{\hat{u}}_{c,0}$ real component (solid line), imaginary component (dashed line), (b) the spectrum of the complex-valued rotor displacement $\underline{z}_r = x + jy$.

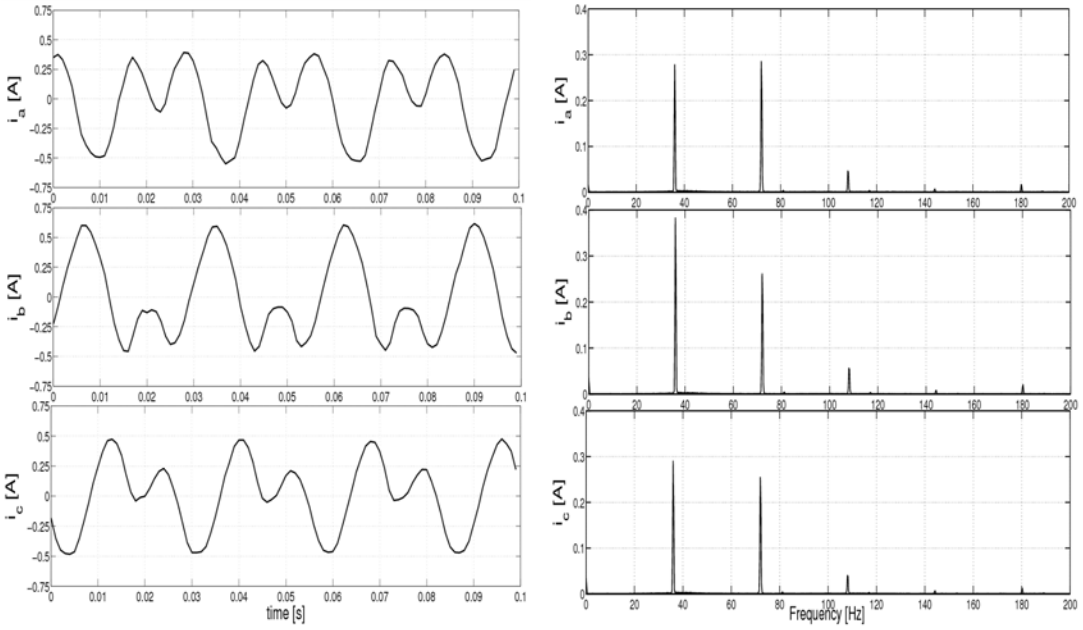

(a) (b)

Figure 34: The measured current in the control winding phases 'a', 'b' and 'c' at rotation speed 36.0 Hz: (a) time-series data and (b) spectrum. The currents are dominated by three frequency components at 36.0 Hz, 72.0 Hz and 108.0 Hz.

5 Discussion

5.1 Electromechanical modelling

In general, the axially non-uniform rotor-dynamic phenomena in electrical machines require electromechanical modelling in 3-D. However, as was pointed out in Sec. 2.1, a full-scale 3-D transient electromechanical FEA is a computationally demanding task for present-day computers. In Publication I, a methodology for coupling the stator and rotor 3-D FEM to an analytical low-order parametric model was presented. The presented model has the following advantages:

1) low-order, computationally efficient,

2) based on physical parameters,

3) parameters can be estimated by using measurements or simulations and

4) can be coupled with a 3-D structural mechanical model.

The model presented by Holopainen [2] is restricted to axially uniform phenomena including cylindrical whirling. The method proposed by Tenhunen *et al.* [83] includes axially non-uniform effects such as skewed rotor bars and stator slots. The method presented in Publication I has an advantage that in addition to including axially non-uniform effects it also couples the 3-D mechanical rotor and stator deformations. Another advantage is that it is computationally efficient. It was pointed out by Tenhunen [3] that the number of slices used in the multi-sliced FEM [29] is strongly restricted by the computational capacities available. Indeed, the central processing unit (CPU) time increases linearly with number of slices.

An advantage of the electromechanical model in Publication I is that the coupling is performed by using structural normal modes. Consequently, the number of nodes included in the electromechanical coupling is negligible in terms of the overall number of degrees of freedom in the full-scale structural mechanics FEM. In fact, the size of the LTI system given by Eqs. (47) and (48) is solely fixed by the number of mechanical vibration modes included into the modal decomposition. For instance, by increasing the number of slices, the number of columns of the system matrix K_c and the number of rows for the modal decomposition matrix Φ increase, but, nevertheless, the size of the matrix $K_c\Phi$ remains the same. Typically, at the low-frequency domain, the flexural rotor vibration is dominated by the few lowest vibration modes. In these cases, the modelling technique developed in Publication I is especially powerful.

The model introduced in Publication I does not cover

1) the effect of skewed rotor bars or stator slots,

2) unipolar flux,

3) saturation and non-linear magnetic materials,

4) parallel paths in the stator winding,

5) higher flux-density harmonics in the air-gap.

The effect of stator and rotor skew was included in the multi-slice FEM presented by Tenhunen *et al.* [83]. In terms of the scope of the electromechanical modelling, the model presented in Publication I lies somewhere between the model presented by Holopainen *et al.* [2] and Tenhunen [29].

The parallel paths in the stator winding, commonly used in electrical machines, may have a strong effect on the UMP. An analytical model, analogous to [2], including the parallel paths was presented by Burakov *et al.* [24]. A more involved electromechanical model would result from coupling [24] in a structural mechanics model in modal form.

5.2 Modelling and identification of built-in force actuator

In Sec. 2.2 and in Publication II and Publication III, a built-in force actuator in a cage induction machine was considered. The examined actuator is based on force-actuation methodology of an induction-type self-bearing machine. In this work, the actuator was used for attenuation of flexural rotor vibration. The actuator-rotor system was (1) simulated by using FEM, (2) modelled analytically and (3) identified experimentally.

In this work, a system simulator of the actuator-rotor based on numerical calculation of the electromagnetic fields in the machine cross-section was built. Previously, the self-bearing actuator has been analysed by using simple mechanical models. The simulator presented in this work enables the usage of general 3-D structural mechanical models in a computationally efficient way. Indeed, the time-discretised electromagnetic FEM is encoded into a SIMULINK block [61] where it is coupled to a structural mechanics block. The mechanics block is encoded to an LTI system which enables the application of various modelling approaches including 3-D FEM in which the system order is reduced by modal decomposition [86].

The system simulator developed enables an enhanced actuator design. In the simulator, the modelled phenomena include: detailed stator and rotor slotting, eccentric rotor motion, rotor-cage currents and saturation of magnetic materials. However, 3-D effects are only partly included in the form of end-winding impedances. A multi-sliced time-discretised FEM analysis introduced by Tenhunen *et al.* [29] would, when coupled with structural mechanics and force actuator, provide means of including 3-D effects.

In the literature, as it was discussed in Sec. 2.2, the rotor cage is a challenge to the self-bearing force actuator. This is due to the design of the cage rotor which enables equalising currents to be induced when the supplementary winding is

excited. This, in turn, affects the actuated force. In the literature, the rotor position controllers are commonly current-fed and the effect of the induced cage currents is compensated by phase-lead and phase-lag elements [108]. In this work, a different approach based on voltage-fed supplementary winding is proposed. In this approach, the induced cage currents are included in the LTI model. The induced cage currents are states of the system. A further advantage of the model is that the cage currents induced by the eccentric rotor motion are also included. Previously, the eccentric-rotor cage currents are not included into any analytical self-bearing actuator-rotor model.

The advances of the presented analytical model include

1) cage currents induced both by eccentric rotor motion and supplementary winding currents,

2) coupling with structural mechanics model.

The fact that the cage currents affect the actuator force raise the need for an enhanced modelling of the actuator-rotor system. In the previous analytical models for the actuator-rotor system, the effect of the UMP induced by eccentric rotor motion has either been neglected, or, modelled by a radial component only. However, the tangential UMP component is important in the sense that it may affect the system stability [5]. The model presented in this work couples the actuator model with an eccentric-rotor UMP model. The commonly-used models for current-fed self-bearing actuators are of the form given by Eq. (26) where a direct current-force relation analogous to that of AMB is provided. In the later developements, the induced cage currents were included [108]. However, these models do not include the UMP induced by eccentric rotor motion which may have an effect on the rotor-dynamics. The model presented by Baoguo *et al.* [50], given by Eqs. (30) and (31), includes radial UMP. Furthermore, it can be coupled to a simple mechanical model in Eqs. (32) and (33). The model presented in this work given by Eqs. (60) – (63) includes a more realistic model for the UMP in which the equalising cage currents are taken into account, as well.

The results from the FE simulation in Publication II and Publication III show that the eccentric-rotor actuator-system can be approximated by the system given by Eqs. (60) – (63). However, it was found that (1) there is non-linearity with respect to the disturbance force level and (2) the validity of the low-order model is restricted by additional unmodelled system dynamics. The unmodelled system dynamics beyond LTI formalism are either LTP (pseudo-linear) or non-linear. Modelling the rotating air-gap field harmonics within linear theory leads in general to an LTP system. In this work, the LTP formalism was avoided in analytical formulations by restricting to a few dominating air-gap harmonics and by using a straight-forward modulation of the voltages and currents in Eqs. (65) – (67).

In Publication IV, the system identification for the actuator-rotor system was carried out. The identification results presented in Fig. 26 and Fig. 27 show that

the system dynamics within the low-frequency domain can be approximated by a low-order LTI system. The LTI system includes 8 real states which are the rotor position and velocity (4), the cage currents (2) and the control winding currents (2).

5.3 Attenuation of rotor vibration

The built-in force actuation mechanism of a self-bearing machine is, primarily, used for rotor positioning to guarantee a non-contact operation analogous to AMBs. However, the mechanism provides means to actively produce force on the rotor which could have other applications, as well. In this work, the force actuator is used solely for vibration attenuation of a flexible rotor supported by ordinary sliding or rolling element bearings. Previously, such a strategy was examined by Chiba *et al.* [42] by using a PID controller for current regulation.

As was pointed out in Sec. 2.3, various control schemes have been demonstrated in AMBs. The same does not hold for the induction-type self-bearing actuators where the control design is strongly restricted to PID controllers. In terms of vibration suppression, the main significance of this work is to apply an unbalance mass compensation algorithm, previously successfully demonstrated in AMBs, to a self-bearing force actuator for vibration suppression. The main advantage of the methodology is that the entire control effort is directed to the attenuation of harmonic vibration components which, typically, are the main source of rotor vibration.

Another advantage of the presented strategy is that the control of the dominating first unbalanced mass harmonic requires a force rotating at the speed of the rotor. In terms of the self-bearing actuator, especially in a machine with small slip, this means that the induced cage currents are small. This in turn leads to small rotor losses and, on the other hand, a better force actuation at the rotation frequency of the rotor. In general, as can be seen from Eqs. (60) – (63), the generation of a control force rotating with angular frequency

$$\omega = -\omega_{p+1} = (p+1)\omega_m - \omega_s = \omega_m - s\omega_s \tag{75}$$

does not induce equalising $p+1$ currents in the rotor cage from the control winding. When the self-bearing force actuator is used in order to compensate the rotor weight, a static force is needed, which induces currents in the rotor cage.

The simulation results for the vibration attenuation at the rated operational conditions predict a good performance of the built-in force actuator and CC algorithm. The results are shown in Fig. 24. However, as was pointed out in Publication III, a pre-compensator was needed in order to smooth the system dynamics stemming from the control winding RL resonance.

The results from the experimental vibration suppression in Fig. 28 and Fig. 29 show that the CC algorithm works well in the simultaneous suppression of multiple harmonic vibration components. In the experiments, however, due to the

flexible and bowed rotor, the rated operation condition of the machine could not be achieved. Hence, the operation point with a main winding supply of 17 Hz, 15A was chosen for experiments (rated 50 Hz, 50 A). At this operation point, a pre-compensator was not needed due to the higher damping of the control winding RL circuit. Despite this, the CC algorithm was successfully demonstrated.

5.4 Future research

In terms of the electromechanical modelling of the actuator-rotor system, in this work the aim was to cover the governing electromechanical phenomena in a low-order linear model. In particular, the LTI formalism was adopted which is a standard framework in control design. The results show that this approach provides a good approximation of the actuator-rotor system. However, because of the restriction to LTI dynamics, some electromechanical effects were left unmodelled. These effects may have a significance in some applications or operation conditions.

In Fig. 35, frequency-domain results from time-discretised FEA are shown for the complete model with non-linear magnetic materials and saturation and, also, for the linearised FE model. In order to perform an impulse test, the voltage impulse (duration 5 ms, peak value 10 V) shown in Fig. 35(a) was supplied to the control winding (real part of the space-vector) and the horizontal component of the output force on the rotor was recorded for calculation of FRF. In the simulation, the rotor was concentric (no eccentricity). It can be seen that the non-linearity has a considerable effect on the system dynamics. Consequently, the validity of the linear FEM (or low-order LTI) is suppressed to a low-frequency domain under 100 Hz.

In terms of systems theory, a more detailed analytical air-gap field analysis including the stator and rotor slotting with saturation leads to a system with time-periodic coefficients [71, 109–111]. Previously, such LTP systems have been encountered in analysis and control of various industrial applications such as rotating machinery [112], inverter locomotives [113], satellites [114] and helicopters [115]. In electrical machines, various air-gap field harmonics may couple with the eccentric rotor motion and produce the UMP giving rise to LTP systems [105]. During recent years, motivated by various applications in engineering, biochemistry and economics, analysis and control of LTPs have been under active research [116–119].

In this work, the experiments were performed in idealised circumstances. The motor was run at no-load and fed by a generator which provided smooth voltage supply compared to frequency converters commonly used to supply variable-speed drives. In the experiments, no coupling between the control winding and main winding was observed. However, in a real application with the frequency-converter supply, the capacitive coupling between the control winding and main winding may induce high-frequency disturbance to the control winding. Exci-

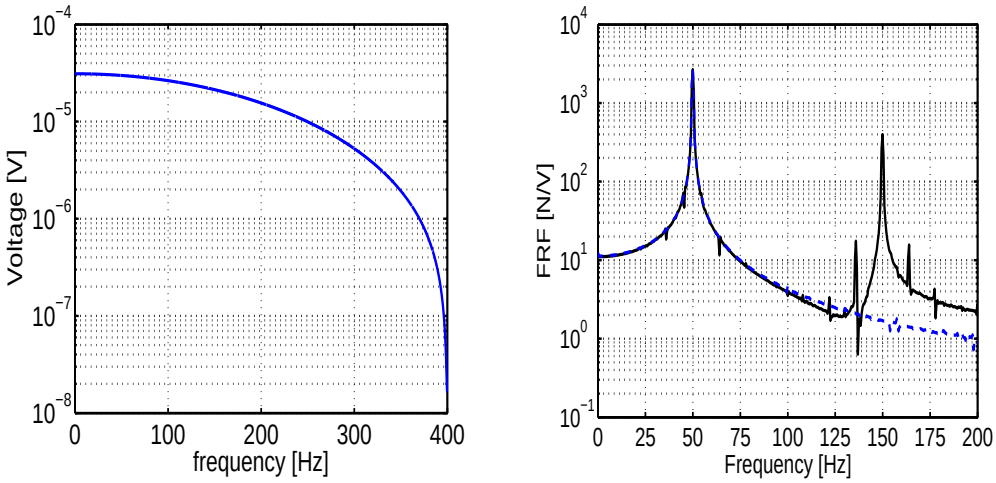

(a) (b)

Figure 35: Comparison of the FRFs calculated by using linear and non-linear FEA: (a) the spectrum of the voltage impulse in the control winding and (b) the voltage-force FRF calculated by a linear FEA (dashed line) and non-linear FEA (solid line). The frequency response is 11 N/V (DC) and 2700 N/V (50 Hz).

tations originated from the machine load and transients impose challenges for the vibration suppression in a real application, as well. In order to bring the approach closer to real applications, these aspects have to be considered in the future. Bearing this in mind, the experimental work related to this study only presents a first step towards a real application in a large electrical machine.

One matter to which attention must be paid to in future developments is the effect of the changing operation conditions on the control operation. It was observed that a change in the rotation speed or the fundamental air-gap flux density changes the system dynamics considerably. Indeed, an increase of the air-gap flux at certain rotation speed enhanced the RL resonance which suppressed the CC control performance. In the model, the effect was included in Eq. (60). In general, however, the system has to be identified again when the operational conditions change. In future developments, the changing operational conditions have to be taken into account. One approach could be the development of an adaptive, or model-predictive, CC algorithm in which the FRFs at harmonic frequencies are modified with respect to the operation point along to the model given by Eqs. (60) – (63). Recent developments in control design including the LQR based pre-compensator enabled a wide-frequency domain operation including critical speed operation [107].

6 Conclusions

In this thesis, a model-based control for the attenuation of flexural rotor vibration in cage induction machines was considered. For actuation of control force, a built-in force actuator based on a self-bearing machine working principle was considered.

In the modelling of eccentric-rotor cage rotor machines, a methodology for coupling an analytical electromechanical model to a 3-D structural mechanics model was presented. The methodology provides a computationally efficient means to model low-frequency rotor vibration in electrical machines. The parametric electromechanical model of an eccentric-rotor machine was coupled with the built-in force actuator. As a results, a model for the coupled actuator-rotor system was introduced.

In order to validate the parametric actuator-rotor model, a system simulator was built based on a detailed time-discretised FEA of the magnetic fields in the machine cross-section. In this work, the simulator was applied for a 30 kW two-pole cage induction machine equipped with an additional four-pole winding for lateral force generation. In the simulations, the machine was at the steady-state operation condition at the rated speed and load. From the results, it was concluded that the actuator-rotor system can be approximated by the low-order linear model within the low-frequency domain. However, it was observed that (1) there is a considerable non-linearity with respect to the disturbance force and (2) the validity of the model is strongly limited to the low-frequency domain roughly up to 100 Hz. Beyond the low-frequency domain, unmodelled system dynamics, presumably dominated by rotor and stator slotting harmonics, suppressed the validity of the low-order model. The parametric model was identified on the low-frequency domain by using time-discretised FEM.

In this thesis, an algorithm for compensating harmonic disturbance forces was applied in the built-in force actuator. Based on the identified parametric model, a control design based on the combined LQR and CC controllers was proposed. The controller was embedded into the system simulator and harmonic disturbance frequencies were compensated successfully.

The identification procedure of the parametric model and the model-based control design was experimentally demonstrated in a 30 kW two-pole cage induction machine in which an additional four-pole winding for radial force generation was installed. The results show that the proposed modelling and model-based control design are suitable in attenuation of rotor vibration in induction machines.

References

[1] E. Lönnrot, *Kalevala (In Finnish, Translation by John Martin Crawford, 1888)*, Suomen Kirjallisuuden Seuran Kirjapaino, Helsinki, 1849.

[2] T. P. Holopainen, A. Tenhunen, E. Lantto, and A. Arkkio, "Unbalanced magnetic pull induced by arbitrary eccentric motion of cage rotor in transient operation, part 1: Analytical model," *Electrical Engineering (Archiv für Electrotechnik)*, vol. 88(1), pp. 13–24, 2005.

[3] A. Tenhunen, "Electromagnetic forces acting between the stator and eccentric cage rotor," *Doctoral dissertation, Helsinki University of Technology, Electrical and Communications Engineering*, pp. 1–40, 2003, http://lib.tkk.fi/Diss/2003/isbn9512266830/.

[4] A. Burakov, "Modelling the unbalanced magnetic pull in eccentric-rotor electrical machines with parallel windings," *Doctoral dissertation, Helsinki University of Technology, Electrical and Communications Engineering*, pp. 1–154, 2007, http://lib.tkk.fi/Diss/2007/isbn9789512290062/.

[5] T. P. Holopainen, "Electromechanical interaction in rotordynamics of cage induction motors," *Doctoral dissertation, Helsinki University of Technology, Electrical and Communications Engineering*, pp. 1–145, 2004, http://www.vtt.fi/inf/pdf/publications/2004/P543.pdf.

[6] K. Kalita, "Integrating rotordynamic and electromagnetic dynamic models for flexible-rotor electrical machines," *PhD thesis, the University of Nottingham*, 2007.

[7] K. Tammi, "Active control of radial rotor vibrations: Identification, feedback, feedforward, and repetitive control methods," *Doctoral dissertation, Helsinki University of Technology, Department of Automation and Systems Technology*, pp. 1–165, 2007, http://www.vtt.fi/inf/pdf/publications/2007/P634.pdf.

[8] N. L-P. Lundström and J-O. Aidanpää, "Dynamic consequences of electromagnetic pull due to deviations in generator shape," *Journal of Sound and Vibration*, vol. 301(1–2), pp. 207–225, 2007.

[9] P. Frauman, A. Burakov, and A. Arkkio, "Effects of the slot harmonics on the unbalanced magnetic pull in an induction motor with an eccentric rotor," *IEEE Transactions on Magnetics*, vol. 43(8), pp. 3441–3444, 2007.

[10] D.G. Dorrell, "Experimental behaviour of unbalanced magnetic pull in 3-phase induction motors with eccentric rotors and the relationship with tooth saturation," *IEEE Transactions on Energy Conversion*, vol. 14, no. 3, pp. 304–309, 1999.

[11] D.G. Dorrell and A.C. Smith, "Calculation of u.m.p in induction motors with series or parallel winding connections," *IEEE Transactions on Energy Conversion*, vol. 9(2), pp. 304–310, 1994.

[12] E. Rosenberg, "Magnetic pull in electrical machines," *Transactions of the american institute of electrical engineers*, vol. 37(2), pp. 1425–1469, 1917.

[13] J. Gukkenheimer and P. Holmes, *Nonlinear Oscillations, Dynamical Systems, and Bifurcations of Vector Fields*, Springer-Verlag, New York, 1983.

[14] G. Genta, *Dynamics of rotating systems*, Springer-Verlag New York, Inc., 2005.

[15] A. Tenhunen, T. P. Holopainen, and A. Arkkio, "Spatial linearity of unbalanced magnetic pull in induction motors during eccentric rotor motions," *COMPEL: The International Journal for Computation and Mathematics in Electrical and Electronic Engineering*, vol. 22(4), pp. 862–876, 2003.

[16] H. Frohne, "Über den einseitigen magnetischen zug in drehfeldmaschinen," *Electrical Engineering (Archiv für Electrotechnik)*, vol. 51, no. 5, pp. 300–308, 1968.

[17] J. Früchtenicht, H. Jordan, and H. O. Seinsch, "Exzentrizitätsfelder als ursache von laufinstabilitäten bei asynchronmaschinen, teil 1 & 2," *Electrical Engineering (Archiv für Electrotechnik)*, vol. 65, pp. 271–292, 1982.

[18] A. Arkkio, M. Antila, K. Pokki, A. Simon, and E. Lantto, "Electromagnetic force on a whirling cage rotor," *IEE Proceedings – Electric Power Applications*, vol. 147, pp. 353–360, 2000.

[19] E. Lantto, A. Arkkio, M. Antila, K. Pokki, and A. Simon, "Electromagnetic forces caused by cage induction motor," *The Seventh International Symposium on Magnetic Bearings (ISMB7), ETH Zurich, August 23–25, 2000.*

[20] K. J. Binns and M. Dye, "Identification of principal factors causing unbalanced magnetic pull in cage induction motors," *Proceedings of IEE*, vol. 120, no. 3, pp. 349–354, 1973.

[21] F. Taegen, "Die bedeutung der läufernutschlitze für die theorie der asynchronmaschine mit käfigläufer," *Electrical Engineering (Archiv für Electrotechnik)*, vol. 48(6), pp. 271–292, 1964.

[22] G. J. Retter, *Matrix and space-phasor theory of electrical machines*, Akadémiai Kiadó, Budapest, 1987.

[23] T. Holopainen, S. Aatola, and A. Arkkio, "Vibration measurements for validation of electromechanical rotor model for cage induction motor," *Proceedings of 8th International Conference on Vibrations in Rotating Machinery (IMechE), University of Wales, Swansea, UK, 7–9.9.2004 (2004), 423 – 432.*

[24] A. Burakov and A. Arkkio, "Low-order parametric force model for eccentric-rotor electrical machine equipped with parallel stator windings and rotor cage," *IET Electric Power Applications*, vol. 1(4), pp. 532–542, 2007.

[25] R. Belmans, A. Vandenput, and W. Geysen, "Influence of unbalanced magnetic pull on the radial stability of flexible-shaft induction machines," *IEE Proceedings – Electric Power Applications*, vol. 134, no. 2, pp. 101–109, 1987.

[26] R. Belmans, A. Vandenput, and W. Geysen, "Calculation of the flux density and the unbalanced pull in two pole induction machines," *Electrical Engineering (Archiv für Electrotechnik)*, vol. 70(3), pp. 151–161, 1987.

[27] M.J. DeBortoli, S.J. Salon, D.W. Burow, and C.J. Slavik, "Effects of rotor eccentricity and parallel windings on induction machine behavior: a study using finite element analysis," *IEEE Transactions on Magnetics*, vol. 29, no. 2, pp. 1676–1682, 1993.

[28] A. Arkkio, "Analysis of induction motors based on the numerical solution of the magnetic field and circuit equations," *Acta Polytechnica Scandinavia, Electrical Engineering Series*, vol. 59, pp. 1–97, 1987, http://lib.hut/Diss/list.html#1980.

[29] A. Tenhunen and A. Arkkio, "Modelling of induction machines with skewed rotor slots," *IEE Proceedings – Electric Power Applications*, vol. 148, no. 1, pp. 45–50, 2001.

[30] G. Schweitzer, H. Bleuer, and A. Traxler, *Active magnetic bearings*, Hochschulverlag AG, ETH Zürich, 244 p. edition, 1994.

[31] G. Schweitzer and E. Maslen, *Magnetic Bearings - Theory, Design, and Application to Rotating Machinery*, Springer Verlag, Berlin, 2009.

[32] A. Chiba and T. Fukao, "Electric rotating machinery with radial position control windings and its rotor radial position controller," *Japan Patent No. 2835522*, January 1989.

[33] A.O. Salazar, W. Dunford, R. Stephan, and E. Watanabe, "A magnetic bearing system using capacitive sensors for position measurement," *IEEE Transactions on Magnetics*, vol. 26, no. 5, pp. 2541–2543, 1990.

[34] J. Bichsel, "Beiträge zum lagerlosen elektro-motor," *Diss. ETH Zürich*, 1990.

[35] A. Chiba, D. T. Power, and M. A. Rahman, "Characteristics of a bearingless induction motor," *IEEE Transactions on Magnetics*, vol. 27(6), pp. 5199–5201, 1991.

[36] A.O. Salazar and R.M. Stephan, "A bearingless method for induction machines," *IEEE Transactions on Magnetics*, vol. 29, no. 6, pp. 2965–2967, 1993.

[37] R. Schöb, "Beiträge zur lagerlosen asynchronmaschine," *Diss. ETH Zürich*, 1993.

[38] A. Chiba, R. Furuichi, Y. Aikawa, K. Shimada, Y. Takamoto, and T. Fukao, "Stable operation of induction-type bearingless motors under loaded conditions," *IEEE Transactions on Industry Applications*, vol. 33(4), pp. 919–924, 1997.

[39] A. Chiba, T. Fukao, O. Ichikawa, M. Oshima, M. Takemoto, and D. G. Dorrell, *Magnetic bearings and bearingless drives*, Elsevier Newnes Press, Boston, MA, 2005.

[40] S.W.K. Khoo, R.L. Fittro, and S.D. Garvey, "An ac self-bearing rotating machine with a single set of windings," *Proceedings of International Conference on Power Electronics, Machines and Drives (Conf. Publ. No. 487)*, pp. 292–297, 2002.

[41] W.K.S. Khoo and S.D. Garvey, "Practical implementation of the bridge configured winding for self-bearing machines," *Proceedings of International Conference on Power Electronics and Drives Systems (PEDS 2005)*, vol. 2, pp. 1146–1151, 2005.

[42] A. Chiba, T. Fukao, and M.A. Rahman, "Vibration suppression of a flexible shaft with a simplified bearingless induction motor drive," *Conference Record of the 2006 IEEE Industry Applications Conference 2006. 41st IAS Annual Meeting.*, vol. 2, pp. 836–842, 2006.

[43] Y. Okada, K. Dejima, and T. Ohishi, "Analysis and comparison of pm synchronous motor and induction motor type magnetic bearings," *IEEE Transactions on Industry Applications*, vol. 31, no. 5, pp. 1047–1053, 1995.

[44] A. Chiba, T. Deido, T. Fukao, and M.A. Rahman, "An analysis of bearingless ac motors," *IEEE Transactions on Energy Conversion*, vol. 9, no. 1, pp. 61–68, 1994.

[45] A. Chiba, D.T. Power, and M.A. Rahman, "No load characteristics of a bearingless induction motor," *Conference Record of the IEEE Industry Applications Society Annual Meeting*, vol. 1, pp. 126–132, 1991.

[46] S. Nomura, A. Chiba, F. Nakamura, K. Ikeda, T. Fukao, and M.A. Rahman, "A radial position control of induction type bearingless motor considering phase delay caused by the rotor squirrel cage," *Conference Record of the Power Conversion Conference, Yokohama 1993*, pp. 438–443, 1993.

[47] A. Chiba and T. Fukao, "Optimal design of rotor circuits in induction type bearingless motors," *IEEE Transactions on Magnetics*, vol. 34(4), pp. 2108–2110, 1998.

[48] T. Kuwajima, T. Nobe, K. Ebara, A. Chiba, and T. Fukao, "An estimation of the rotor displacements of bearingless motors based on a high frequency equivalent circuits," *Proceedings of 4th IEEE International Conference on Power Electronics and Drive Systems, 2001*, vol. 2, pp. 725–731, 2001.

[49] T. Tera, Y. Yamauchi, A. Chiba, T. Fukao, and M.A. Rahman, "Performances of bearingless and sensorless induction motor drive based on mutual inductances and rotor displacements estimation," *IEEE Transactions on Industrial Electronics*, vol. 53(1), pp. 187–194, 2006.

[50] W. Baoguo and W. Fengxiang, "Modeling and analysis of levitation force considering air-gap eccentricity in a bearingless induction motor," *Proceedings of the Fifth International Conference on Electrical Machines and Systems*, vol. 2, pp. 934–937, 2001.

[51] T. Zhang, H. Zhu, and Y. Sun, "Rotor suspension principle and decoupling control for self-bearing induction motors," *Proceedings of CES/IEEE 5th International Power Electronics and Motion Control Conference (IPEMC '06)*, vol. 1, pp. 1–5, 2006.

[52] J. Cai and G. Henneberger, "Radial force of bearingless wound-rotor induction motor," *Proceedings of 8th International symposium on magnetic bearings, August 26–28, 2002, Mito, Japan*, vol. 1, pp. 1–5, 2002.

[53] F. D. Guo and D. Chen Chu, "The unbalanced magnetic pull and its effects on vibration in a three-phase generator with eccentric rotor," *Journal of Sound and Vibration*, vol. 254(2), pp. 297–312, 2002.

[54] S. Watanabe, "Vibration controller for rotating machine," *Japanese Patent JP11027975*, 1999.

[55] W.K.S. Khoo, S.D. Garvey, K. Kalita, and P.R. Houlston, "Vibration control with lateral force produced in electrical machines," *Proceedings of 8th*

International Conference on Vibrations in Rotating Machinery (IMechE), University of Wales, Swansea, UK, 7–9.9.2004 (2004), 713–722.

[56] A. Chiba and T. Fukao, "The maximum radial force of induction machine type bearingless motor using finite element analysis," *Proceedings of the Fourth International Symposium on Magnetic Bearings (ISMB4), vdf Hochschulverlag AG, Zurich, Switzerland, August 23–26, 1994.*

[57] J. Cai and G. Henneberger, "Transient fem computation of radial force and torque for bearingless wound-rotor induction motors," *Proceedings of the Fifth International Conference on Electrical Machines and Systems*, vol. 2, pp. 991–994, 2001.

[58] U.A.U. Amirulddin, G.M. Asher, P. Sewell, and K.J. Bradley, "Dynamic field modelling of torque and radial forces in vector-controlled induction machines with bearing relief," *IEE Proceedings – Electric Power Applications*, vol. 152, no. 4, pp. 894–904, 2005.

[59] J.M.S. Ferreira, M. Zucca, A.O. Salazar, and L. Donadio, "Analysis of a bearingless machine with divided windings," *IEEE Transactions on Magnetics*, vol. 41, no. 10, pp. 3931–3933, 2005.

[60] W.K.S. Khoo, "Bridge configured winding for polyphase self-bearing machines," *IEEE Transactions on Magnetics*, vol. 41, no. 4, pp. 1289–1295, 2005.

[61] S. Kanerva, "Simulation of electrical machines, circuits and control systems using finite element method and system simulator," *Doctoral dissertation, Helsinki University of Technology, Department of Electrical and Communications Engineering*, pp. 1–92, 2005, http://lib.tkk.fi/Diss/2005/isbn9512276100/.

[62] S. Seman, "Transient performance analysis of wind-power induction generators," *Doctoral dissertation, Helsinki University of Technology, Department of Electrical and Communications Engineering*, pp. 1–112, 2006, http://lib.tkk.fi/Diss/2006/isbn9512284235/.

[63] W. Kauss, A. Gomes, R. Stephan, and D. David, "Lqr control of a bearingless machine implemented with a dsp," *Proceedings of 11th International Symposium on Magnetic Bearings (ISMB11), Nara, Japan, August 26–29, 2008.*

[64] T. Katou, A. Chiba, and T. Fukao, "Magnetic suspension force in an induction bearingless motor with a squirrel cage rotor," *Electrical Engineering in Japan*, vol. 159, no. 3, pp. 77–87, 2007.

[65] C. Huettner, "Vibration control for an implantable blood pump on a bearingless slice motor," *JSME International Journal, Series C: Mechanical Systems, Machine Elements and Manufacturing*, vol. 46, no. 3, pp. 908–915, 2003.

[66] J. S. Rao, *Vibratory Condition Monitoring of Machines*, Narosa Publishing House, New Delhi, India, 2000.

[67] G. Genta, *Vibration of Structures and Machines: Practical Aspects*, Springer-Verlag New York, Inc., 1999.

[68] C. R. Burrows and M. N. Sahinkaya, "Vibration control of multi-mode rotor-bearing systems," *Proceedings of the Royal Society of London, Series A, Mathematical and Physical Sciences*, vol. 386(1790), pp. 77–94, 1983.

[69] C.R. Burrows, M.N. Sahinkaya, and S. Clements, "Active vibration control of flexible rotors: an experimental and theoretical study," *Proceedings of the Royal Society of London*, vol. 422, pp. 123–146, 1989.

[70] L.A. Sievers and A.H. von Flotow, "Linear control design for active vibration isolation of narrow band disturbances," *Proceedings of the 27th IEEE Conference on Decision and Control*, vol. 2, pp. 1032–1037, 1988.

[71] S.R. Hall and N.M. Wereley, "Linear control issues in the higher harmonic control of helicopter vibrations," *Proceedings of 45th Annuual Forum of the American Helicopter Society, Boston, USA*, pp. 955–971, 1989.

[72] S. Beale, B. Shafai, P. LaRocca, and E. Cusson, "Adaptive forced balancing for magnetic bearing control systems," *Proceedings of the 31st IEEE Conference on Decision and Control*, vol. 4, pp. 3535–3539, 1992.

[73] S.J. Fedigan C.R. Knospe, R.W. Hope and R.D. Williams, "Adaptive online rotor balancing using digital control," *Proceedings of MAG '93 Magnetic Bearings, Magnetic Drives, and Dry Gas Seals Conference, Technomic Publishing, Lancaster, PA, July 1993.*

[74] P. S. Keogh, C. R. Burrows, and T. Berry, "On-Line Controller Implementation for Attenuation of Synchronous and Transient Rotor Vibration," *Journal of Dynamic Systems, Measurement, and Control*, vol. 118, pp. 315–321, 1996.

[75] E. Lantto, "Robust control of magnetic bearings in subcritical machines," *Doctoral dissertation. Acta Polytechnica Scandinavica, The Finnish academy of technology*, pp. 1–143, 1999, http://lib.tkk.fi/Diss/199X/isbn9512255758/.

[76] P. S. Keogh, M. O. T. Cole, and C. R. Burrows, "Multi-State Transient Rotor Vibration Control Using Sampled Harmonics," *Journal of Vibration and Acoustics*, vol. 124, pp. 186, 2002.

[77] E. Lantto and V. Tommila, "A supercritical 250 kw industrial air compressor prototype," *The Eleventh International Symposium on Magnetic Bearings (ISMB11), Nara, Japan, August 26–29, 2008.*

[78] C.R. Knospe, R.W. Hope, S.M. Tamer, and S.J. Fedigan, "Robustness of adaptive unbalance control of rotors with magnetic bearings," *Journal of Vibration and Control*, vol. 2, pp. 33–52, 1996.

[79] S. Daley, J. Hätönen, and K. Tammi, "Instantaneous harmonic vibration control of a flexible rotor," *Proceedings of the International Symposium on Active Control of Sound and Vibration, Adelaine, Australia, September 18 – 20, 2006.*

[80] S.J. Fedigan C.R. Knospe, R.W. Hope and R.D. Williams., "Experiments in the control of unbalance response using magnetic bearings," *Mechatronics*, vol. 5(4), pp. 385–400, 1995.

[81] T. Glad and L. Ljung, *Control Theory*, Taylor & Francis, Bodmin UK, 2000.

[82] C.R. Knospe, S.J. Fedigan, R. W. Hope, and R.D. Williams, "A multitasking dsp implementation of adaptive magnetic bearing control," *IEEE Transactions on Control Systems Technology*, vol. 5(2), pp. 230–238, 1997.

[83] A. Tenhunen, T. Benedetti, T. P. Holopainen, and A. Arkkio, "Electromagnetic forces of the cage rotor in conical whirling motion," *IEE Proceedings – Electric Power Applications*, vol. 150(5), pp. 563–568, 2003.

[84] D.G. Dorrell, T.J.E. Miller, and C.B. Rasmussen, "Inter-bar currents in induction machines," *IEEE Transactions on Industry Applications*, vol. 39, no. 3, pp. 677–684, 2003.

[85] R. Garch, R. Nordmann, and H. Pfützner, *Rotordynamik*, Springer Verlag, Berlin, 2. auflage edition, 2000.

[86] R. R. Craig Jr., "A review of time-domain and frequency-domain component mode synthesis method," *International Journal of Analytical and Experimental Modal Analysis*, vol. 2(2), pp. 59–72, 1987.

[87] K. Kobayashi, M. Yamashita, A. Chiba, and T. Fukao, "Principles of self-excitation at radial force winding terminals in bearingless induction motors with a squirrel cage rotor," *Conference Record of the IEEE Industry Applications Conference*, vol. 1, pp. 235–240, 2000.

[88] T. P. Holopainen, A. Tenhunen, E. Lantto, and A. Arkkio, "Unbalanced magnetic pull induced by arbitrary eccentric motion of cage rotor in transient operation, part 2: Verification and numerical parameter estimation," *Electrical Engineering (Archiv für Electrotechnik)*, vol. 88(1), pp. 25–34, 2005.

[89] A. Burakov and A. Arkkio, "Comparison of the unbalanced magnetic pull mitigation by the parallel paths in the stator and rotor windings," *IEEE Transactions on Magnetics*, vol. 43, no. 12, pp. 4083–4088, 2007.

[90] K.P. Kovacs, "Two-pole induction-motor vibrations caused by homopolar alternating fluxes," *IEEE Transactions on Power Apparatus and Systems*, vol. 96(4), pp. 1105–1108, 1977.

[91] E.H. Maslen and J.R. Bielk, "A stability model for flexible rotors with magnetic bearings," *Journal of Dynamic Systems, Measurement, and Control*, vol. 114, no. 1, pp. 172–175, 1992.

[92] R.K. Ursem and P. Vadstrup, "Parameter identification of induction motors using differential evolution," *Proceedings of IEEE Congress on Evolutionary Computation (CEC 2003)*, vol. 2, pp. 790–796, 2003.

[93] F. Alonge, F. D'Ippolito, and F.M. Raimondi, "Least squares and genetic algorithms for parameter identification of induction motors," *Control Engineering Practice*, vol. 9(6), pp. 647–657, 2001.

[94] K. V. Price, R. M. Storn, and J. A. Lampinen, *Differential Evolution: A Practical Approach to Global Optimization*, Springer Verlag, 2005.

[95] S. Kukkonen and J. Lampinen, "Constrained real-parameter optimization with generalized differential evolution," *Proceedings of IEEE Congress on Evolutionary Computation (CEC 2006)*, pp. 207–214, 2006.

[96] P. van Overschee and B. DeMoor, *Subspace Identification of Linear Systems: Theory, Implementation, Applications*, Kluwer Academic Publishers, 1996.

[97] L. Ljung, *System identification*, Prentice-Hall Inc., New Jersey, USA, 1987.

[98] A. Sinervo, "Modeling and control of flexural rotor vibration of a two-pole cage induction motor," M.S. thesis, Helsinki University of Technology, Faculty of electronics, Communications and Automation, Department of electrical Engineering, Espoo, Finland, 2008.

[99] B. Heller and V. Hamata, *Harmonic field effects in induction machines*, Elsevier Scientific Publishing Company, Oxford, 1977.

[100] O. Bottauscio, M. Chiampi, L. Donadio, and M. Zucca, "Experimental setup for the measurement of induction motor cage currents," *Journal of Magnetism and Magnetic Materials*, vol. 290–291, no. 2, pp. 1322–1325, 2005.

[101] P.S. Hamer, B.M. Wood, J.J. McClurg, and W.L. Billington, "Large 3600 r/min induction motors operating below their first system resonant speed," *IEEE Transactions on Industry Applications*, vol. 31, no. 5, pp. 1177–1185, 1995.

[102] W.R. Finley, M.M. Hodowanec, and W.G. Holter, "An analytical approach to solving motor vibration problems," *IEEE Transactions on Industry Applications*, vol. 36, no. 5, pp. 1467–1480, 2000.

[103] R.R. Neto, D.L. Bogh, and M. Flammia, "Some experiences on rigid and flexible rotors in induction motors driving critical equipment in petroleum and chemical plants," *IEEE Transactions on Industry Applications*, vol. 44, no. 3, pp. 923–931, 2008.

[104] D.Yu. Skubov and I.V. Shumakovich, "Stability of the rotor of an induction motor in the magnetic field of the current windings," *Mechanics of Solids 34 (1999) 28–40 (Translated from Mekhanika Tverdogo Tela (1999) 36–50).*

[105] B. S. Yang, Y. H. Kim, and B. G. Son, "Instability and imbalance response of large induction motor rotor by unbalanced magnetic pull," *Journal of Vibration and Control*, vol. 10, no. 3, pp. 447–460, 2004.

[106] J. Orivuori, "Active control of rotor vibrations in electric drives," M.S. thesis, Helsinki University of Technology, Department of Automation and Systems Technology, Espoo, Finland, 2008.

[107] J. Orivuori, A. Laiho, A. Sinervo, K. Zenger, and A. Arkkio, "Suppression of rotor vibrations of an electric machine at the critical speed by optimal state feedback controller," *The European Control Conference 2009, Budapest, Hungary, August 23–26, 2009 (in press).*

[108] T. Hiromi, T. Katou, A. Chiba, M. Rahman, and T. Fukao, "A novel magnetic suspension-force compensation in bearingless induction-motor drive with squirrel-cage rotor," *IEEE Transactions on Industry Applications*, vol. 43(1), pp. 66–76, 2007.

[109] G. W. Hill, "On the part of the lunar perigee which is a function of the mean motions of the sun," *Acta Mathematica*, vol. 8, pp. 1–36, 1886.

[110] G. Floquet, "Sure les équations différentielles lineaire a coefficients périodiques," *Annales de L'Ecole Normale Supérieure*, vol. 12, pp. 47–89, 1883.

[111] N. M. Wereley, "Analysis and control of linear periodically time varying systems," *PhD thesis, Dept. of Aeronautics and Astronautics, M.I.T.*, pp. 1–223, 1990.

[112] F. Oncescu, A. A. Lakis, and G. Ostiguy, "Investigation of the stability and steady state response of asymmetric rotors, using finite element formulation," *Journal of Sound and Vibration*, vol. 245(2), pp. 303–328, 2001.

[113] E. Möllerstedt and B. Bernhardsson, "Out of control because of harmonics-an analysis of the harmonic response of an inverter locomotive," *IEEE Control Systems Magazine*, vol. 20(4), pp. 70–81, 2000.

[114] T. R. Kane and P. M. Barba, "Attitude stability of a spinning satellite in an elliptic orbit," *Journal of Applied Mechanics*, vol. 33, pp. 402–405, 1966.

[115] D. A. Peters and K. H. Hohenemser, "Application of the floquet transition matrix to problems of lifting rotor stability," *Journal of American Helicopter Society*, vol. 16, pp. 25–33, 1971.

[116] S. C. Sinha and D. H Wu, "An efficient computational scheme for the analysis of periodic systems," *Journal of Sound and Vibration*, vol. 151, pp. 91–117, 1991.

[117] P. Montagnier, C.C. Paige, and R.J. Spiteri, "Real Floquet Factors of Linear Time-Periodic Systems," *Systems & Control Letters*, vol. 50, pp. 251–262, 2003.

[118] K. Zenger, "Dynamic time-variable transformations of linear differential systems," *Proceedings of the 15th International Conference on Systems Science, Wroclaw, Poland, September 7–10*, pp. 241–250, 2004.

[119] V. S. Deshmukh and S. C. Sinha, "Control of Dynamic Systems with Time-Periodic Coefficients via the Lyapunov-Floquet Transformation and Backstepping Technique," *Journal of Vibration and Control*, vol. 10, pp. 1517–1533, 2004.

Series title, number and
report code of publication

VTT Publications 712
VTT-PUBS-712

Author(s)
Antti Laiho

Title

Electromechanical modelling and active control of flexural rotor vibration in cage rotor electrical machines

Abstract

The main objective of this thesis is to develop new tools for model-based control of flexural rotor vibration in cage induction machines. In order to exert the control force on the rotor, a built-in force actuator based on self-bearing principle is considered. A low-order parametric electromechanical model coupling the eccentric-rotor machine, the actuator and rotor-dynamics is developed. Furthermore, numerical analysis of the actuator-rotor system is considered. The numerical analysis is based on time-discretised finite element analysis of the electromagnetic fields in the two-dimensional cross-section of the machine. The finite element analysis is used to estimate the parameters of the low-order model. The numerical analysis provides a tool for both designing the actuator and testing the control algorithms.

In the thesis, a control algorithm, previously used mainly in active magnetic bearings for compensation of harmonic disturbance forces, is applied by using the built-in force actuator. In the simulations, the control algorithm is embedded in the numerical analysis. The modelling and model-based control are verified by experiments. A 30 kW two-pole cage induction motor with an extended rotor shaft is used for measurements.

The results both from simulations and experiments show that, by using the built-in force actuator, the model-based controller is suitable for flexural rotor vibration suppression in a cage induction machine. In particular, the stable operation at the critical speed of the machine can be achieved by using the methodology presented in this research.

ISBN
978-951-38-7348-6 (soft back ed.)
978-951-38-7349-3 (URL: http://www.vtt.fi/publications/index.jsp)

Series title and ISSN	Project number
VTT Publications 1235-0621 (soft back ed.) 1455-0849 (URL: http://www.vtt.fi/publications/index.jsp)	26153

Date	Language	Pages
August 2009	English, Finnish abstr.	91 p. + app. 84 p.

Name of project	Commissioned by
SA-VIBRA-TIMEPER	Academy of Finland

Keywords	Publisher
induction machine, electromagnetic actuator, rotor-dynamics, self-bearing machine, bearingless drive, mechanical vibration, active control	VTT Technical Research Centre of Finland P.O. Box 1000, FI-02044 VTT, Finland Phone internat. +358 20 722 4520 Fax +358 20 722 4374

Julkaisun sarja, numero ja raporttikoodi

VTT Publications 712
VTT-PUBS-712

Tekijä(t)
Antti Laiho

Nimeke

Sähkömekaaninen mallinnus ja aktiivinen roottorin poikittaisvärähtelyjen hallinta häkkiroottorilla varustetussa induktiokoneessa

Tiivistelmä

Tämän väitöskirjan tavoite on uusien menetelmien kehittäminen poikittaisten roottorivärähtelyjen mallipohjaiseen vaimennukseen häkkiroottorilla varustetussa induktiokoneessa. Työssä käytetään laakerittoman sähkökoneen voimantuottomekanismia voiman tuottamisessa roottoriin. Tutkimuksessa rakennetaan matalakertalukuinen sähkömekaaninen malli, joka kytkee toisiinsa roottorin epäkeskon liikkeen, voima-aktuaattorin ja roottoridynamiikan. Työssä tutkitaan lisäksi aktuaattori-roottori-systeemin numeerista analyysiä. Numeerinen analyysi perustuu sähkömagneettisten kenttien aika-diskretisoituun elementtimenetelmäperustaiseen analyysiin koneen kaksiulotteisessa poikkileikkauksessa. Elementtimenetelmää käytetään matalakertalukuisen mallin parametrien estimoinnissa. Numeerinen analyysi antaa työkaluja aktuaattorin suunnitteluun ja säätöalgoritmien testaukseen.

Tässä työssä sovelletaan aiemmin pääasiassa aktiivimagneettilaakereissa harmonisten herätteiden kompensoinnissa käytettyä säätöalgoritmia käyttäen koneen sisäänrakennettua voima-aktuaattoria. Simuloinneissa säätöalgoritmi on sisällytetty numeeriseen analyysiin. Työssä mallinnus ja mallipohjainen säätö verifioidaan kokeellisesti. Mittauksissa käytetään kaksinapaista häkkiroottorilla ja pidennetyllä roottoriakselilla varustettua 30 kW:n induktiokonetta.

Sekä simulaatioista että kokeista saadut tulokset osoittavat, että sisäänrakennettua voima-aktuaattoria hyödynnettäessä mallipohjainen säädin soveltuu poikittaisten roottorivärähtelyjen aktiivivaimennukseen häkkiroottorilla varustetussa induktiokoneessa. Erityisesti tässä työssä esitetty menetelmä mahdollistaa koneen stabiilin toiminnan kriittisellä pyörimisnopeudella.

ISBN
978-951-38-7348-6 (nid.)
978-951-38-7349-3 (URL: http://www.vtt.fi/publications/index.jsp)

Avainnimeke ja ISSN	Projektinumero
VTT Publications 1235-0621 (nid.) 1455-0849 (URL: http://www.vtt.fi/publications/index.jsp)	26153

Julkaisuaika	Kieli	Sivuja
Elokuu 2009	Englanti, suom. tiiv.	91 s. + liitt. 84 s.

Projektin nimi	Toimeksiantaja(t)
SA-VIBRA-TIMEPER	Suomen Akatemia

Avainsanat	Julkaisija
induction machine, electromagnetic actuator, rotor-dynamics, self-bearing machine, bearingless drive, mechanical vibration, active control	VTT PL 1000, 02044 VTT Puh. 020 722 4520 Faksi 020 722 4374

VTT PUBLICATIONS

ISBN 978-951-38-7348-6 (soft back ed.)
ISSN 1235-0621 (soft back ed.)

ISBN 978-951-38-7349-3 (URL: http://www.vtt.fi/publications/index.jsp)
ISSN 1455-0849 (URL: http://www.vtt.fi/publications/index.jsp)